New Approaches towards Phosphorescent Iridium Complexes for Applications in Organic Light-Emitting Diodes and Photocatalysis

Dissertation

Zur Erlangung

des Doktorgrades der Naturwissenschaften

(Dr. rer. nat.)

an der Fakultät für Chemie und Pharmazie

der Universität Regensburg

vorgelegt von

Andreas Hohenleutner

aus München

Regensburg – 2013

The experimental work was carried out between November 2009 and December 2012 at the University of Regensburg, Institute of Organic Chemistry under the supervision of Prof. Dr. Burkhard König.

The PhD-thesis was submitted on:	Thursday January 24th 2013
Date of the colloquium:	Friday February 22nd 2013

Board of Examiners:

Prof. Dr. Robert Wolf	(Chairman)
Prof. Dr. Burkhard König	(1st Referee)
Prof. Dr. Joachim Wegener	(2nd Referee)
Prof. Dr. Hartmut Yersin	(Examiner)

to Vidya

and

to my family

Acknowledgements

First and foremost, I would like to thank my supervisor Prof. Burkhard König. For the opportunity to work in his group over the last years, for the fascinating topic but most of all for the possibility to independently develop my work and the cooperations within the NEMO network. I am very happy I decided to stay in Regensburg for my PhD.

I want to thank Prof. Joachim Wegener, Prof. Hartmut Yersin and Prof. Robert Wolf for taking the time to be the members of my doctoral committee.

I would like to express my gratitude to our partners at Merck KGaA, especially Dominik Joosten and Philipp Stössel, for getting us started, sharing their advice, expertise, data and materials, their approachability and the general straightforward and fruitful collaboration as well as personal help.

I am grateful to Markus Leitl and Prof. Hartmut Yersin for the fruitful collaboration. I learned a lot from the interesting discussions about the photophysics of our compounds.

The German Federal Ministry for Education and Research and the DAAD INDIGO program supported my work financially. I am very grateful for this and for the possibility to attend a number of exciting conferences within the last years.

Dr. Rudolf Vasold for his constant support and help with all kind of big and small problems and for sharing his expertise and knowledge with us over the last years.

I would like to thank all members of the Central Analytical Department for the friendly and helpful manner and of course diverse measurements.

I owe my thanks to Julia Sporer, Christian Ehrenreich, Mike Yeon Myung, Nadja Simeth, Alexander Lamers, Milada Schulzova, Manuel Bause, Janina Gonschor, Julian Greindl, Andreas Fuchs, Clemens Enzian and Christian Ziegler for their time and commitment during research internships or longer projects. I learned a lot from supervising you guys.

All permanent staff of the König Group for help, support and the friendly atmosphere. In particular Regina Hoheisel for her help with cyclic voltammetry.

All past and present members of the König group; especially Thea, Mouchumi, Benno, Anna, Michl, the several Caros, Durga, Thomas, Tobi, Harry, Tanja, Supratim, Balki, Troppi, Malte, and all the ones I forgot… For sharing expertise and advice, coffee and after work beers, skiing and hiking trips, international evenings and Friday lunch get-togethers, barbecue- and PhD-parties … All of you are way more than colleagues to me and that's what made the last three years an amazing time. THANK YOU!

Masha: For spreading smiles, car trips to Switzerland, discussions till dawn, an enjoyable collaboration, rescuing my sley(!), and for becoming a very good friend over the last years.

Susa: For the collaboration and friendship all these years (must be 10 by now?), for enduring my moods, sharing the ups and downs of doing a PhD, for India and for being one of the nicest and most selfless persons I know.

Josef: For parties till dawn, organizing the skiing trips, common sailing licences and trips, organizing parties and being a friend.

Sanne: For your attitude, lots of good times on skiing trips, long discussions and of course the "Monday evenings" in the kitchen or on the balcony. We miss you here…

Tasha: For the coffee breaks, long talks about nearly everything, skiing and hiking trips, DJ'ing for us on almost every party and for becoming such a close friend.

I am extremely grateful to all my friends and colleagues (or both), whom I am not personally mentioning here. Sorry guys, there is just not enough space…

I want to thank Susa, Tasha, Masha, Markus and Vidya for proofreading parts of the manuscript for this thesis.

I will be eternally grateful to my parents for raising me to be the person I am now and for loving and supporting me in every way I could ever think of for the last 28 Years. I cannot thank you enough!

Vidya, for your endless love and support, for enduring my moods (especially in the last months), for all the time we spent together… and the future ahead. I am the happiest person for having you in my life. I love you.

Table of Contents

CHAPTER 1

1. CHEMICAL DEGRADATION IN ORGANIC LIGHT-EMITTING DEVICES: MECHANISMS AND IMPLICATIONS FOR THE DESIGN OF NEW MATERIALS*

* This chapter was accepted for publication in Advanced Materials. Authors: Susanna Schmidbauer, Andreas Hohenleutner and Burkhard König. SS and AH contributed equally.

1.1 INTRODUCTION

From the first discovery of light emission from anthracene single crystals in 1965,[1] organic electroluminescence has developed into a field of immense research interest with hundreds of groups around the world working to improve materials and devices. While it initially did not get much scientific attention, the first heterojunction device by Tang and Van Slyke in 1987[2] sparked academic and commercial interest in the subject and the advances in the efficiency of organic light-emitting devices since then have been tremendous. In particular the discovery of the triplet harvesting effect by Baldo et al. was responsible for a leap in the internal quantum efficiencies of the devices, enabling the conversion of nearly 100% of the charge carriers into photons.[3] As the recombination of electrons and holes yields triplet (75%) and singlet (25%) excitons and organic materials are usually only capable of emission from singlet states (fluorescence) this used to limit the achievable internal quantum efficiency. Using phosphorescent transition metal complexes as the emitting materials could overcome this limitation. Emission of light takes place from the triplet states of these compounds and singlet excitons are rapidly converted into triplets via efficient inter system crossing (ISC). By now, organic light-emitting devices have made their way into mass production for display applications and are also expected to find application in the commercial lighting market in the near future. Besides high efficiencies and low power consumptions, it is also important that the devices have a high operational stability. Degradation in OLEDs can be caused by the formation of dark spots, the occurrence of electrical shorts leading to a sudden decrease in luminance (catastrophic failure) or intrinsic degradation. Dark spot formation and catastrophic failure can be suppressed by carefully optimized and controlled fabrication conditions and an adequate encapsulation of the devices and thus is no longer considered an obstacle for commercial applications. Intrinsic degradation is characterized by the decrease of overall luminance over time during continuous driving. This is accompanied by a rise of the operating voltage necessary to maintain operation at a constant current. This type of degradation is believed to result mainly from the deterioration of organic (and in some cases metal-organic) molecules in the device. The location and nature of this chemical degradation is highly dependent on the employed materials as well as the device structure and the occurring processes can be manifold even for a single device. It is due to this complexity that chemical degradation is still the least understood of the different modes of degradation. To enable the development of new materials with high performances and stabilities however, it is important to understand the chemical nature of defects in the organic layers and the reactions that lead to their formation.

In this progress report, we will try to shed light on the chemistry behind intrinsic degradation in OLEDs by giving an overview on recent advances in the elucidation of chemical degradation mechanisms, how they can be investigated and how the gained knowledge can impact the design of new materials. It is not our aim to present a comprehensive review about intrinsic degradation and operational lifetimes, which would include many aspects of device engineering and go beyond the scope of this manuscript, but rather to limit our discussion to the chemical aspects of device degradation. Nevertheless, to provide a basis for the understanding of the processes, we have to discuss some of the physical mechanisms responsible for the formation of defect sites in OLEDs.

1.2 POSSIBLE REASONS FOR DEFECT FORMATION

In general it is believed that intrinsic device degradation is caused by the chemical conversion of a fraction of molecules in the organic layers of the device. The degradation products can then act as non-radiative recombination centers, luminescent quenchers or deep charge traps. Luminance loss can be caused by the former two or, if the emitting dopant itself is destroyed during device operation, simply by the lack of emitting centers. Deep charge traps are sites that can "trap" an electron or hole due to suitable energy levels and thus causes a localization of charges at the defect sites. Accumulation of these immobilized charges then leads to a rise of the operating voltage. It should be noted that a single defect site is not necessarily limited to one of the mentioned roles but might in fact act as an electron- and hole-trap as well as a quenching site at the same time. The formation of these defects can be caused by different processes and proceed via a variety of possible pathways.

1.2.1 CHARGE CARRIER INDUCED DEGRADATION

Instability of the molecules corresponding radical cations or radical anions can lead to defect formation by bond rupture or via radical reactions with surrounding molecules. The degradation is in this case caused by the holes and electrons moving through the organic materials and can thus be labeled charge carrier induced degradation. In efficient, state-of-the-art OLEDs, chemical degradation in the bulk of the transport layers - that is not in the vicinity of the emitting layer - is likely to be of this origin. The formed defects can act as traps for the charges moving through the device and should in general mainly result in a rise of the operating voltage.

1.2.2 EXCITON INDUCED DEGRADATION

Due to the presence of excitons, the situation is a bit more complex in the emitting layer and at its interfaces with the adjacent transport or blocking layers. Excitons can participate in defect formation either via direct degradation of molecules in the excited state or via bimolecular quenching reactions.[4] Destructive deactivation can occur via direct excitation to a repulsive potential or via thermal population of higher lying dissociative states of a molecule. These dissociation processes can produce charged fragments or radicals that can in turn react with surrounding molecules and thus lead to deterioration of the organic or metal-organic materials.

Bimolecular annihilation reactions involving excitons constitute another pathway.[4-7] The annihilation of two excitons leads to the population of higher lying excited states that can undergo further reactions via two possible pathways: Direct dissociative processes similar to the ones induced by normal excitonic degradation, or degradation via the so called “hot molecule mechanism” (see Figure 1). In this case, internal conversion from an excited singlet state gives a highly vibrationally excited electronic ground state S_0**.[8] This “hot molecule” has an equivalent vibrational temperature of 2000-4000 K and can dissociate directly (path A) or via excitation by another photon (or energy transfer from another exciton, path B). The absorption bands of these hot molecules show a thermal broadening causing an enhanced absorption at lower energies.

Energy transfer from an exciton to a polaron (radical cation or anion) yields a polaron excited state (excited radical) that might decay via similar pathways.[9-10] The importance of this particular route is highlighted by the fact that exciton-polaron annihilation has even been proposed to be the dominant mechanism for different phosphorescent devices.[10]

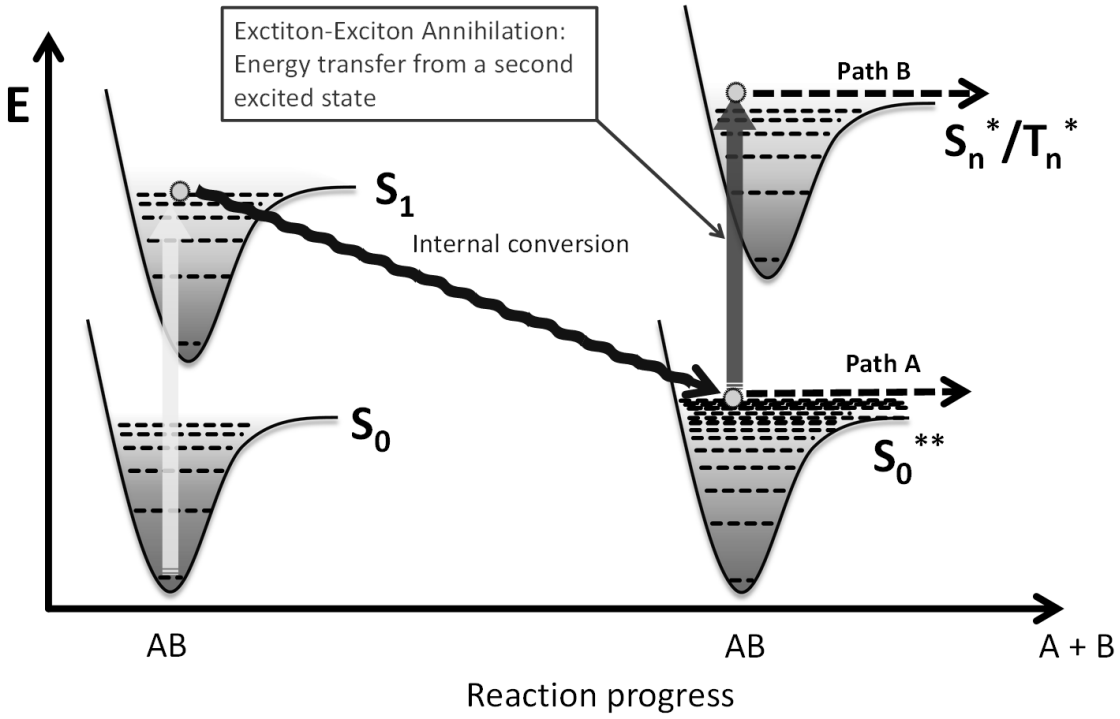

Figure 1-1. The "hot molecule" mechanism. Internal conversion from an excited singlet state gives a highly vibrationally excited electronic ground state S0**. This "hot molecule" can dissociate directly or via excitation by another photon (or energy transfer from another exciton).

1.3 USEFUL TECHNIQUES FOR THE ELUCIDATION OF CHEMICAL DEGRADATION MECHANISMS

Physical methods can provide information on the amount and location of trapped charges, luminescence quenchers and non-radiative recombination sites and often also on the electronic/(photo)-physical processes leading to their formation. However, they usually do not allow to draw conclusions regarding their chemical nature.

Since the organic layers in an OLED device are typically only several nm thick, the amount of material available for analysis is usually very small. The actual degradation products will only amount to a small fraction of the material even after extended operation. A defect density of 0.1% in the emission layer for example can already lead to 50% loss in luminance.[4] Considering the likely participation of different pathways and their mostly radical nature, the degradation of OLEDs is furthermore expected to lead to a multitude of deterioration products

rather than to a single potentially easily identifiable one. The elucidation of chemical degradation mechanisms and products therefore presents a significant challenge.

1.3.1 CHEMICAL ANALYSIS TECHNIQUES

However, there are many reports on the chemical analysis of OLEDs and a number of techniques that have proven useful in gaining insight on the chemical deterioration products and pathways. Spectroscopic methods can provide information on the electronic and chemical structure of degradation products. Techniques that have been employed include UV-Vis, infrared-, nuclear magnetic resonance as well as electron paramagnetic resonance spectroscopy.[11-15] Nonetheless, to gain detailed structural information from these methods, isolation of the degradation products from the bulk material is usually necessary. With the limited amount available, this represents a significant impediment. High performance liquid chromatography (HPLC) is a technique that allows the analysis and separation of complicated mixtures and the detection of very small quantities of materials. It can additionally be supplemented through above mentioned analysis methods to successfully identify degradation products.[11] HPLC and its combination with mass spectrometry (HPLC-MS) has been employed successfully to investigate degradation pathways in organic light emitting devices for example by comparing chromatogram peaks and the corresponding ions of pristine and aged devices.[11, 16-17] While most chemical analysis techniques require dissolving the organic layers of the device before the measurements, mass spectrometry using a laser desorption ionization (LDI) source is a powerful method for the direct analysis of organic thin films and even fully processed OLED devices. The molecules of a solid sample are ionized and accelerated via excitation with a UV-laser pulse in a strong electric field inside a vacuum chamber. This ionization mode traditionally requires preparation of the analytes within a suitable matrix material to enable excitation and ionization of the materials (MALDI; matrix assisted laser desorption ionization). An OLED device however presents an ideal LDI sample in itself and can thus be analyzed directly. The combination of electron accepting (electron transport layers/n-dopants) and electron donating (hole transport layers/p-dopants) together with the strong UV-absorption of most organic OLED materials enable an efficient excitation, desorption and ionization of the sample. The high sensitivity of the LDI method facilitates the detection and identification of degradation products even as trace impurities and has enabled the elucidation of a variety of chemical degradation pathways.

1.3.2 THEORETICAL CALCULATIONS

Quantum chemical calculations are a popular tool for the prediction of properties of molecules and materials in their ground and excited states, the elucidation of chemical and photochemical reaction pathways and the interpretation of experimental results. Especially density functional theory (DFT) calculations have become a standard tool in the development of new materials for organic electronics. Computational chemistry can help to assess the feasibility of reaction pathways that molecules can undergo. Energies and geometries of the participating electronic states and reaction intermediates can be predicted and thus contribute to the understanding of charge and exciton induced processes in the organic materials. Calculations have for example been employed to identify "structurally weak" parts of molecules by determining bond dissociation energies or to identify deactivation routes and possible exciton induced degradation pathways for phosphorescent emitters.[18-22]

1.4 CHEMICAL DEGRADATION MECHANISMS IN ORGANIC LEDS AND STRATEGIES FOR STABILITY IMPROVEMENT

With the different processes leading to the formation of degradation products and defect states, respectively, in combination with the variety of materials present in a typical device, it is likely that not only one pathway is responsible for the OLED instability. It is the sum of all degradation events in the different layers leading to device failure. Therefore even minor instabilities in the materials have to be elucidated and eliminated to ensure highly efficient and durable OLED devices. In the following sections we will review the degradation behavior of some materials that were investigated until now, trying to identify (re)occurring mechanisms starting with the hole conducting, followed by the electron conducting materials and ending with phosphorescent emitters. Not only the pure degradation mechanisms are summarized, but also some concluding remarks are drawn for rational changes in the molecule structures, which might lead to an improvement in device stability.

1.4.1 DEGRADATION OF HOLE CONDUCTING MATERIALS

Aromatic amines are widely used in organic light emitting diodes due to their physical and electrochemical properties. They are a well investigated class of molecules for the use as hole transporting (NPD, spiro-TAD, TAPC), electron blocking (spiro-TAD) as well as host materials (CBP, CDBP, DMFL-CBP, TCTA) in phosphorescent devices. Much effort has been expended so far to shed light on the behavior of aromatic amines in driven OLEDs. Investigations showed that aromatic amines in the HTLs do not suffer any chemical degradation in single-carrier devices (electron- and hole-only devices, respectively). It was also observed that degradation mainly occurs in the vicinity of the HTL/EML-interface, where recombination and therefore exciton formation takes place. Both facts infer that aromatic amine degradation is mainly caused by excited states rather than charge carriers.[8, 14] Estimating the bond dissociation energies of several arylamines via DFT calculations provided some indications about the nature of the degradation pathway: [14, 23] $C(sp^2)$-$C(sp^2)$ bonds exhibit homolytic bond dissociation energies of at least 110 kcal/mol whereas C-N bond energy-levels are at least ~30 kcal/mol lower (Figure 1-2) and lie therefore in the same energy range as the first singlet excited state of the arylamines. The vulnerability of arylamines might consequently lie in the high probability of C-N bond dissociation in excited molecules.

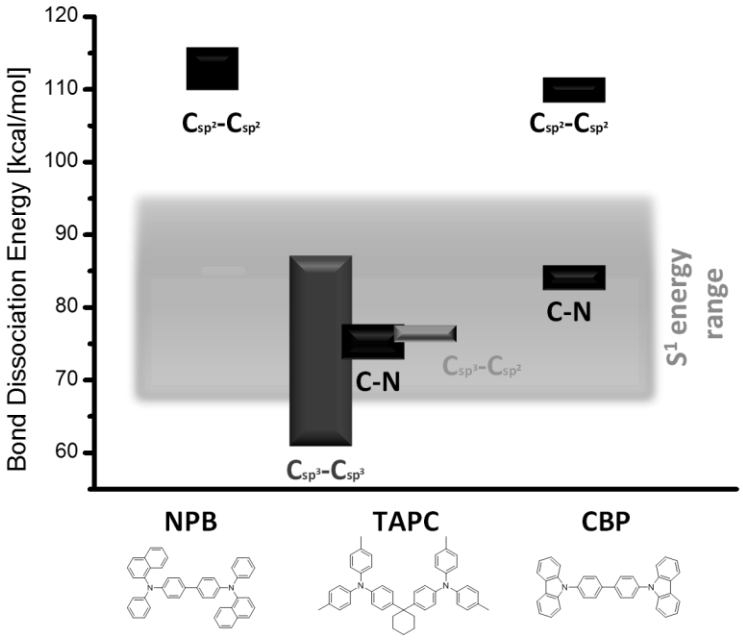

Figure 1-2: Dissociation energies of different bond-types in the hole condcuting materials NPB, TAPC and CBP.

Kondakov et al. assumed that the C-N bond cleavage is of homolytic rather than heterolytic nature due to the endothermicity of the latter.[14] The so generated reactive radical species undergo unselective subsequent reactions with adjacent neutral molecules resulting in long-lived π-conjugated radical species. Due to their lower lying LUMO, energy transfer from the excited matrix or dopant molecules can occur. The very low oscillator strength of the following transition leads to the non-emissive character of these excited states. Thus, the formed radicals can not only act as deep and irreversible carrier traps but also as luminescence quenchers.[11] With respect to the chemical degradation pathway, these radicals can additionally undergo hydrogen transfer, disproportion or radical addition reactions with a neighboring radical to form neutral, saturated degradation products (Scheme 1-1).

Several groups successfully analyzed different aged OLED devices via HPLC/MS techniques. By this means, degradation products derived from C-N bond dissociation and following reactions could be identified for a variety of arylamines, thus supporting the proposed general degradation pathway. Some of these products and more details and peculiarities of the mechanism will be discussed in the following section.

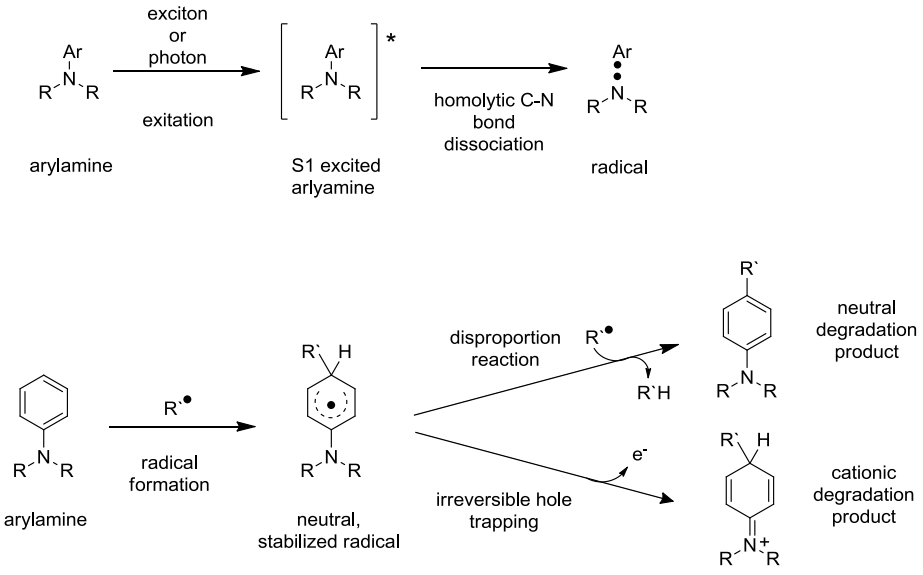

Scheme 1-1: General degradation pathway of aromatic amines in driven OLED devices.

The unequivocally identified degradation products of the host material CBP (4,4'-bis(carbazol-9-yl)biphenyl) are shown in Figure 1-3.[11, 14] Three different species (BPC, C and 3-CCBP), derived from C-N bond cleavage and subsequent reactions, could be isolated from aged OLED devices via HPLC separation. After 4000 h of operation at 40 mA/cm$_2$ (LT_{50} = 80 h),

approximately 20% of CBP had degraded. The main degradation product formed was BPC (about 1/3 of the degraded CBP molecules).The yields of the remaining two derivatives were much lower. Gel permeation chromatographic (GPC) analysis also revealed the presence of high-molecular-weight products.

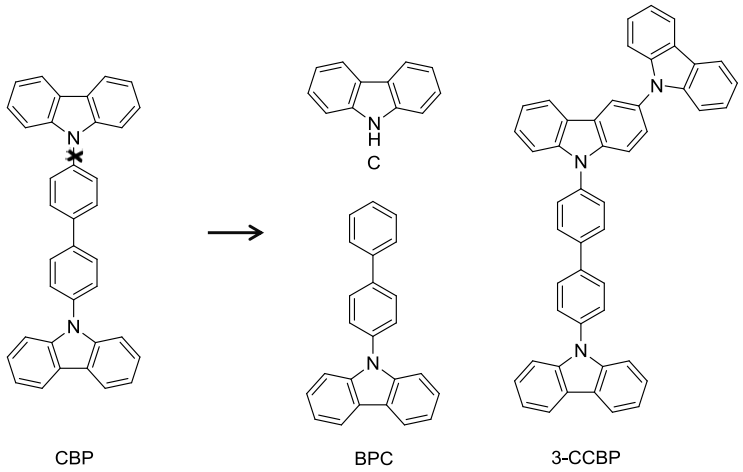

Figure 1-3: Host material CBP and degradation products identified by Kondakov et al.

In the carbazole-containing matrix material TCTA (4,4',4"-tris(carbazol-9-yl)triphenylamine) bond cleavage does not affect the carbazolyl moiety, but the central triphenylamine core.[16, 24] Sivasubramaniam et al. could also identify [TCTA-carbazole]-fragments in MS investigations in minor amounts, but these could be attributed to degradation processes during thermal vapor deposition.[25] Different mechanisms for the formation of these products have been proposed: Leo et al. assumed a heterolytic dissociation of the C-N bond, yielding a cationic amine species and a phenylcarbazole anion, which reacts in a nucleophilic substitution with adjacent TCTA molecules to TCTA+PC. In contrast, Sivasubramaniam et al. postulated a radical pathway for the formation of this product.[16] Additionally, miscellaneous substitution products with moieties of the adjacent hole transport material NPB (*N,N'*-bis(naphthalen-1-yl)-*N,N'*-bis(phenyl)-benzidine, degradation behavior discussed below)could be identified (Figure 1-4, middle).

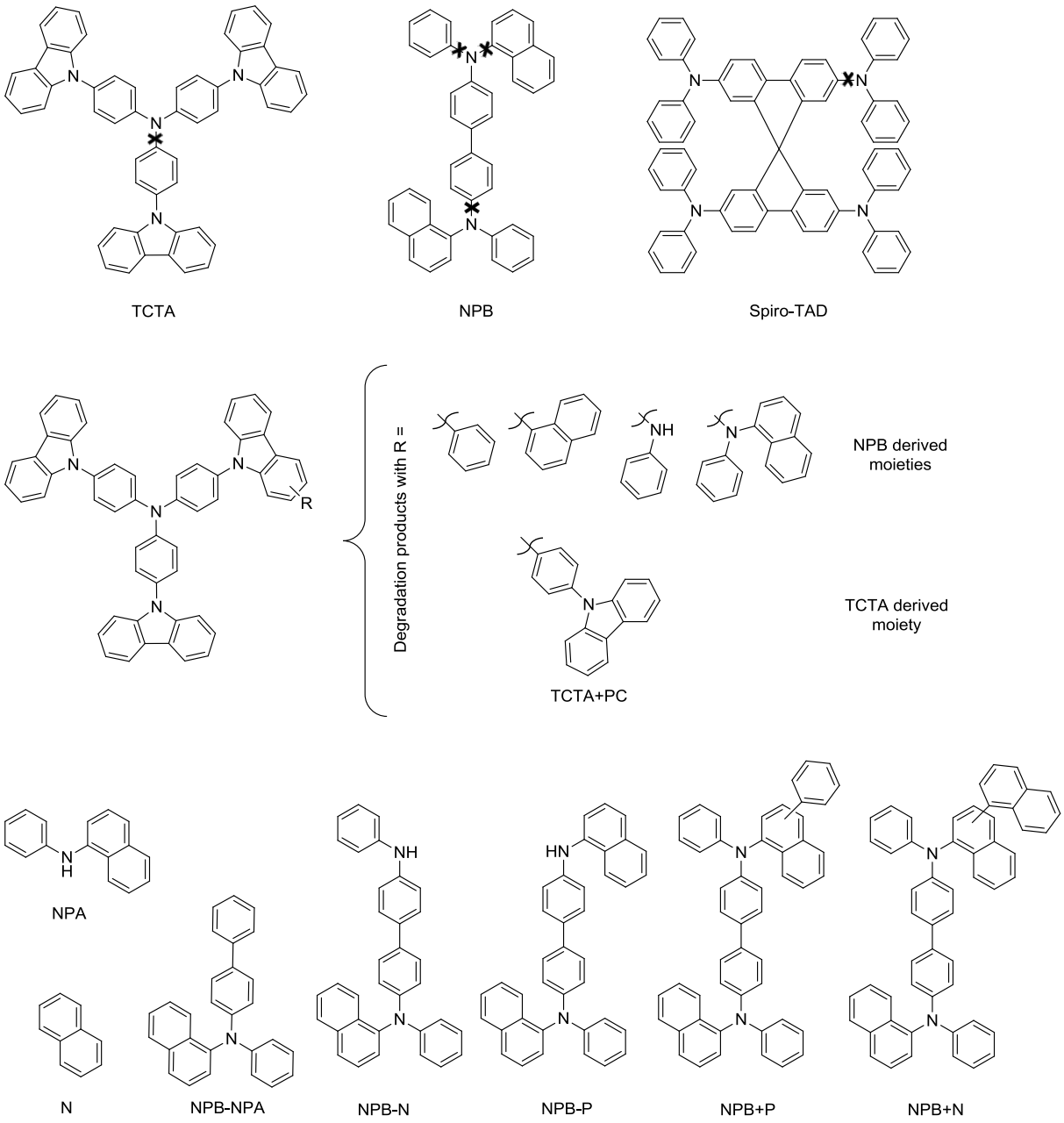

Figure 1-4: Degradation behavior of the arylamines TCTA, NPB, and spiro-TAD. Top: weak bonds of the molecules, which are responsible for degradation due to bond dissociation. Middle: identified degradation products of TCTA, resulting from substitution reactions with fragments of other TCTA molecules or of the adjacent material NPB. Bottom: identified degradation products of NPB, resulting from bond dissociation and substitution reactions of these moieties with neigbouring NPB molecules.

In mass spectrometric investigations Leo et al. found that the electron blocking material Spiro-TAD (2,2',7,7'-tetrakis(*N,N*-diphenylamino)-9,9-spirobifluorene) undergoes an analogous dissociation between the spiro-bifluorene core and the diphenylamine (Figure 1-4, top).[24]

Quantum chemical calculations on the hole transport material NPB revealed that the numerous non-equivalent C-N bonds have almost identical bond dissociation energies, which explains the multitude of different degradation products that could be detected for this material. Products NPB-NPA, NPA and N (Figure 1-4, bottom) could be unambiguously identified.[23] Further derivatives, lacking a phenyl (NPB-P) or naphthyl (NPB-N) moiety respectively, can be assumed according to mass spectrometric analysis of the degraded device, [25-26] as well as products formed by radical attacks (NPB+N, NPB+P).[23]

Investigating the degradation behavior of the hole transport material TAPC (Di-[4-(*N,N*-ditolyl-amino)-phenyl]cyclohexane), Kondakov et al. did not only identify the expected C-N bond dissociation and resulting substitution products of TAPC (DTA, TAPC-T and TAPC-DTA, **Figure 1-5**). [23] Species like TAPC-DTPA and DTPA could be observed, which obviously originate from C-C bond cleavage. This is also reasonable keeping in mind that the bond dissociation energies of bonds containing C(sp^3) centers are about 30 kcal/mol lower than these of double bonds, therefore having equal energies as the first singlet excited state of TAPC (Figure 1-2). Another degradation route, specific for molecules incorporating saturated rings, starts with the homolytic cleavage of C(sp^3)-C(sp^3) bonds. Due to the ring structure not two radicals are formed, but one single biradical which can easily undergo dimerization or polymerization reactions to high molecular weight compounds. The enormous increase of driving voltage in aged devices containing TAPC additionally suggests the accumulation of trapped charges in the bulk of the TAPC layer. This indicates that degradation not only occurs via excitons at the vicinity of the HTL/EML interface, but is at least partly caused by charge carriers, following a still unidentified degradation pathway.

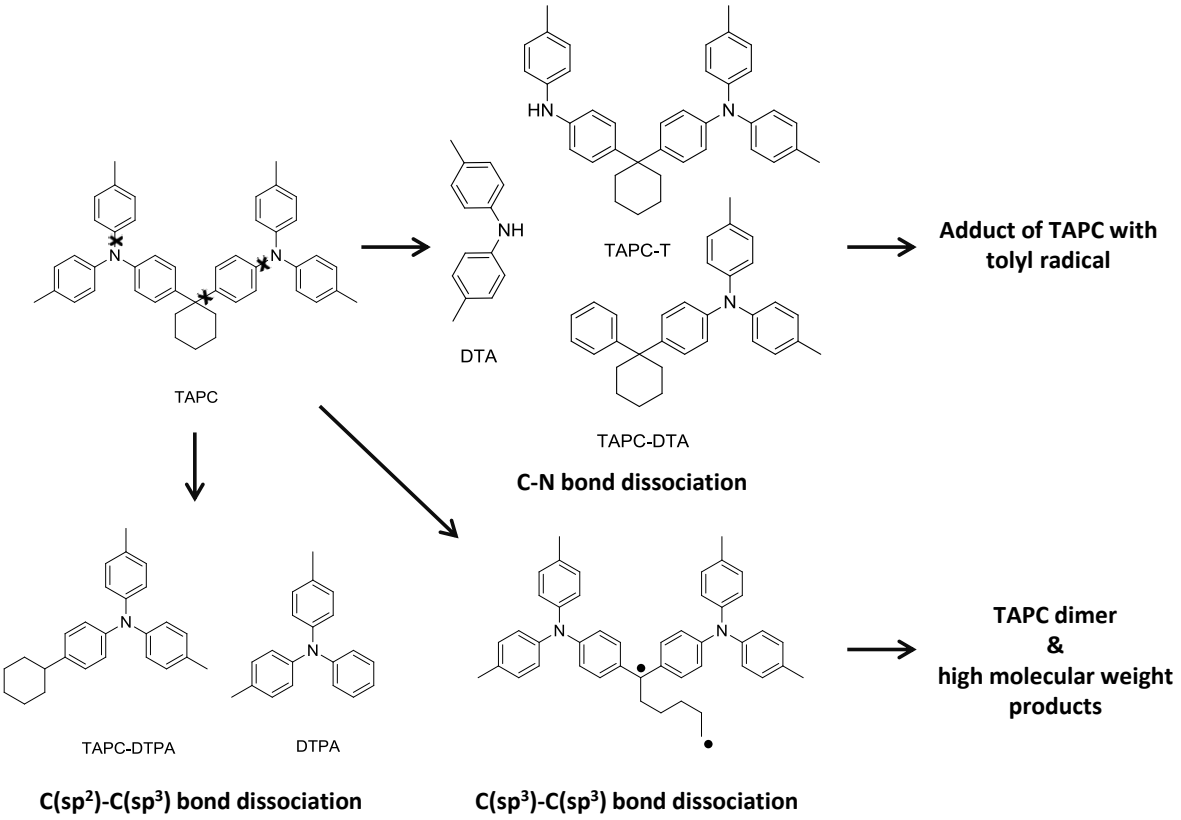

Figure 1-5: Different pathways of TAPC-degradation: low dissociation energies of C-N, C(sp^3)-C(sp^3)- and C(sp^2)-C(sp^3) bonds lead to miscellaneous degradation products.

In terms of stability, interesting effects could be observed for CBP derived materials, which are related to the planarity and π-conjugation of the molecules (Figure 1-6).[24, 27] DMFL-CBP follows a similar degradation pathway as CBP, namely C-N bond cleavage. In contrast, the 3,3'-methylated CDBP, predominantly degrades via C-C bond dissociation (Figure 1-6). Choi et al. explained this observation based on the dihedral angles of the molecules.[27] While DMFL-CBP has a planar structure, CBP and CDBP are twisted with torsion angles of 35 and 90 °, respectively. In the latter configuration, having the two phenyl groups perpendicular to each other, the π-conjugation of this molecule is broken. This results in a decreased C-C bond dissociation energy and as a result in an increased likelihood of bond-cleavage.

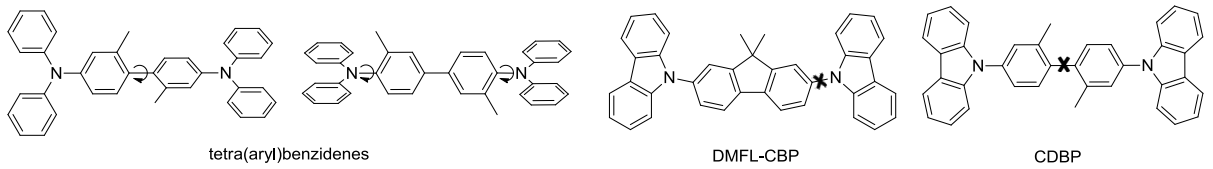

Figure 1-6: Substitution induced torsion of tetra(aryl)benzidenes and resulting changes in bond strength for DMF-CBP and CDBP.

Low et al. showed additionally that methylation in 2,2'- or 3,3'-position of the biphenyl core in tetra(aryl)benzedenes results in increased oxidation potentials.[28] This effect seems to result from the non-planarity of the system - and therefore the restricted conjugation between the two phenyl moieties and the lone pairs of the nitrogen- caused by the sterical hindrance of the methyl substituents. Rigidification of the biphenyl moiety leads to an extended π-conjugated system and a decreased oxidation potential. It is known that the oxidation potentials can be directly correlated to the ionization potentials of the materials. Adachi et al. proposed a linearity between the ionization potential and device lifetime and explains this with low initial driving voltages of devices incorporating easily ionizable hole transport materials.[29] Several groups demonstrated in experimental and theoretical investigations a linear dependence of the ionization potential and the Hammett parameter of the substituents attached to a triarylamine core structure,[30-32] giving way to a rational design of materials with appropriate ionization potentials.

1.4.2 DEGRADATION OF ELECTRON CONDUCTING MATERIALS

Almost all known hole transport materials are based on aromatic amines containing either triarylamine or carbazole moieties. For electron transport materials in contrast, a much wider structural diversity of materials is available. The employed materials range from phosphinoxides over a variety of nitrogen and oxygen containing heterocyles (oxadiazoles, triazines, pyridines, phenantrolines, benzimidazoles, etc.) and metal organic compounds to fully aromatic hydrocarbons. As a matter of course, there is not "one general" pathway explaining the chemical degradation behavior of electron conducting materials. We will start this section with a "bridge material", the ambipolar carbazole containing phosphine oxide CZPO2. This material exhibits both electron and hole conducting properties and follows, at least partly, the same exciton induced degradation pathway as the hole transporting materials. Quantum chemical calculations on CZPO2 by Chiu et al. revealed that the C-P bond dissociation energy is equal to that of C-N bonds, which enables the cleavage through the first singlet excited state **(Figure**

1-7).[33] This results in both, dissociation of the carbazole (discussed in the previous section) and the phosphinoxide unit from the benzene core. The main cause for a fast degradation compared to "pure" arylamines however, is the instability of the radical anion species formed through electron transport, resulting in the decrease of the C-P bond dissociation energy to almost half the original value. In contrast, the formation of the radical cation species of the carbazole unit leads to a stabilization of the C-N bond (about 10 kcal/mol). Therefore C-P bond containing materials might undergo bond cleavage not only, but also due to the presence of negative charge carriers.

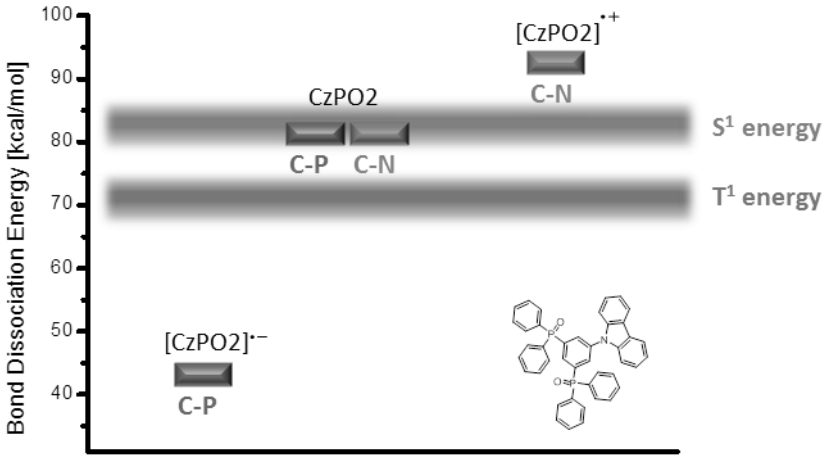

Figure 1-7: Dissociation energies of the differnet bond-types of the bipolar condcuting material CzPO2.

One important and well investigated class of fluorescent host and electron transporting materials are azaaromatic compounds, like quinolines (AlQ_3, $BAlQ_2$), phenanthrolines (BPhen) or benzimidazoles. Much effort has been spent so far on elucidating the degradation mechanism of these materials, especially of AlQ_3. Unipolar current devices of AlQ_3 as well as devices with tunable hole injection efficiency clearly indicated that hole injection in this material leads to device degradation.[34-36] Investigations by Papadimitrakopoulos et al., showing the irreversible oxidation behavior of AlQ_3 in cyclic voltammetry measurements,[37] are consistent with the thesis of the hole current induced formation of unstable cationic $AlQ_3^{\bullet+}$ species.[38-39] Scholz et al. assumed after LDI-TOF-MS measurements that excited AlQ_3 molecules undergo a reversible ligand-dissociation to AlQ_2^+ (Scheme 1-2).[40] While MS signals at 648 amu suggest the subsequent reaction of the cationic species with the adjacent hole blocking material BPhen (4,7-

di(phenyl)-1,10-phenanthroline), no information could be obtained whether a charge transfer species [AlQ_2+BPhen]$^+$ or even a coordinatively bound complex [AlQ_2BPhen]$^+$ is generated.[41] Initially assumed dimerization reactions of AlQ_3 to the charged $Al_2O_5^+$ species[40] turned out to occur exclusively at a very high density of excited molecules, like for example during the laser ionization process for mass spectrometric investigations and are therefore most likely no relevant degradation pathway in OLEDs.[41] The free chinoline ions, resulting from the dissociation process, can react to non-emissive, fluorescence quenching degradation products.[37, 40]

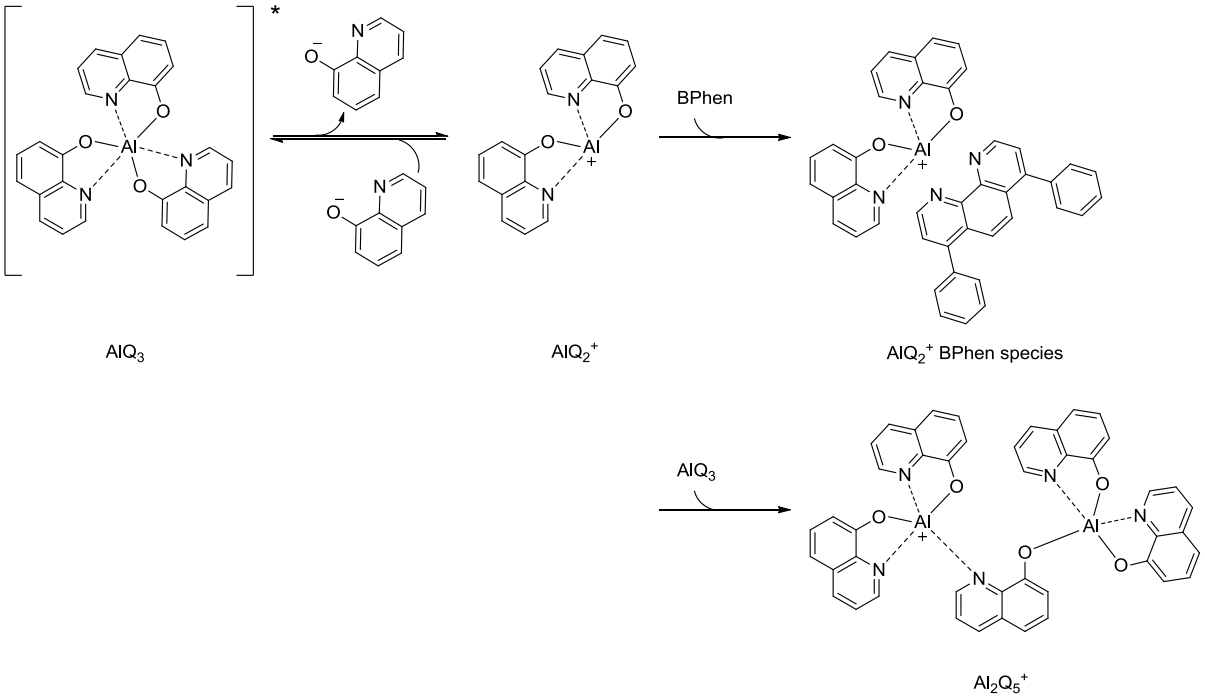

Scheme 1-2: Dissociation and degradation pathways of tris(8-hydroxy-quinolinato)aluminium AlQ_3.

Later on the destructive role of hole accumulation at the layer-interface was qualified, realizing that high electron density in the AlQ_3 layer causes similar irreversible luminescence efficiency loss in the device. It is assumed that electron traps of still unknown nature (chemical degradation is suggested) with a luminance efficiency of < 1 % compared to AlQ_3 are formed near the interface.[35, 42]

As quenching sites prevent emission from a large number of molecules surrounding them, it is obvious that even a relatively small amount of degraded AlQ_3 molecules has a pronounced effect on the quantum efficiency of the whole device. Hence it is imperative to prevent accumulation of charges (both electrons and holes) in or at the interface of the AlQ_3 layer. As it is known that the

transit time of holes through the HTL is up to 3 orders of magnitude faster than for the electrons through AlQ_3,[43-44] it is important to finetune the balance between electron and hole injection and mobility. Using hole transport materials with low ionization potentials is only one example, which can improve device stability. The resulting energy barrier between the HTL and the AlQ_3 layer impedes the hole injection in the latter.[29, 38] This reduces hole induced AlQ_3 degradation. A complementary route to enhance the device durability is to improve electron mobility. This was for example achieved by doping AlQ_3 with materials like $BAlQ_2$[45] or BPhen.[45-46]

Investigations of the hole blocking and electron transport material BPhen showed besides faster electron transit properties compared to AlQ_3 some drawbacks concerning the chemical stability in stressed devices. Dimerization as well as trimerization of BPhen molecules (Scheme 1-3) could be observed, leading to charge traps in the form of charged and neutral oligomers at the EML/HBL interface.[24, 40] These products can generally be ascribed to nucleophilic reactions of the lone electron pair of the sp^2-hybridized nitrogen atom of an azaaromatic compound with an adjacent radical cationic species.[36] BPhen degradation seems to be dependent on the total charge passing through the device and occurs mainly at high voltages.[47] BCP generally shows a higher stability compared to BPhen, as dimer formation could only be observed to a lower extent and trimer formation not at all.[40] This can be explained by the sterical hindrance of the methyl groups in the 2-positions of BCP, which leads to the conclusion that the introduction of bulkier substituents can improve the stability of the phenanthroline materials by shielding the sp^2-nitrogens and impede interaction with reactive species in the vicinity. In phosphorescent OLED devices BPhen can also form adducts with emitter fragments (see emitter section).[48-49] Both degradation pathways can result in the formation of gap states for charge carriers and excitons, causing significant luminance loss. Interestingly, complexation reactions of BPhen with the cathode materials Ag or Cs[41, 47, 50] are highly desired as an emerging interlayer, formed at the ETL/cathode interface during the evaporation of the cathode material, acts as a doped injection layer, enhancing electron injection into the ETL.[50]

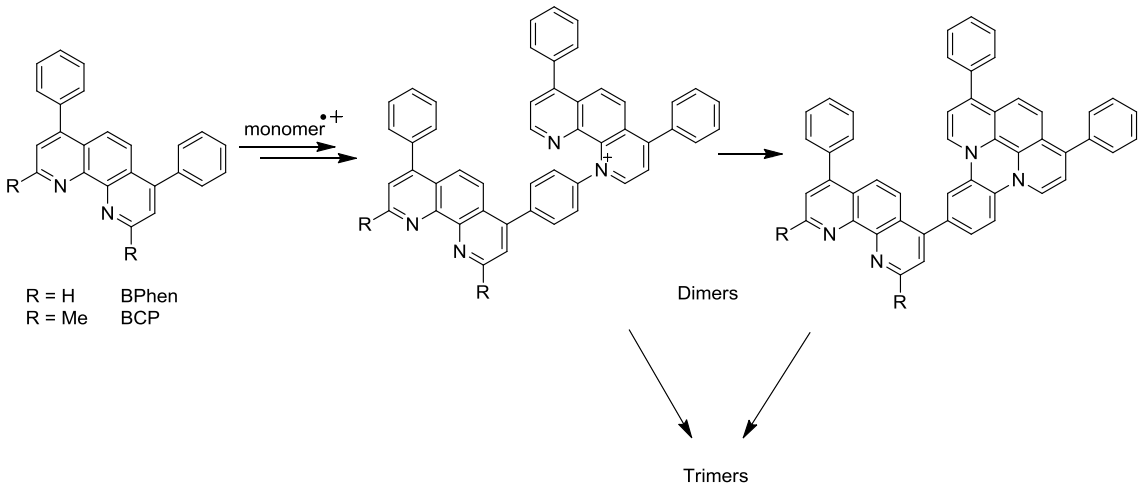

Scheme 1-3: Oligomerization reactons of the phenantroline based electron transporters.

With the electron transport material $BAlQ_2$ instead of BPhen, device lifetime can be improved significantly.[51] Compared to BPhen, $BAlQ_2$ seems to exhibits better chemical stability as no coordination products with phosphorescent emitters could be identified so far. Initially, this molecule was also considered to be inert regarding self-dimerization.[40] But it turned out that it undergoes this degradation pathway as well:[47] the excited complex suffers dissociation of the phenylphenolate ligand (Scheme 1-4). The so formed $[Al(Me\text{-}Q)_2]^+$ species can either undergo a subsequent back-reaction or a coordination with another charged $BAlQ_2$ to the dimer $[BAlQ_2{+}Al(Me\text{-}Q)_2]^+$. De Moraes et al. found this degradation to be dependent on the current density and assumed it to be caused by bimolecular annihilation reactions (see 2nd section). [47] They also observed a direct correlation between dimer-formation and device lifetime.

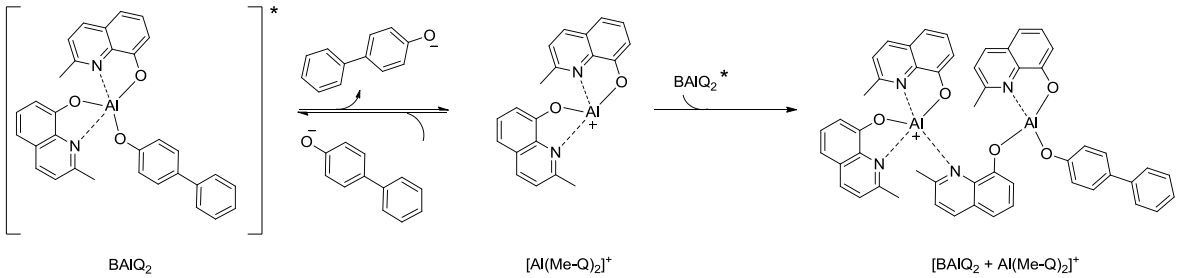

Scheme 1-4: Dissociation and dimerization reactions of the electron transport material $BAlQ_2$.

Fully aromatic hydrocarbons were always considered being favorable inert host materials as they lack –disadvantageous features like weak bonds (C-N, C-metal, N-metal, C-P) and highly reactive nucleophilic centers (lone pairs). Therefore homolytic bond dissociations and nucleophilic addition reactions are no critical issues for this class of host materials. But having a

very closer look at devices incorporating hydrocarbons like ADN and rubrene, respectively, Kondakov et al. noticed a slow but steady and irreversible decrease of these molecules in chromatography based analysis of photoexcited devices.[52] Degradation mechanisms comparable to those of the arylamines can be ruled out as the weakest covalent bond in ADN has a dissociation energy of ~ 120 kcal/mol. The S_1 state energy of about 70 kcal/mol is therefore too low for exctiton induced bond dissociation. Electron paramagnetic resonance (EPR) measurements nonetheless confirmed the generation of free spins during photoexcitation, formally carbon centered radicals. Oligomeric degradation products could be detected in significant amounts by gel permeation chromatography (GPC). It is assumed that the formation of these high-molecular-weight products takes place due to excited state reactions of adjacent molecules resulting in dehydrogenation reactions. Mass spectrometric investigations and additional comparison of the chromatographic retention times and absorption spectra with an authentic sample revealed the major low-molecular-mass product to be cADN (Scheme 1-5). The photocyclic ringclosing reaction of ADN to cADN is quite surprising as this reaction type commonly generates 6-membered-ring-derivatives. In contrast, 5-membered ring closure requires high-energy intermediates, formally biradicals. Quantum chemical calculations confirmed, in case of ADN, a stable biradical intermediate ADN••, which can trap both electrons and holes. Various hydrogen transfer reactions of this biradical with ion radicals or neutral adjacent molecules can occur to form neutral and charged radical species.[53] These can act as deep traps, non-radiative recombination centers and quenchers. Due to its absorpption properties and the negligible fluorescent quantum yield (< 1 %), the cyclization product cADN acts as an efficient fluorescence quencher.

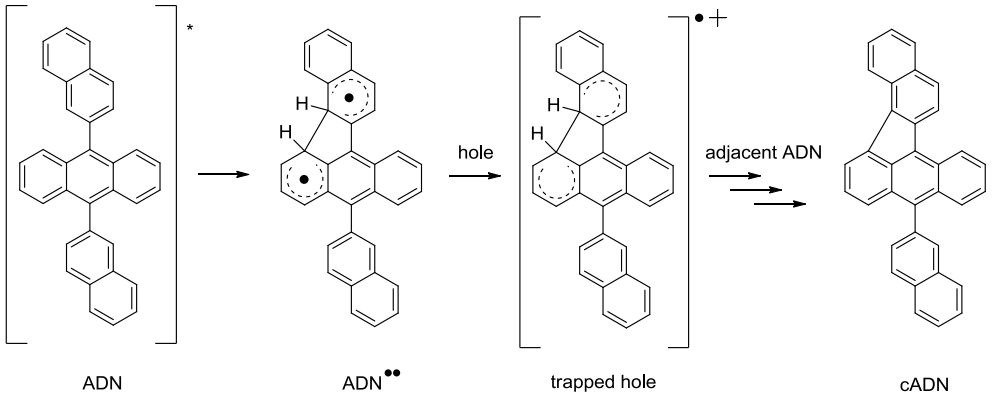

Scheme 1-5: Radical degradation pathway of ADN.

Compared to the transformation reactions of the arylamines, the quantum yields for photochemical degradation of the hydrocarbons are extremely low: it takes up to $1x10^{11}$ excitation events to degrade one single molecule of ADN.[52] Nonetheless, this minor degradation pathway also has a non-negligible influence on device stability. Further analysis of ADN and its *t*butyl substituted analogue TBADN by Wang et al. revealed the appearance of an "intermolecular species" during device operation which is assumed to contribute to the loss of color purity and efficiency.[54] The mechanism of the formation and the nature of this species could not be elucidated so far, but dimerization reactions or morphological changes due to aggregation are suggested. This species shows a characteristic bathocromically shifted emission compared to the original anthracen derivatives which results in increased emission in the green part of the spectrum. Furthermore this species is capable of charge trapping and energy quenching, causing the efficiency loss of aged devices. As this degradation phenomenon occurs through aggregation processes of the anthracenes and the color shift is more pronounced in the ADN devices, the introduction of sterically demanding groups could minimize this degradation pathway. In this study it was also shown that mixing the anthracene layer with CBP also inhibits the formation of these intermolecular species.

It can be concluded that the degradation behavior of electron conducting materials can be quite different: charge as well as exciton induced degradation was found for different types of compounds. And some degradation phenomena cannot be explained to date. In the case of dimerization and accumulation processes, the introduction of bulky groups seems to be a useful tool for prevention.

1.4.3 STRATEGIES FOR THE STABILITY IMPROVEMENT OF TRANSPORT MATERIALS

The degradation of transport materials can proceed via a variety of different pathways and can have different causes. Nevertheless, some common or reoccurring problems can be identified: The presence of "weak bonds" with dissociation energies close to the first excited state pose a problem concerning material stability: For many amine based hole transport materials as well as phosphine oxide electron transporters, the energy of the first singlet excited state lies within the same range as the energies of C-N, C-P, $C(sp^2)$-$C(sp^3)$ and $C(sp^3)$-$C(sp^3)$ bonds. This can lead to exciton induced bond rupture and subsequent reactions. Consequently, the bond strengths directly affect the stability of the molecule and hence the device lifetime. Overcoming this problem, at least to some extent, can be achieved by minimizing the number of weak bonds within the molecules. Rigidifying the molecular structure, for example via bridging neighboring

aryl moieties can reduce excited state initiated degradation reactions due to decreased rotational flexibility and is already considered a useful tool also to increase the thermal stability and decrease the oxidation potentials. The latter lead to a lower injection barrier at the anode/HTL interface, therefore to a reduced initial driving voltage. This principle of bridged molecules has also found entry to commercial applications (Figure 1-8).[55-58]

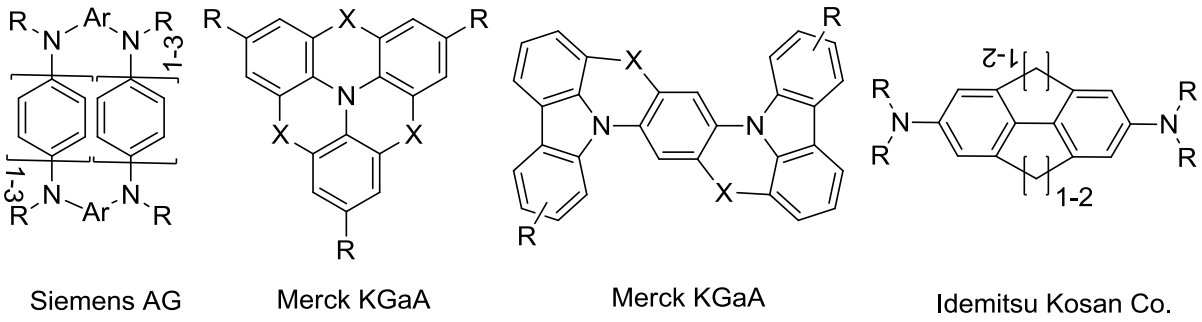

Figure 1-8: Examples for bridged aromatic amines used in commercial applications.

Another "weak link" was identified for N-heterocyclic materials. The nitrogen lone pair was found to contribute to degradation reactions resulting in oligomerization reactions with radical species or complexation with coordinatively unsaturated compounds. Shielding the sp^2-N with sterically demanding groups decreases the interactions of its lone pair with reactive intermediates. Thus the possibility of undergoing degrading reactions can be reduced drastically.

A parameter which used to influence device lifetime is the thermal stability of the materials. If the device operating heat or other heat treatments exceed the specific glass transition temperature T_g of the materials, interdiffusion between the organic layers as well as crystallization of the amorphous material can occur. Therefore molecules with high T_g values are very desirable. After enormous scientific research concerning this topic it is nowadays well understood how to tune the T_g simply by influencing the molecular structure:[59-60] high glass transition temperatures can be achieved by (i) increasing the number of π-electrons, (ii) introducing bulky, heavy and/or rigid moieties for enlarging the molecule and decreasing the rotational freedom and (iii) incorporating an intermolecular hydrogen bonding site for the formation of super molecular structures. These guidelines were applied to already known compounds with appropriate electronic and spectroscopic properties which are suffering

thermal lability (like TAD, TPD, AlQ_3) for the development of high thermally stable materials (Figure 1-9).

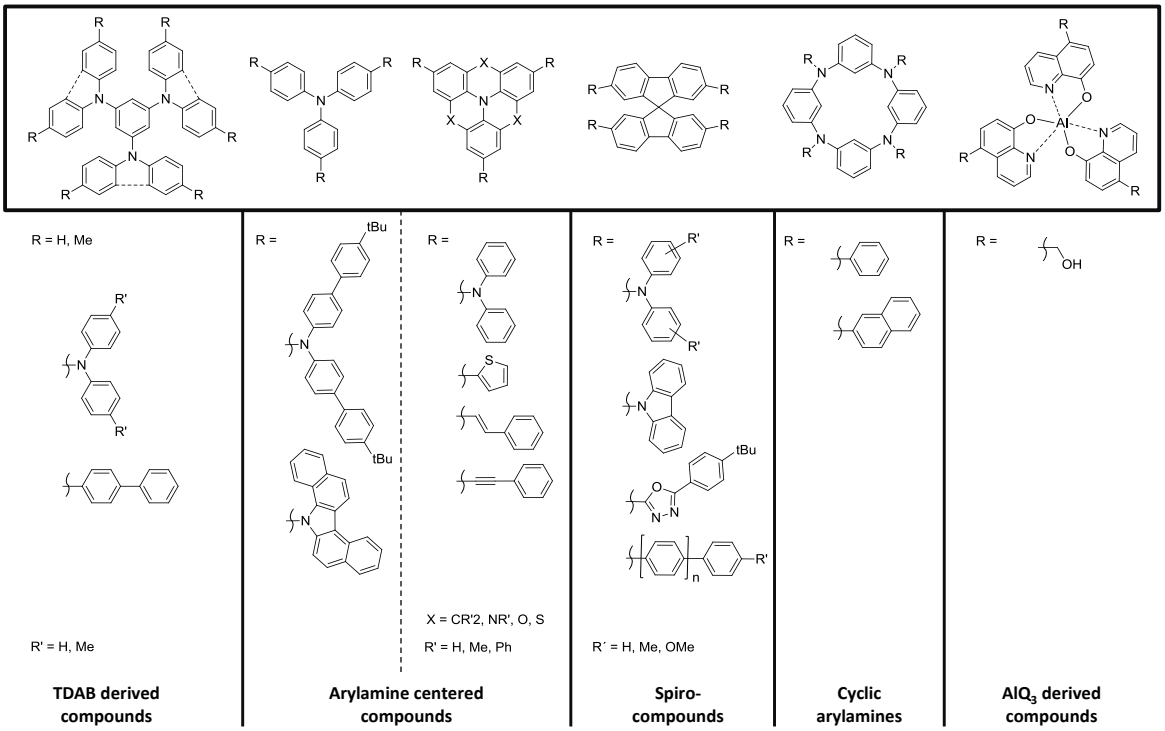

Figure 1-9. Some examples of thermally stable materials in OLED application: TDAB derived,[61-63] arylamine centered[56, 64-65] and spiro[66] compounds as well as cyclic arylamines[55, 67] and an AlQ_3 derivative.[68]

1.4.4 DEGRADATION OF PHOSPHORESCENT EMITTERS

Degradation products of transport and host materials can be a significant problem for the operational stability of OLEDs and the use of more robust materials can enhance the device lifetime. Nevertheless, the great impact that the type of phosphorescent dopant can often have on the device lifetimes, cannot be adequately explained by a deterioration of the host and transport materials alone. In fact, while investigating the degradation of CBP in OLEDs containing $Ir(ppy)_3$ Kondakov et al. noticed that the phosphorescent dopant is deteriorating even faster than other materials and reasoned that it might therefore play a significant role in the degradation of the investigated devices.[11]

In phosphorescent devices, charge carrier induced degradation might play a role for host as well as guest materials in the emitting layer – depending on the contribution of the dopant to electron or hole transport. Exciton induced direct degradation and especially bimolecular

annihilation reactions on the other hand are likely to be induced by guest (dopant) excitons since the excited state lifetimes of the phosphorescent metal-organic dopants is significantly longer (typically 0.5 - 5 μs)[69] than of the organic host materials. Recent investigations by Siboni and Aziz on triplet polaron annihilation furthermore indicated that positive charges (holes) located on the phosphorescent dopant are more efficient quenchers for triplet polaron annihilation than charges located on the host material for the same system. [10] This indicates the importance of the stability of the phosphorescent guest for the overall operational lifetime of the devices and explains the huge efforts that are currently being expended to develop stable phosphorescent emitters.

The analysis of chemical degradation mechanisms and products for these materials however proves to be significantly more difficult compared to other materials as the emitting layers typically contain only up to 15% of the phosphorescent dopants. Even though the low abundance of these species in the organic layers represents an additional challenge, there are a number of reports on the detection and structural identification of degradation products for phosphorescent emitters.

Direct LDI-MS analysis of driven devices, as developed and employed by Leo et al., for example proved to be a valuable tool for the investigation of these species. [24] By comparing the mass-spectra of pristine and driven phosphorescent devices they were able to demonstrate, that cyclometallated homo- and heteroleptic iridium emitters can undergo ligand dissociation reactions during device operation.[40, 70-72] A possible explanation for this degradation pathway is the thermal population of higher lying metal-centered states upon excitation. This phenomenon has been proven to be responsible for the temperature dependent emission quenching of a number of transition metal complexes at room temperature.[73-74] Spectroscopic investigations in correlation with DFT calculations for a number of green to blue emitting iridium compounds suggested that the thermal population of higher lying triplet metal centered states (^{3}MC, also called dd* or ligand field states) leads to the rupture of an Ir-N bond.[20, 75] The five coordinate species that is formed has been calculated to have a trigonal bipyramidal geometry with one ligand being monodentate after bond dissociation (Figure 1-10). This ligand showed a twisted geometry where the dihedral angle between the phenyl moiety and the heterocycle was > 50 °. At room temperature, these high energy states are thermally accessible only via the high excitation energies of blue emitting complexes while the activation energy is too high for green and red phosphorescent compounds. Nevertheless, it is conceivable that upon

exciton-exciton or exciton-polaron annihilation (see 2nd section) these states become accessible and therefore play a role in the degradation of these materials as well.

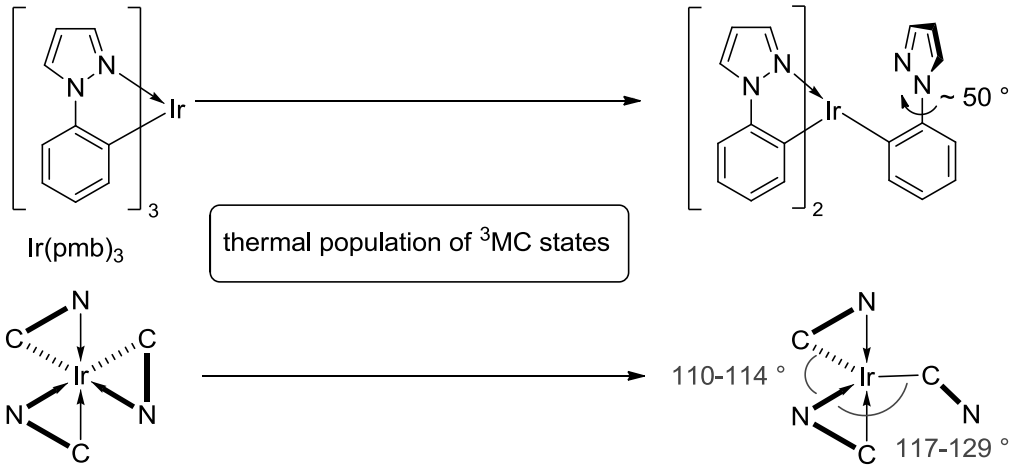

Figure 1-10: Bond rupture via the thermal poulation of higher lying ^{3}MC/dd* states .[20]

After excitation and thermal population of the ^{3}MC states, the partly dissociated ligand might fully dissociate to give a fragment of type $(C^N)_2Ir^+$ (Scheme 1-6). The weaker Ir-heteroatom bonds in ancillary ligands are more prone to bond rupture and thus can explain the often observed diminished stability of heteroleptic emitters compared to homoleptic ones in OLED devices. Recently, it was shown that the cleavage of N^O and O^O ancilliary ligands of iridium complexes can also be induced by the presence of protons. The authors reasoned that since protons can be present in devices, for example due to the use of PEDOT:PSS as hole injection material, acid induced degradation could also be one of the responsible mechanisms for the observed device degradation of heteroleptic emitters.[76]

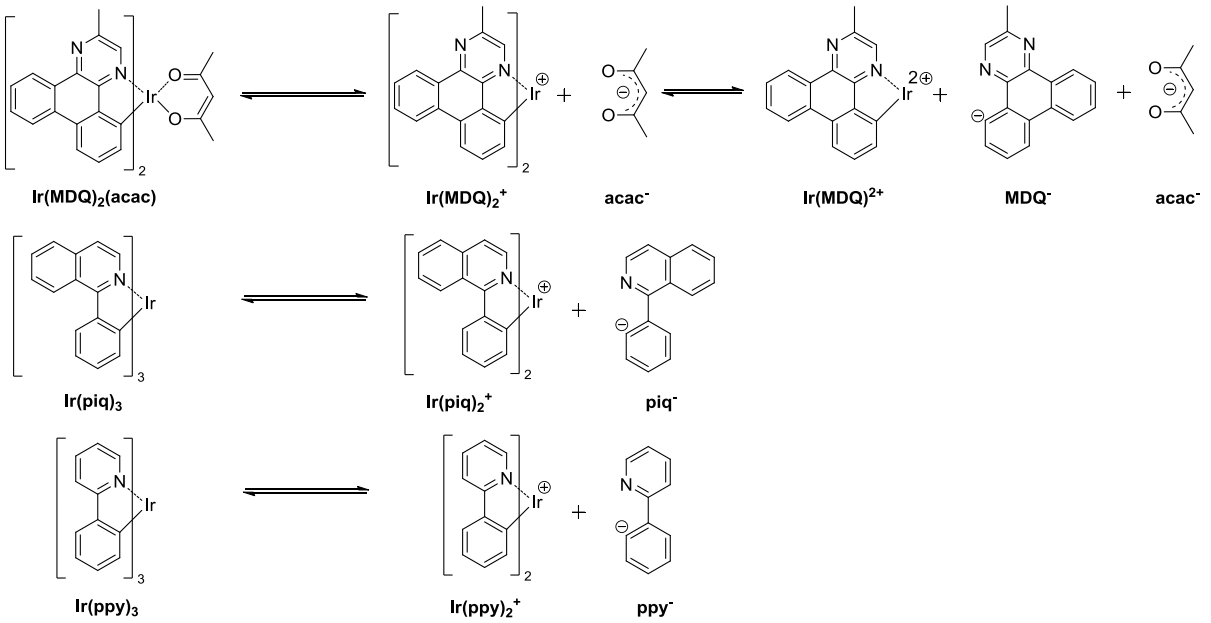

Scheme 1-6: Ligand disscoiation pathways for red and green phosphorescent iridium complexes.

While these dissociation processes should in principle be reversible, the resulting charged, coordinatively unsaturated fragments are likely to undergo further reactions with surrounding molecules. For a variety of different homo- and heteroleptic iridium emitters such as $Ir(MDQ)_2(acac)$, $Ir(piq)_3$, $Ir(ppy)_3$ and FIrpic, the complex fragments were shown to undergo reactions with molecules of the adjacent transport layers. For $Ir(MDQ)_2(acac)$ and $Ir(piq)_3$-based red phosphorescent OLEDs, the interaction strength between emitter fragments and different HBL materials (BPhen, TPBi, AlQ_3) correlated directly with the obtained device lifetimes.[51, 77] The stronger the interaction between the employed hole blocker and the dopant fragments, the lower was the operating stability of the corresponding devices. This emphasizes that OLED degradation and the stability of single components cannot be discussed without considering the chemical interactions between the different materials present in a device.

This ligand dissociation has been observed for dopants of different molecular structure and emission color in a variety of device structures and is backed by spectroscopic and quantum chemical investigations. It can therefore be considered a somewhat general pathway that might be responsible for the deterioration of phosphorescent dopants. Nevertheless, depending on the structure of the employed complexes there are multiple other possibilities for their degradation. Some groups or bonds of the dopants might be particularly prone to dissociation or bond rupture due to weaker bond strengths. However, the observed dissociation reactions cannot always be rationalized via bond dissociation energies. Especially interesting is the case of the sky blue phosphorescent emitter FIrpic: While highly efficient blue OLEDs could be achieved

with this emitter, its extremely low operational stability prevents its use for commercial applications. It was observed that in addition to the ligand dissociation processes known for other emitters, a loss of CO_2 from the picolinate ligand takes place (Scheme 1-7). This renders the dissociation step irreversible and could thus account for its exceptionally low stability in devices.[71] Furthermore, the cleavage of fluorine substituents upon thermal vapor deposition as well as through electrical aging was detected via the comparison of HPLC-MS data of unprocessed materials, pristine and driven devices (Scheme 1-7).[17] This dissociation of fluorine atoms could recently also be shown for another blue emitter (Fir6) and might provide an explanation for the often observed detrimental effect of fluorination on device lifetimes.[78] The exact mechanism of this fluorine cleavage nevertheless is still unknown. The carbon fluoride bond is one of the strongest single bonds known and an explanation via bond energies is therefore invalid in this case. It also remains unclear whether the reactions proceed via an ionic or a radical pathway and how the hydrodehalogenation takes place. Due to the detection of fluorinated degradation products of other materials in the examined devices, an exchange of the fluorine atoms between the emitter and neighboring molecules was suggested.

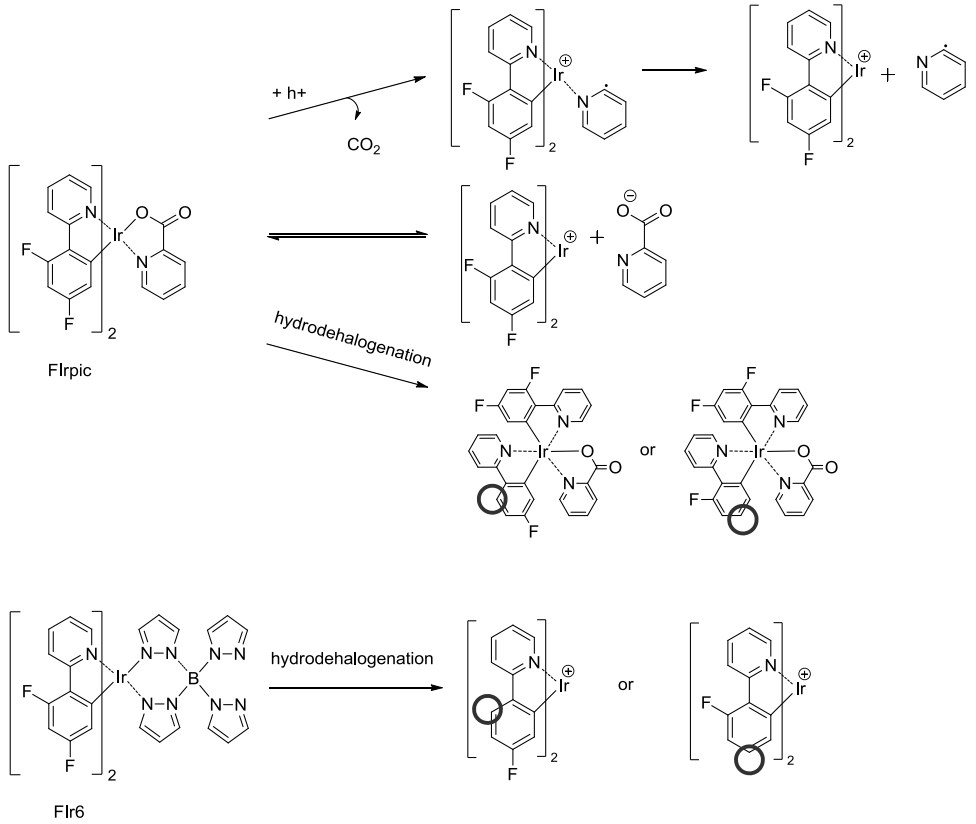

Scheme 1-7: Degradation products of blue phosphorescent emitters FIrpic and FIr6 as detected via LDI-TOF MS. The exact meachanism of the fluorine cleavage remains unclear.

An interesting example for the identification of problematic structural features was presented by UDC (Universal Display Corporation) who found that N-phenyl substituted phenylimidazole (pim) based blue emitters showed significantly enhanced lifetimes compared to the corresponding N-methyl substituted ones.[79] In order to rationalize this, Treboux et al. performed an analysis of the triplet potential energy surface of these compounds.[18] They calculated that a homolytic dissociation of the methyl group of $Ir(Me\text{-}pim)_3$ slightly stabilizes the excited complex and therefore presents a likely pathway for its faster degradation. The authors reason that since the excited state has significant MLCT character, the additional electron, transferred to the imidazole heterocycle upon exctitation, disrupts the aromaticity which can be regained by dissociation of the methyl radical. The dissociation of a phenyl radical from $Ir(Ph\text{-}pim)_3$ on the other hand would destabilize the complex and is therefore disfavored - accounting for the higher stability of this material (Figure 1-11).

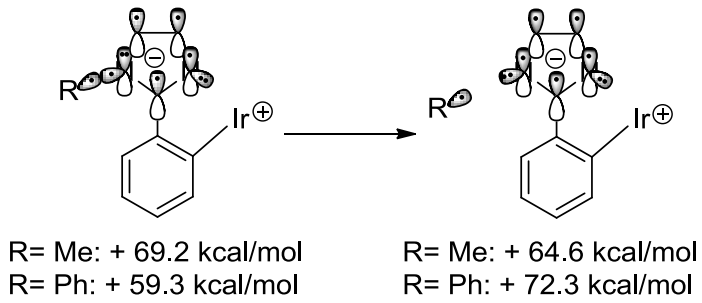

Figure 1-11: Schematic representation of the MLCT exctited states before and after dissociation of $Ir(Me\text{-}pim)_3$ and $Ir(Ph\text{-}pim)_3$ and corresponding calculated energies.[18-19]

One of the major challenges in the OLED field to date is still the development of a stable phosphorescent blue. While there has been considerable progress in the lifetime of blue emitters and materials with lifetimes of up to 20,000 h are now commercially available,[80] most of the more stable materials do not exhibit a deep blue color but rather show sky/light blue phosphorescence. Compared to lifetimes (LT_{50}) of several hundred thousand hours for red and green phosphorescence, there is still a significant improvement in the stability required. The difficulty in their development lies in the inherent properties of blue emitting materials. Their large band gap render their reduced or oxidized form a potent reductant or oxidant, respectively, and a variety of redox processes might be induced via these species. Furthermore, the higher excited state energies often increase the accessibility of higher lying electronic states leading to dissociation and bond rupture processes as already discussed above.

1.4.5 STRATEGIES FOR THE STABILITY IMPROVEMENT OF PHOSPHORESCENT DOPANTS

When designing new materials with enhanced stabilities to reduce degradation and improve operational device stabilities, there are a few possible approaches. One way is to eliminate or reinforce parts of the structure that are known to be susceptible to degradation. Methyl groups in phenylimidazole based complexes or fluorine substituents in the case of FIrpic or FIr6 are obvious examples for these approaches.

As degradation of the emitting layer often involves the participation of excitons, the exciton lifetime is likely to have a significant impact on the stability of the devices. The deactivation of excited states is always governed by a competition between the radiative decay and all non-radiative deactivation routes including possible exciton induced degradation pathways. A higher radiative rate (which at a given quantum yield corresponds to a shorter excited state lifetime) thus not only increases the external quantum efficiency of a device but also reduces the likelihood of direct degradation. Furthermore, a shorter excited state lifetime significantly reduces the exciton density in the emission layer and therefore the probability of bimolecular annihilation reactions leading to the deterioration of the materials. For an in depth discussion on on the triplet state photophysics of organo-transition metal compounds and strategies to obtain high radiative rates, the interested reader may be referred to recent excellent reviews on the subject by Yersin et al. and references therein.[69, 81]

Another promising handle to improve operational lifetimes is to reduce the probability of the ligand dissociation mechanism that has been discussed above. One strategy is to make the dissociative ^{3}MC states less accessible. The use of strongly coordinating ligands should raise the metal centered state energies and might thus decrease the rate of destructive deactivation. A promising approach for achieving blue phosphorescence while maintaining a sufficient energy gap between the emissive and the ^{3}MC-states are therefore Ir-carbene complexes. $Ir(pmb)_3$ for example exhibits a significantly higher ^{3}MC state energy (28 000 cm^{-1}) compared to complexes with C^N ligands (21 700 to 24 000 cm^{-1}).[20, 82]

Favoring the radiative decay over non-radiative, possibly destructive deactivation modes could also be achieved by limiting the freedom of the excited molecules to rearrange and thus preventing the dissociation of the metal-ligand bonds. Increased rigidity of the complexes can be achieved by bridging the two ring systems of the cyclometallating ligands as in $Ir(bzq)_3$ (Figure 1-12). Rigidified ligands are a reoccurring theme in patent literature, which shows that this approach is also being employed in industry.[83-85] Figure 1-12 illustrates some of the parent

structures of bridged green and blue emitting phosphorescent iridium complexes found in academic and patent literature.

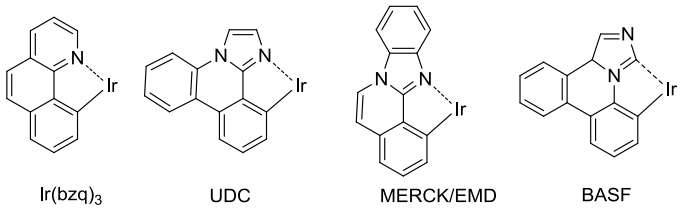

Figure 1-12: Structures of iridium complexes with rigidified ligands as found in academic and patent literature.[83-85]

Increasing the rigidity, raising the ligand field strength and thus the activation energy for quenching via the mentioned dd* states can also be achived by using higher dentate ligands. This effect has been shown to greatly enhance quantum yields in a variety of Pt complexes when going from bidentate to tri- or even tetra-dentate ligands.[86-88] In fact, it was recently reported that OLEDs incorporating a red phosphorescent tetradentate Pt complex could reach similar performance and lifetimes as ones with the Iridium based emitter $Ir(piq)_3$ in comparable device setups.[89]

Optimization of the emitter environment is another interesting approach to increase stability. It was found that the population of metal centered states can be reduced or suppressed by a rigid matrix and photoinitiated ligand dissociation reactions can be suppressed in certain cases.[69, 90] By optimizing interactions between the emitter and the host materials in order to provide a rigid environment, it might be possible to significantly reduce destructive deactivation of the excited states. Moreover, a careful selection of host materials might also prevent possible reactions between emitter and host molecules such as the adduct formation mentioned above. Researchers at Fujifilm utilized this strategy by screening the stability of different host:guest combinations under UV-irradiation and were thus able to significantly improve the operational stability of blue phosphorescent devices.[91]

1.5 CONCLUSIONS

In summary, we discussed the different chemical processes responsible for the intrinsic degradation of state-of-the-art organic light-emitting diodes. The initial step in the observed degradation reactions is often a bond dissociation process. This can be homo- or heterolytic, caused either by charge carriers, excitons or bimolecular annihilation reactions between two exctitons or excitons and polarons. The resulting species are highly reactive charged or radical fragments that can undergo further reactions with surrounding molecules and thus form charge traps or luminescent quenching sites.

The observed products, in combination with the results of quantum chemical calculations, shed light on the type of bonds, structural features or electronic states that are problematic with regard to chemical stability. The insights gained via the elucidation of these reaction pathways have direct implications for the design of new materials. Some promising approaches such as rigidification, shielding of potentially reactive moieties or tuning of energy levels to limit accessibility of certain electronic states have already been employed. The investigations also clearly show that the interactions between different materials can be of utmost importance and should be taken into consideration when trying to improve operational stabilities. An interesting example is the degradation of red phosphorescent devices containing $Ir(piq)_3$ or $Ir(MDQ)_2(acac)$ where the stability of the phosphorescent dopant seems to depend heavily on the employed hole blocking material.

Even though some of the reaction pathways could be resolved for certain materials commonly used in OLEDs, chemical degradation is a complex subject. To gain deeper insights into the processes for different types of materials, a combined effort of physicists, engineers, analytical and theoretical chemists will be required. In depth knowledge of these processes will eventually enable to overcome the shortcomings and limitations of present materials to realize highly efficient and stable organic light emitting diodes.

1.6 REFERENCES

[1] M. Pope, H. P. Kallmann, P. Magnante, *J. Chem. Phys.* **1963**, *38*, 2042-2043.
[2] C. W. Tang, S. A. VanSlyke, *Appl. Phys. Lett.* **1987**, *51*, 913-915.
[3] M. A. Baldo, D. F. O'Brien, Y. You, A. Shoustikov, S. Sibley, M. E. Thompson, S. R. Forrest, *Nature* **1998**, *395*, 151-154.
[4] N. C. Giebink, B. W. D'Andrade, M. S. Weaver, P. B. Mackenzie, J. J. Brown, M. E. Thompson, S. R. Forrest, *J. Appl. Phys.* **2008**, *103*, 044509.
[5] J. Kalinowski, W. Stampor, J. Mężyk, M. Cocchi, D. Virgili, V. Fattori, P. Di Marco, *Phys. Rev. B* **2002**, *66*, 235321.
[6] M. A. Baldo, S. R. Forrest, *Phys. Rev. B* **2000**, *62*, 10958-10966.
[7] M. A. Baldo, C. Adachi, S. R. Forrest, *Phys. Rev. B* **2000**, *62*, 10967-10977.
[8] N. Nakashima, K. Yoshihara, *J. Phys. Chem.* **1989**, *93*, 7763-7771.
[9] N. C. Giebink, B. W. D'Andrade, M. S. Weaver, J. J. Brown, S. R. Forrest, *J. Appl. Phys.* **2009**, *105*, 124514.
[10] H. Z. Siboni, H. Aziz, *Appl. Phys. Lett.* **2012**, *101*, 063502-063504.
[11] D. Y. Kondakov, W. C. Lenhart, W. F. Nichols, *J. Appl. Phys.* **2007**, *101*, 024512-024517.
[12] V. Jankus, C. Winscom, A. P. Monkman, *J. Chem. Phys.* **2009**, *130*, 074501.
[13] C. Y. Kwong, A. B. Djurišić, W. C. H. Choy, D. Li, M. H. Xie, W. K. Chan, K. W. Cheah, P. T. Lai, P. C. Chui, *Materials Science and Engineering: B* **2005**, *116*, 75-81.
[14] D. Y. Kondakov, T. D. Pawlik, W. F. Nichols, W. C. Lenhart, *Journal of the Society for Information Display* **2008**, *16*, 37-46.
[15] V. Jankus, C. Winscom, A. P. Monkman, *J. Chem. Phys.* **2009**, *130*, 074501.
[16] V. Sivasubramaniam, F. Brodkorb, S. Hanning, O. Buttler, H. P. Loebl, V. van Elsbergen, H. Boerner, U. Scherf, M. Kreyenschmidt, *Solid State Sci.* **2009**, *11*, 1933-1940.
[17] V. Sivasubramaniam, F. Brodkorb, S. Hanning, H. P. Loebl, V. van Elsbergen, H. Boerner, U. Scherf, M. Kreyenschmidt, *J. Fluorine Chem.* **2009**, *130*, 640-649.
[18] G. Treboux, J. Mizukami, M. Yabe, S. Nakamura, *J. Photopolym. Sci. Technol.* **2008**, *21*, 347-348.
[19] G. Treboux, J. Mizukami, M. Yabe, S. Nakamura, *Chem. Lett.* **2007**, *36*, 1344-1345.
[20] T. Sajoto, P. I. Djurovich, A. B. Tamayo, J. Oxgaard, W. A. Goddard, M. E. Thompson, *J. Am. Chem. Soc.* **2009**, *131*, 9813-9822.
[21] D. Y. Kondakov, C. T. Brown, T. D. Pawlik, V. V. Jarikov, *J. Appl. Phys.* **2010**, *107*, 024507.
[22] D. Y. Kondakov, *J. Appl. Phys.* **2008**, *104*, 084520.
[23] D. Y. Kondakov, *J. Appl. Phys.* **2008**, *104*, 084520-084529.
[24] S. Scholz, K. Walzer, K. Leo, *Adv. Funct. Mater.* **2008**, *18*, 2541-2547.
[25] V. Sivasubramaniam, *Dissertation* **2010**.
[26] S. Scholz, R. Meerheim, B. Lussem, K. Leo, *Appl. Phys. Lett.* **2009**, *94*, 043314-043313.
[27] A. Choi, T. Yamaguchi, C.-H. Han, *Res. Chem. Intermed.*, 1-9.
[28] P. J. Low, M. A. J. Paterson, D. S. Yufit, J. A. K. Howard, J. C. Cherryman, D. R. Tackley, R. Brook, B. Brown, *J. Mater. Chem.* **2005**, *15*, 2304-2315.
[29] C. Adachi, K. Nagai, N. Tamoto, *App. Phys. Lett.* **1995**, *66*, 2679-2681.
[30] S. O. Okutsu, T.; Tamano, M.; Enokida, T., *IEEE Trans. Electron Dev.* **1997**, *44*, 1302-1306.
[31] J.-H. Pan, H.-L. Chiu, L. Chen, B.-C. Wang, *Comp. Mater. Sci.* **2006**, *38*, 105-112.
[32] J. Pan, Y. Chou, H. Chiu, B. Wang, *Aust. J. Chem.* **2009**, *62*, 483-492.
[33] N. Lin, J. Qiao, L. Duan, H. Li, L. Wang, Y. Qiu, *J. Phys. Chem. C* **2012**, *116*, 19451-19457.
[34] Z. D. Popovic, H. Aziz, N.-X. Hu, A.-M. Hor, G. Xu, *Synth. Met.* **2000**, *111–112*, 229-232.
[35] Y. Luo, H. Aziz, G. Xu, Z. D. Popovic, *Chem. Mater.* **2007**, *19*, 2079-2083.
[36] V. V. Jarikov, D. Y. Kondakov, *J. Appl. Phys.* **2009**, *105*, 034905-034908.

[37] F. Papadimitrakopoulos, X. M. Zhang, D. L. Thomsen, K. A. Higginson, *Chem. Mater.* **1996**, *8*, 1363-1365.
[38] H. P. Aziz, Z. D.; Hu, N.-X.; Hor, A.-M.; Xu, G., *Science* **1999**, *283*, 1900-1902.
[39] Z. D. Popovic, H. Aziz, A. Ioannidis, N.-X. Hu, P. N. M. dos Anjos, *Synth. Met.* **2001**, *123*, 179-181.
[40] S. Scholz, C. Corten, K. Walzer, D. Kuckling, K. Leo, *Org. Electr.* **2007**, *8*, 709-717.
[41] S. Scholz, B. Lussem, K. Leo, *Appl.Phys. Lett.* **2009**, *95*, 183309-183303.
[42] D. Y. Kondakov, *J. Appl. Phys.* **2005**, *97*, 024503-024505.
[43] S. C. Tse, H. H. Fong, S. K. So, *J. Appl. Phys.* **2003**, *94*, 2033-2037.
[44] T.-Y. Chu, Y.-H. Lee, O.-K. Song, *App. Phys. Lett.* **2007**, *91*, 223509-223503.
[45] R. Meerheim, S. Scholz, G. Schwartz, S. Reineke, S. Olthof, K. Walzer, K. Leo, Proc. SPIE. **2008**, *6999*, 699917-1 - 699917-9.
[46] H. H. Fong, W. C. H. Choy, K. N. Hui, Y. J. Liang, *Appl. Phys. Lett.* **2006**, *88*, 113510-113513.
[47] I. R. de Moraes, S. Scholz, B. Lüssem, K. Leo, *Org. Electr.* **2012**, *13*, 1900-1907.
[48] S. Scholz, R. Meerheim, K. Walzer, K. Leo, *SID Symp. Digest Thech. Pap*., **2008**, 69991B-69991B.
[49] I. R. de Moraes, S. Scholz, B. Lussem, K. Leo, *Appl. Phys. Lett.* **2011**, *99*, 053302-053303.
[50] S. Scholz, Q. Huang, M. Thomschke, S. Olthof, P. Sebastian, K. Walzer, K. Leo, S. Oswald, C. Corten, D. Kuckling, *J. Appl. Phys.* **2008**, *104*, 104502-104510.
[51] R. Meerheim, S. Scholz, S. Olthof, G. Schwartz, S. Reineke, K. Walzer, K. Leo, *J. Appl. Phys.* **2008**, *104*, 014510-014518.
[52] D. Y. Kondakov, C. T. Brown, T. D. Pawlik, V. V. Jarikov, *J. Appl. Phys.* **2010**, *107*, 024507-024508.
[53] D. Y. Kondakov, C. T. Brown, T. D. Pawlik, *SID Symp. Digest Tech. Pap.* **2010**, *41*, 43-46.
[54] Q. Wang, Y. Luo, H. Aziz, *J. Appl. Phys.* **2010**, *107*, 084506-084506.
[55] A. M. Kanitz, Georg, Felix; Nuyken, Oskar; Simmerer, Jürgen., *Patent,* Siemens AG, **2001**.
[56] A. V. Parham, Horst; Heun, Susanne, Heil, Holger; Stößel, Philipp; Fortte, Rocco, *Patent* Merck Patent GmbH, **2007**.
[57] A. H. P. Parham, *Patent,* Merck Patent GmbH, **2011**.
[58] C. F. Hosokawa, Masakazu., *Patent,* Idemitsu Kosan Co., **2001**.
[59] Y. Shirota, *J. Mater. Chem.* **2000**, *10*, 1-25.
[60] L. S. Hung, C. H. Chen, *Mater. Sci. Eng. R.* **2002**, *39*, 143-222.
[61] K. Katsuma, Y. Shirota, *Adv. Mater.* **1998**, *10*, 223-226.
[62] W. Ishikawa, K. Noguchi, Y. Kuwabaru, Y. Shirota, *Adv. Mater.* **1993**, *5*, 559-561.
[63] P. Kundu, K. R. Justin Thomas, J. T. Lin, Y. T. Tao, C. H. Chien, *Adv. Funct. Mater.* **2003**, *13*, 445-452.
[64] H. Ogawa, H. Inada, Y. Shirota, *Macromol. Symp.* **1998**, *125*, 171-180.
[65] J. P. Chen, H. Tanabe, X.-C. Li, T. Thoms, Y. Okamura, K. Ueno, *Synth. Met.* **2003**, *132*, 173-176.
[66] J. Salbeck, N. Yu, J. Bauer, F. Weissörtel, H. Bestgen, *Synth. Met.* **1997**, *91*, 209-215.
[67] M. Xu, C. Yi, C.-J. Yang, J.-H. Wang, Y.-Z. Liu, B. Xie, X.-C. Gao, P. Wang, D.-C. Zou, *Thin Solid Films* **2008**, *516*, 7720-7726.
[68] S. Yin, Y. Hua, X. Chen, X. Yang, Y. Hou, X. Xu, *Synth.Met.* **2000**, *111–112*, 109-112.
[69] H. Yersin, A. F. Rausch, R. Czerwieniec, T. Hofbeck, T. Fischer, *Coord. Chem. Rev.* **2011**, *255*, 2622-2652.
[70] I. R. de Moraes, S. Scholz, B. r. Lüssem, K. Leo, *Appl. Phys. Lett.* **2011**, *99*, 053302.
[71] I. R. d. Moraes, S. Scholz, B. Lüssem, K. Leo, *Org. Electr.* **2011**, *12*, 341-347.
[72] S. Scholz, R. Meerheim, B. Lussem, K. Leo, *Appl. Phys. Lett.* **2009**, *94*, 043314.
[73] F. Barigelletti, D. Sandrini, M. Maestri, V. Balzani, A. Von Zelewsky, L. Chassot, P. Jolliet, U. Maeder, *Inorg. Chem.* **1988**, *27*, 3644-3647.

[74] A. Islam, N. Ikeda, K. Nozaki, Y. Okamoto, B. Gholamkhass, A. Yoshimura, T. Ohno, *Coord. Chem. Rev.* **1998**, *171*, 355-363.
[75] L. Yang, F. Okuda, K. Kobayashi, K. Nozaki, Y. Tanabe, Y. Ishii, M.-a. Haga, *Inorg. Chem.* **2008**, *47*, 7154-7165.
[76] E. Baranoff, B. F. E. Curchod, J. Frey, R. Scopelliti, F. Kessler, I. Tavernelli, U. Rothlisberger, M. Grätzel, M. K. Nazeeruddin, *Inorg. Chem.* **2011**, *51*, 215-224.
[77] S. Scholz, R. Meerheim, B. Lüssem, K. Leo, *SID Symp. Digest Tech. Pap.* **2009**, *40*, 681-684.
[78] R. Seifert, I. R. de Moraes, S. Scholz, M. C. Gather, B. Lüssem, K. Leo, *Org. Electr*.
[79] C. Lin, P. B. Mackenzie, R. Walters, J.-Y. Tsai, C. S. Brown, J. Deng, *Patent,* Universal Display Coorporation, **2006**.
[80]
[81] H. Yersin, A. F. Rausch, R. Czerwieniec, in *Physics of Organic Semiconductors* (Eds.: C. Adachi, R. Holmes, W. Bruetting), Wiley-VCH, **2012**, p. 371.
[82] R. J. Holmes, S. R. Forrest, T. Sajoto, A. Tamayo, P. I. Djurovich, M. E. Thompson, J. Brooks, Y. J. Tung, B. W. D'Andrade, M. S. Weaver, R. C. Kwong, J. J. Brown, *Appl. Phys. Lett.* **2005**, *87*, 243507-243503.
[83] D. B. Knowles, C. Lin, P. B. Mackenzie, J.-Y. Tsai, R. Walters, S. A. Beers, C. S. Brown, W. H. Yeager, E. Barron, Universal Display Coorporation, **2008**.
[84] P. Stoessel, H. Heil, D. Joosten, C. Pflumm, A. Gerhard, E. Breuning, *Patent,* Merck Patent GMBH, **2010**.
[85] O. Molt, C. Lennartz, E. Fuchs, K. Kahle, N. Langer, C. Schildknecht, J. Rudolph, G. Wagenblast, S. Watanabe, *Patent,* BASF SE, **2009**.
[86] A. F. Rausch, L. Murphy, J. A. G. Williams, H. Yersin, *Inorg. Chem.* **2011**, *51*, 312-319.
[87] D. A. K. Vezzu, J. C. Deaton, J. S. Jones, L. Bartolotti, C. F. Harris, A. P. Marchetti, M. Kondakova, R. D. Pike, S. Huo, *Inorg. Chem.* **2010**, *49*, 5107-5119.
[88] D. Ravindranathan, D. A. K. Vezzu, L. Bartolotti, P. D. Boyle, S. Huo, *Inorg. Chem.* **2010**, *49*, 8922-8928.
[89] H. Fukagawa, T. Shimizu, H. Hanashima, Y. Osada, M. Suzuki, H. Fujikake, *Adv. Mater.* **2012**, *24*, 5099-5103.
[90] D. W. Thompson, C. N. Fleming, B. D. Myron, T. J. Meyer, *J. Phys. Chem. B* **2007**, *111*, 6930-6941.
[91] W. Sotoyama, T. Satoh, M. Kinoshita, M. Tobise, K. Kawato, T. Ise, H. Takizawa, S. Yamashita, *Fujifilm Research and Development* **2010**, *No.055*, 24-28.

CHAPTER 2

2. RAPID COMBINATORIAL SYNTHESIS AND CHROMATOGRAPHY BASED SCREENING OF PHOSPHORESCENT IRIDIUM COMPLEXES FOR SOLUTION PROCESSING*

* This chapter was published as: Hohenleutner, A., Schmidbauer, S., Vasold, R., Joosten, D., Stoessel, P., Buchholz, H. and König, B. Rapid Combinatorial Synthesis and Chromatography Based Screening of Phosphorescent Iridium Complexes for Solution Processing. *Adv. Funct. Mater.* **2012,** *22,* 3406–3413. AH and SS contributed equally to this work.

2.1 INTRODUCTION

Iridium complexes have been employed as dyes for biological labeling[1-3] and sensing of different analytes,[4-5] as photon upconversion agents,[6-7] dyes for dye-sensitized solar cells (DSSCs),[8] photocatalysts for CO_2 reduction and water splitting[9-12] and more recently as efficient catalysts in the emerging field of organo photoredox catalysis.[13-15] While their unique properties make them promising candidates in all of the above mentioned areas, their current most important application is their use as emitters in organic light-emitting devices (OLEDs). Spurred by the discovery of the triplet harvesting effect by Forrest et al. in 1998,[16] enabling a theoretical internal quantum efficiency of 100 %, the number of reported phosphorescent iridium complexes has grown significantly over the last decade. The preference of cyclometallated iridium complexes for OLED applications can be rationalized by their extremely high triplet quantum yields,[17-18] the predictability and tunability of their emission color over the whole visible spectrum, good thermal and photo-stability compared to other transition metal complexes as well as their good synthetic accessibility.[19-21] For OLEDs produced via thermal vapor deposition, the excellent performance of these devices has already allowed the technology to enter mass production. However, there are still important challenges to be met. Even though there has been substantial progress in improving the operational lifetime of phosphorescent emitters, further improvement in the stability of these materials is highly desirable to obtain highly efficient and long term stable devices. To realize large area display and lighting applications at a competitive price, it is furthermore of interest to develop materials with sufficient solubility in suitable solvents to enable processing from solution for example via ink jet printing.

While modern computational methods can provide reliable information on the emission colors and energy,[22-26] the colour purity and in particular the stability of the iridium complexes cannot be predicted in such a straightforward fashion. To deepen the understanding of these compounds and gain insight into structure-property relationships concerning those essential criteria, it is still necessary to synthesize and characterize a large number of compounds.

While combinatorial chemistry is a well-established tool for the rapid synthesis of potential biologically active molecules[27] or catalysts[28] there have been surprisingly few reports of combinatorial methods for the synthesis and screening of new phosphorescent emitters for OLEDs. Bernhard et al. reported the parallel synthesis of a number of iridium complexes and the screening of their photophysical properties directly from the reaction mixture, omitting any

purification steps.[26] In 2006, Li et al. synthesized a library of iridium complexes by parallel solid phase synthesis and identified possible hits via their "on bead" emission.[29] Recently then, Nazeeruddin et al. prepared a library of 90 heteroleptic complexes via a similar approach as Bernhard's with a slightly modified procedure at room temperature.[30] However, as the purity of materials is absolutely vital for the operational device lifetime, the laborious, time consuming and therefore expensive purification of potential new emitters is still inevitable to obtain information about the stability of those compounds. Since the rapid purification of combinatorial libraries via chromatographic methods is a well established technique in pharmaceutical industry,[31-33] we have developed a screening for phosphorescent iridium complexes based on this methodology. Having a small amount of the purified compounds available, we can determine the photophysical properties of the new compounds and initially assess their stability under continuous excitation.

2.2 RESULTS AND DISCUSSION

2.2.1 Synthesis

To develop the combinatorial synthesis and screening we chose to focus on structures derived from the epitomal $Ir(ppy)_3$ which despite being one of the first reported[34-35] phosphorescent emitters remains to be the one of the most efficient and widely used dopants for phosphorescent OLEDs to date.[36] Incorporation of suitable dendritic structures at the periphery of an emitter is known to give special benefits to the original phosphorescent emitter: self quenching can be suppressed via simple shielding of the emissive core by branched side chains. Following this strategy, high solid state quantum efficiencies were obtained using ethylhexyloxy chains as dendritic structures.[19] However, this benefit was limited by the fact that charge-carrier mobility and glass transition temperature T_g may be decreased. These drawbacks could be eliminated using arylated dendrons.[37-39] Another advantage using these structures is the enhanced solubility for a better compatibility regarding solution processing. Utilizing palladium mediated C-C and C-N coupling reactions (Buchwald-Hartwig and Suzuki-Miyaura respectively), arylated dendritic structures can be attached to the emitting iridium core starting from the Br-functionalized $Ir(ppy)_3$ derivative **1**[40] in order to obtain efficient and soluble phosphorescent emitters in excellent yields and purity.[41-43] The method is particularly advantageous for a combinatorial approach, as the introduction of structural diversity takes place in the last step of the synthesis. The time consuming preparation and purification of a

variety of ligands can thus be avoided as boronic acids and diarylamines are widely available from commercial suppliers. Utilizing this post modification procedure, we synthesized 4 libraries, two of them via a Buchwald-Hartwig protocol and two via Suzuki-Miyaura reactions (Scheme 2-1). For each of the libraries we combined precursor **1** with three different amines/boronic acids in a one-pot reaction, giving way to a total of 10 possible products per reaction.

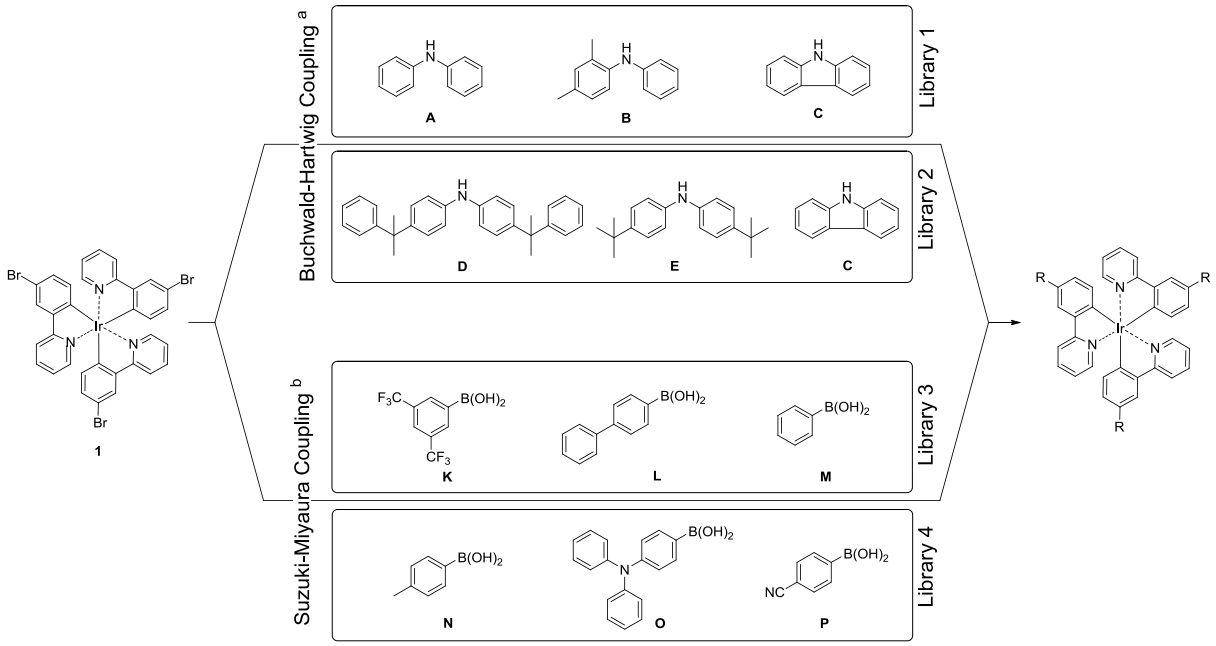

Scheme 2-1: Synthesis of libraries 1-4. Reaction conditions: a) $Pd(OAc)_2$, $P(^tBu)_3$, NaO^tBu, toluene/dioxane, 130 °C, 4 h. b) $Pd(OAc)_2$, P(o-tolyl)$_3$, K_3PO_4, toluene/dioxane/water, 85 °C, 10 h.

Scheme 2-1 exemplarily shows the synthesis of library 3 with all possible products. We assigned a letter to each of the coupling partners, so that all compounds prepared via the combinatorial approach can be described by a three letter code - each letter representing one introduced substituent. **MMM** for example is the compound where all three bromine functionalities have been replaced by a phenyl group via the Suzuki coupling with phenylboronic acid **M**. This combinatorial strategy facilitates the rapid generation of a large number of structurally diverse compounds as it enables the synthesis of up to 10 products with only one reaction to be performed. As a control, we synthesized and characterized several homoleptic reference complexes via conventional reactions. Their absorption and emission spectra were recorded and showed excellent agreement with the ones obtained from the combinatorial synthesis and screening.

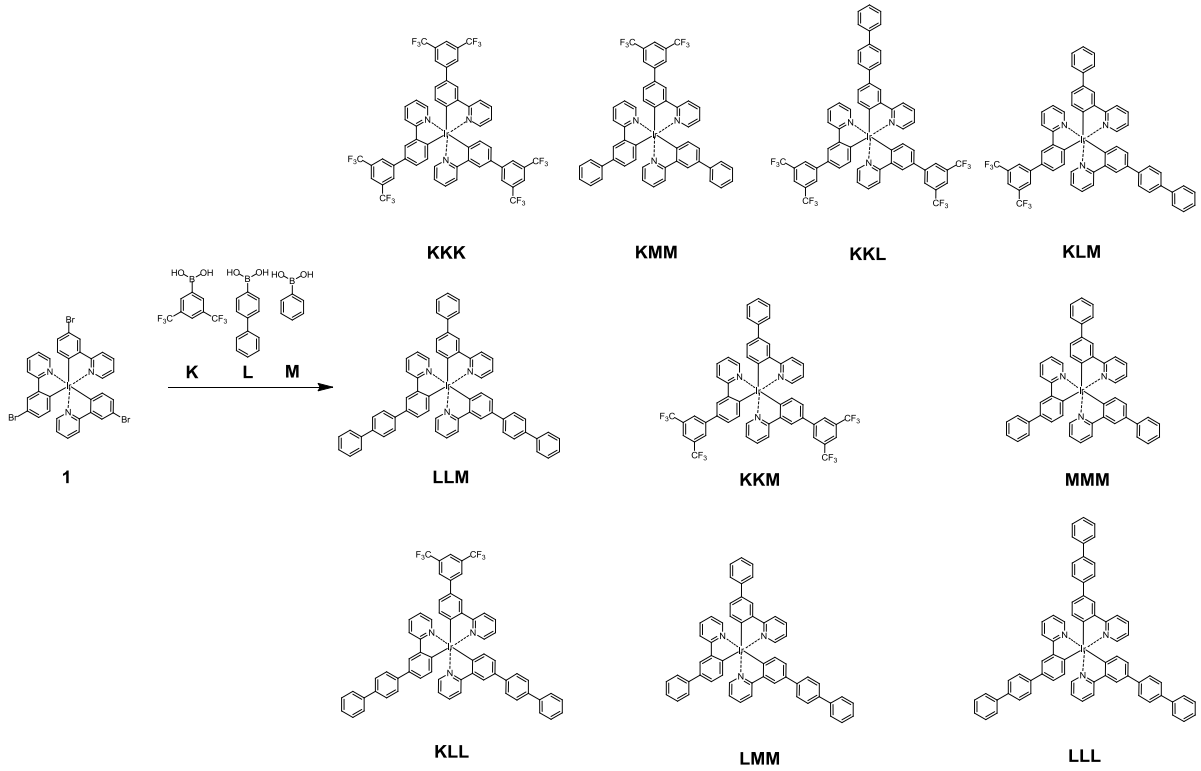

Scheme 2-2: Synthesis of library 4 with all 10 expected products.

2.2.2 SCREENING

To enable the separation and characterization of the compounds in our libraries on a suitable timescale, a chromatography based screening was developed. Figure 2-1 outlines the screening setup. In a first step, the crude reaction mixture is separated via a semipreparative HPLC system. A diode array detector (DAD) and a fluorescence detector (FLD) allow a peak based automated fraction collection and the simultaneous recording of absorption and phosphorescence spectra.

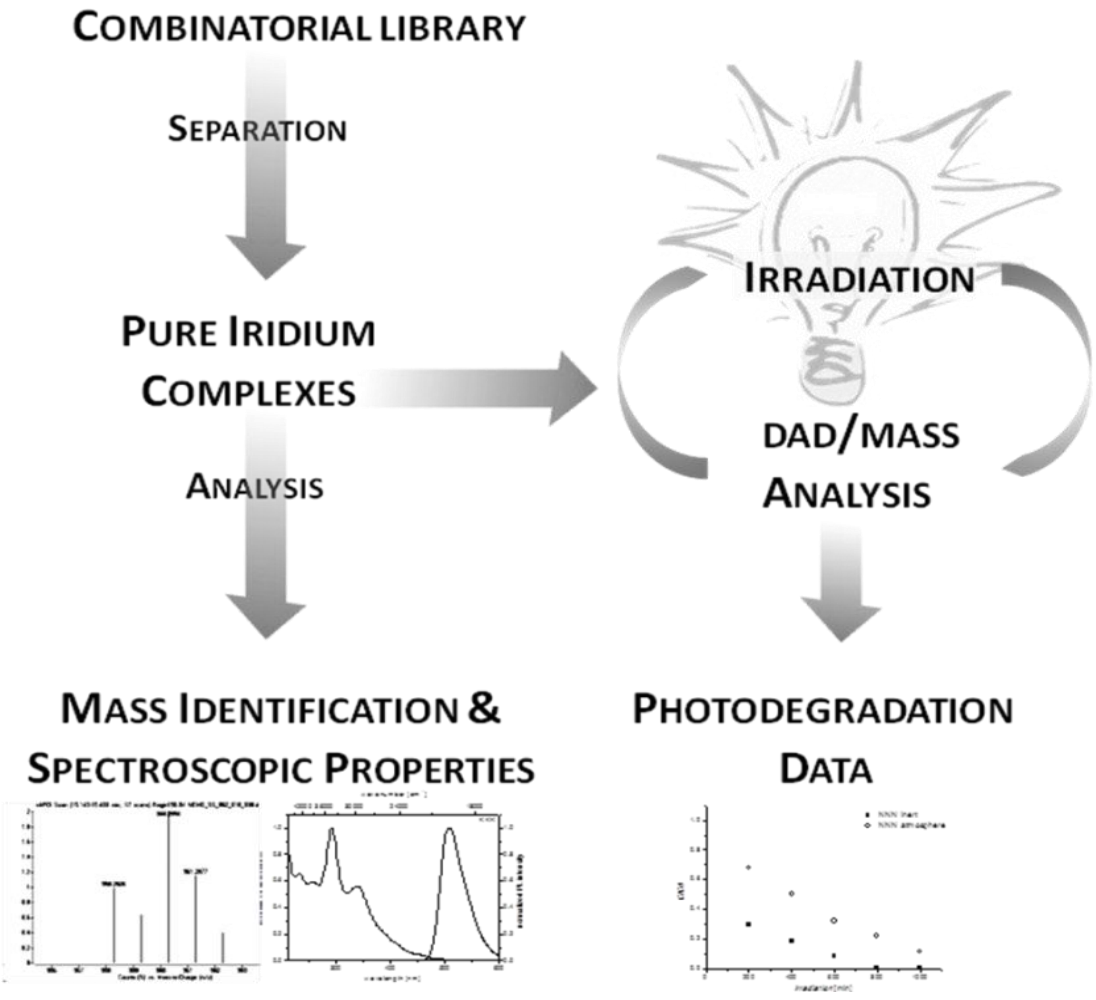

Figure 2-1: Schematic representation of the purification and screening process.

Figure 2-1 shows 3D-absorption- and emission-plots obtained from the separation of library 2. The eluted compounds were collected into vials, quantified and identified via LC-MS and then subjected to repeated irradiation and HPLC analysis to investigate the irradiation induced degradation of the compounds.

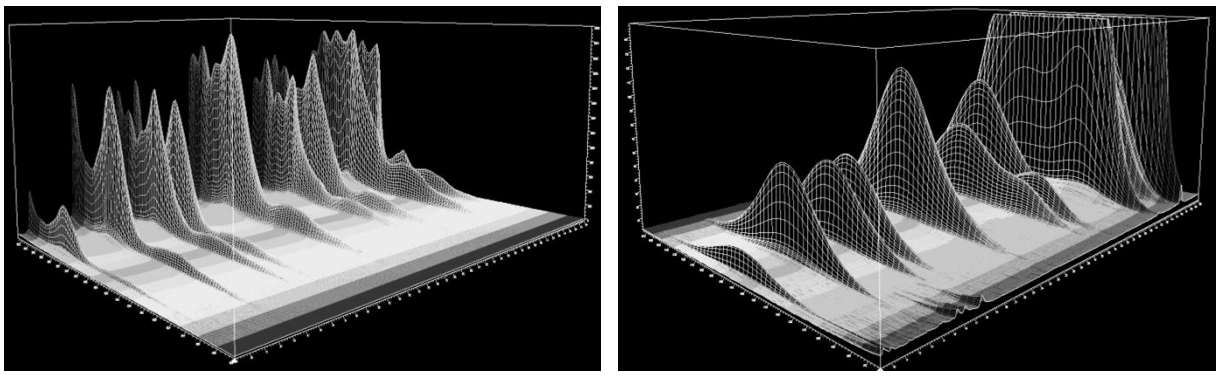

Figure 2-2: 3D-Plots from the separation of library 2. Left: Absorption intensity (z-axis) plotted against the wavelength (y-axis) and retention time (x-axis). Right: Emission intensity (z-axis) plotted against the wavelength (y-axis) and retention time (x-axis). The colors do not represent the colors as perceived by the eye.

2.2.3 SEPARATION AND SPECTROSCOPIC PROPERTIES

Of the 40 theoretically possible compounds, 36 could be separated and identified via LC-MS. The yields for the single compounds were estimated via the integrated area obtained from the chromatograms at 305 nm, assuming similar molar absorption coefficients for the different compounds. Apart from library 2 which showed a nearly statistical distribution of products, no clear trends in the reactivity of reactants could be elucidated. Their absorption and emission spectra (see the supporting information) were recorded and the full width at half maximum (FWHM) was determined as an indicator of color purity. Table 2-1 gives an overview of all identified compounds, their maximum emission wavelengths and FWHM values as well as the m/z values obtained by LC-MS analysis.

Table 2-1: Overview over all synthesized complexes with their yields, maximum emission wavelengths, FWHM values, PL quantum yields as well as the m/z (100 %) values obtained via LC-MS.

	Code	Formula	m/z (100 %)[a]	λ_{max} [nm]	FWHM	Quantum	Yield [%][c]
Library 1	**AAB**	$IrC_{71}H_{55}N_6$	1185.4227 (M+H)+	571	59	0.24	6
	BBC	Ir $C_{73}H_{59}N_6$	1211.4395 (M+H)+	575	56	0.25	2
	AAA	$IrC_{69}H_{51}N_6$	1157.3917 (M+H)+	569	58	0.25	10
	ABC	$IrC_{71}H_{53}N_6$	1183.4076 (M+H)+	574	57	0.25	14
	AAC	$IrC_{69}H_{49}N_6$	1155.3771 (M+H)+	570	61	0.25	25
	BCC	$IrC_{71}H_{51}N_6$	1181.3921 (M+H)+	577	55	---	7
	ACC	$IrC_{69}H_{47}N_6$	1153.3613 (M+H)+	569	64	0.28	27
	CCC	$IrC_{69}H_{45}N_6$	1151.3442 (M+H)+	519	47	0.82	8
Library 2	**EEE**	$IrC_{93}H_{99}N_6$	1493.7676 (M+H)+	576	58	0.18	3
	EED	$IrC_{103}H_{103}N_6$	1617.7987 (M+H)+	576	60	0.16	12
	CEE	$IrC_{85}H_{81}N_6$	1379.6264 (M+H)+	575	61	0.19	11
	EDD	$IrC_{113}H_{107}N_6$	1741.8296 (M+H)+	575	59	0.19	14
	CED	IrC_{95} H_{85} N_6	1503.6566 (M+H)+	575	62	0.17	24
	CCE	$IrC_{77}H_{63}N_6$	1265.4846 (M+H)+	577	67	0.17	11
	CDD	$IrC_{105}H_{89}N_6$	1627.6853 (M+H)+	575	62	0.19	11
	CCD	$IrC_{87}H_{67}N_6$	1388.5133 (M+H)+	522	70	0.26	11
	CCC	$IrC_{69}H_{45}N_6$	1151.3435 (M+H)+	519	44	0.82	3
Library 3	**KKK**	$IrC_{57}H_{30}N_3F_{18}$	1292.1887 (M+H)+	507	52	0.74	12
	KKM	$IrC_{55}H_{32}N_3F_{12}$	1156.2156 (M+H)+	512	45	0.71	6
	KKL	$IrC_{61}H_{36}N_3F_{12}$	1232.2460 (M+H)+	512	44	0.82	30
	KMM	$IrC_{53}H_{34}N_3F_6$	1020.2376 (M+H)+	515	43	0.71	2
	KLM	$IrC_{59}H_{38}N_3F_6$	1096.2711 (M+H)+	516	47	0.62	11
	KLL	$IrC_{65}H_{42}N_3F_6$	1172.2998 (M+H)+	517	41	0.64	15
	MMM	$IrC_{51}H_{36}N_3$	884.2608 (M+H)+	519	41	0.77	1
	LMM	$IrC_{57}H_{40}N_3$	960.2931 (M+H)+	519	43	0.63	5
	LLM	$IrC_{63}H_{44}N_3$	1036.3240 (M+H)+	519	46	0.66	9
	LLL	$IrC_{69}H_{48}N_3$	1112.3546 (M+H)+	520	47	0.81	9
Library 4	**NNN**	$IrC_{54}H_{42}N_3$	926.3083 (M+H)+	520	46	0.85	7
	NNO	$IrC_{65}H_{49}N_4$	1079.3663 (M+H)+	522	45	0.77	6
	NOO	$IrC_{76}H_{56}N_5$	1232.4257 (M+H)+	522	49	0.77	15
	OOO	$IrC_{87}H_{63}N_6$	1385.4813 (M+H)+	525	45	0.71	35
	NNP	$IrC_{54}H_{39}N_4$	937.2922 (M+H)+	518	47	0.83	16
	NOP	$IrC_{65}H_{46}N_5$	1090.3481 (M+H)+	520	43	0.65	4
	OOP	$IrC_{76}H_{53}N_6$	1243.4054 (M+H)+	521	44	0.54	5
	NPP	$IrC_{54}H_{36}N_5$	948.2694 (M+H)+	515	44	0.76	11
	OPP	$IrC_{65}H_{43}N_6$	1101.3259 (M+H)+	517	44	---	1

[a] obtained via LC-MS (APCI); [b] determined relative to the standard quinine hemisulfate monohydrate;

While the complexes prepared via the Suzuki couplings all emit in the green region, introduction of the electron donating arylamine moieties para to the metal leads to a significant bathochromic shift of the emission wavelength into the orange region. This is caused by the electron donating effect of the arylamine substituents, effectively increasing the donation to the metal via the Ir-C bond, destabilizing the metal centered HOMO and thus reducing the HOMO-LUMO energy gap. The same trend, although not as pronounced, could also be observed depending on the substituents of the aryl or diarylamine groups. Increasing electron donating character leads to a red shifted emission while electron withdrawing substituents cause a blue shift of the emission maximum (Figure 3). The electronic influence of the substituents on the emission energy can be rationalized using Hammett parameters for para substitution. Plotting the emission maxima against σ_{para} of the substituents shows a good correlation with the notable exception of carbazole (Figure 2-3).

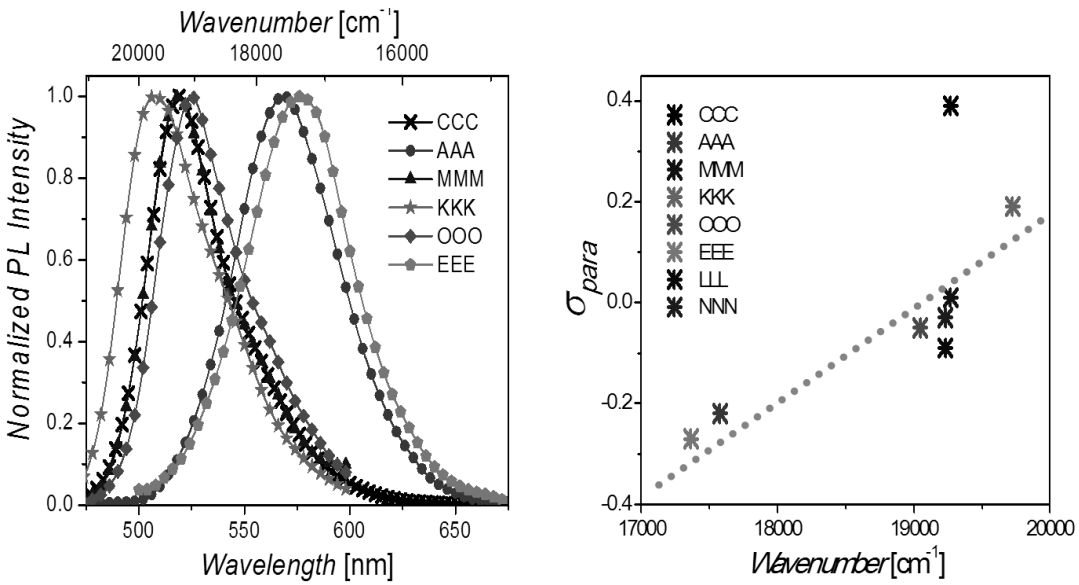

Figure 2-3: Phosphorescence spectra of selected homoleptic complexes illustrating the influence of electron donating and withdrawing groups on the emission energy (left). Hammett parameter σ_{para} plotted against the emission maxima (right). The dotted line is only a guide for the eye.

To gain further insight on the photophysical properties of the compounds we also estimated the phosphorescence quantum yields Φ_P of the complexes relative to a standard in a separate experiment. The obtained Φ_P values vary greatly from 0.17 to 0.82. The compounds can be divided into two categories according to their quantum efficiencies: The first group exhibits good to excellent Φ_P values of 0.6-0.8 and consists of the complexes obtained via the Suzuki-

Miyaura reactions as well as the fully carbazole substituted **CCC.** The second group - obtained via Buchwald-Hartwig couplings - has diarylamine substituents and exhibits smaller Φ_P values between 0.17 and 0.25.

It is well established that motional relaxation can be responsible for non radiative transitions and that in return enhanced molecular rigidity and restricted intramolecular motion results in improved radiative rates.[19] Ono et al. examined the influence of different hole trapping moieties such as diphenylamine, carbazole and phenoxazine on $Ir(ppy)_3$ based complexes with the phenylpyridine ligands substituted at the 4-position of the phenyl ring.[45] They found significantly lower quantum yields for the conformationally free diphenylamine substituted compounds while the more rigid carbazole substituent gave an excellent Φ_P. These observations are in good agreement with our obtained quantum yields for **CCC** (Φ_P = 0.82) and **AAA** (Φ_P = 0.25). This trend continues when looking at the different arylamine substituents in relation to each other - the higher the conformational flexibility of the arylamine substituents, the lower the Φ_P values seem to be. Compounds containing flexible substituents such as dimethylbenzyl (**D**) or *tert*-butyl (**E**) (Φ_P = 0.17-0.19) show slightly reduced phosphorescence efficiencies compared to the methyl- or non-substituted diphenylamines **A** and **B** ($\Phi_P \sim 0.25$). Interestingly, the substitution with triphenylamine (**O**) did not lead to a significant reduction of Φ_P which indicates that the introduction of flexibility on the periphery of the molecule further away from the emitting center does not significantly reduce the quantum yields. Since the introduction of structurally flexible substituents is a common strategy for increasing solubility, this antagonistic relationship between conformational flexibility and phosphorescence efficiency should be kept in mind when designing emitters suitable for solution processing. Increasing the solubility by introducing flexibility at the periphery while preserving the rigidity near the emitting center could therefore be a promising strategy for realizing highly efficient phosphorescence from soluble molecules.

Interesting effects could be observed regarding the emission characteristics of heteroleptic compounds containing ligands of different energies: Compounds with two arylamine and one carbazole substituents show emission that seems to be dominated by the lower energy transition centered on the arylamine substituted ligand, manifesting in emission maxima around 570-575 nm and quantum yields between 0.17 and 0.25.

For complexes containing two carbazoles as well as one arylamine substituent dual emission effects could be observed: While compounds **CCE** (**E** = bis(4-tert-butylphenyl)amine) and **CCA**

(**A** = diphenylamine) exhibit an orange emission with a small shoulder in the green region (Figure 4), complex **CCD** containing two carbazole and one 4,4'-bis(α,α-dimethyl-benzyl)diphenylamine (**D**) substituent shows green phosphorescence with a shoulder in the orange region. To gain more information on this pronounced difference in the emission behavior of **CCD** and **CCE**, we synthesized **DDD** (which could not be obtained from the chromatographic separation of library 2) via a conventional reaction and determined its quantum yield. Φ_P (**DDD**) was found to be 0.20, which is similar to that of **EEE** (Φ_P = 0.18). Since these emission efficiencies are quite similar, the reasons for the different phosphorescence characteristics must lie elsewhere. Detailed spectroscopic investigations might provide a deeper insight into this phenomenon in the future. Emitters with dual emission properties exhibit broad banded emission making them very promising candidates for white organic light-emitting diodes.[46] The combinatorial synthesis of focused libraries directed at the tuning of dual emission properties could be a valuable tool to facilitate the development of new emitters in this field.

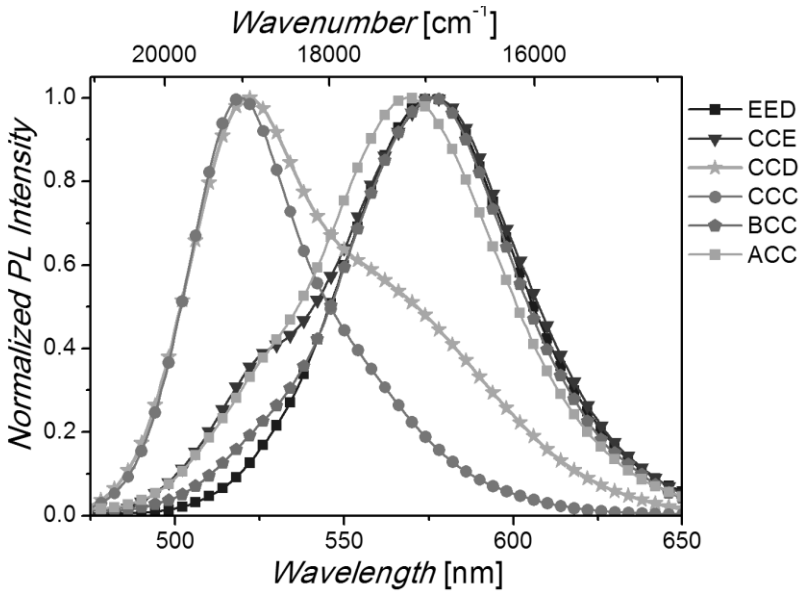

Figure 2-4: Phosphorescence spectra of compounds EED, CCE, CCD, CCC, BCC and ACC.

2.2.4 PHOTODEGRADATION STUDIES

While there is still not much known about the exact degradation mechanisms of emitters in PhOLEDs, most recent investigations suggest an important role of excited states.[47-49] Population of higher lying thermally accessible states for example may lead to bond rupture and possibly cause ligand dissociation.[50-51] Researchers at Fujifilm already used the analysis of irradiation induced degradation as a tool to assess the stability of new emitters. They successfully identified a new long lived phosphorescent blue emitter by spincoating layers of host material doped with a phosphorescent guest and examining the photoluminescence degradation under UV irradiation.[52] To gain a first hint on the stability of our compounds under continuous excitation, we examined the irradiation induced degradation of the complexes in solution. We found LEDs with an emission maximum of 400 nm to be the ideal light source as they allow the direct excitation of the MLCT absorption band and at the same time enable the irradiation through a chromatography glass vial. Toluene was chosen as the solvent for the photodegradation studies as it is a comparably inert and non coordinating solvent and is furthermore one of the preferred solvents for solution processing of organic light-emitting devices. The irradiation was performed once under atmospheric and once under oxygen free conditions.[44]

$Ir(ppy)_3$ and similar compounds are known to be very effective sensitizers of singlet oxygen,[53-55] so we initially expected that the presence of those highly reactive oxygen species would lead to faster degradation under atmospheric conditions. When looking at the results of the photostabilities of the complexes we were surprised to find that for most compounds, the presence of oxygen in the solution seemed to increase the photostability instead.

A possible explanation for this unexpected observation could be that singlet oxygen is deactivated relatively fast in toluene. This implies that the observed degradation in toluene occurs mainly via the excited molecules themselves. Oxygen efficiently quenches the ^{3}MLCT excited state at near diffusion controlled rates, leading to much shorter excited state lifetimes and may thus reduce the probability of degradation via those states. A comparison of the homoleptic complexes showed that the overall trends in the photostability are similar under atmospheric and inert conditions. The fastest photodegradation could be observed for compounds **AAA** and **NNN** (Figure 2-5). The tris-phenyl substituted **MMM** showed a moderate photostability whereas the fully carbazole- and 3,5-*bis*(trifluoromethyl)phenyl- substituted complexes (**CCC** and **KKK** respectively) turned out to be the most stable of all screened

compounds. Figure 2-5 (right) illustrates the influence of the different substituents on the degradation sensitivity for library 3. The presence of trifluoromethyl groups in the substituent (ligand **K**) seems to significantly increase the photostability of the complexes. This effect can be observed for compounds containing one to three bis(trifluoromethyl)phenyl groups under inert and atmospheric conditions alike.

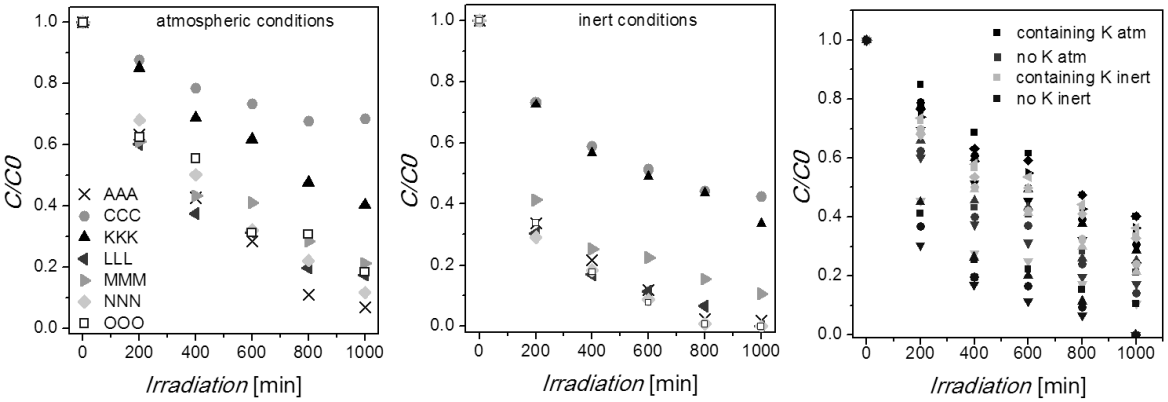

Figure 2-5: Photodegradation of the homoleptic complexes under atmospheric (left) and inert (center) conditions. Substitution effects on the photodegradation of library 3 (right).

Further studies with a larger number of compounds will be necessary to establish structure-property relationships for the photostabilities in solution. More detailed investigations on the nature and products of the degradation pathways in solution as well as a comparison with device stabilities of selected emitters could shed light on the correlations and differences between the photo- and device-degradation of this class of compounds.

2.3 CONCLUSIONS

In conclusion we demonstrated that the described post modification strategy combined with a chromatographic separation and screening enables the rapid synthesis and characterization of potential new OLED emitters. We examined the photophysical properties of the compounds by obtaining absorption and emission spectra directly from the chromatographic separation. Trends in the dual emission behavior of selected heteroleptic complexes were observed that upon further studies might to lead to the development of promising new compounds for white light emitting OLEDs. The determination of phosphorescence quantum yields in a separate experiment illustrated the antagonistic relationship between molecular flexibility and phosphorescence efficiency and helped to elucidate a promising new design principle for soluble and highly efficient phosphorescent emitters. By investigating the photodegradation of the libraries in solution, we found surprising trends and could identify compounds with increased stabilities compared to the rest of the libraries. Once a larger dataset will be available, a more detailed understanding of the degradation mechanisms and structure property relationships might help in the discovery of phosphorescent transition metal complexes with improved stabilities. The reported chromatography based screening of organo-transition metal complexes is not restricted to the development of new OLED emitters but may be easily applied for the accelerated discovery of materials for diverse other fields such as dyes for dye sensitized solar cells or new photoredox catalysts.

2.4 EXPERIMENTAL

fac-Tris(5'-bromo-2-phenylpyridine)iridium was provided by Merck KGaA.[56] All solvents and other commercially available reagents were purchased from Alfa Aesar or Sigma Aldrich and were used as received without further purification. The solvents were used in p.a. quality and degassed via purging with nitrogen over 1 hour prior to use. For the chromatographic separation and analysis (sample preparation and mobile phase) we used LiChrosolv® solvents, (DCM, THF and hexane) which were purchased from Merck KGaA.

2.4.1 General Procedure for the Combinatorial Buchwald-Hartwig Coupling

Tris(5'-bromo-2-phenylpyridine)iridium (0.1 mmol), an equimolar mixture of the secondary arylamines (0.4 mmol) and NaO^tBu (0.8 mmol) were placed in a headspace vial. The vial was then flushed with nitrogen and sealed with a silicone/PTFE septum. Toluene (9 mL), 1,4-dioxane (5 mL) and 1 mL of catalyst solution (containing 0.03 mmol $Pd(OAc)_2$ and 0.18 mmol $P(^tBu)_3$ in degassed toluene) were added subsequently. The mixture was then stirred at 130 °C for 4 h in a custom made aluminum heating block. After the reaction mixture had cooled down to room temperature, the reaction mixture was washed with water and brine and dried over $MgSO_4$. The solvents were removed in vacuo to give an orange residue.

2.4.2 GENERAL PROCEDURE FOR THE COMBINATORIAL SUZUKI-MIYAURA COUPLING

Tris(5'-bromo-2-phenylpyridine)iridium (0.1 mmol), an equimolar mixture of the boronic acids (0.5 mmol) and K3PO4 (0.8 mmol) were combined in a headspace vial. The vial was then flushed with nitrogen and sealed with a silicone/PTFE septum**.** Degassed toluene, dioxane and water (5 mL each) and 1 mL catalyst solution (containing 0.03 mmol Pd(OAc)2 and 0.18 mmol P(o-tolyl)3 in 10 mL degassed toluene) were added. The reaction mixture was stirred at 85 °C for 10 h in a custom made aluminum heating block. The toluene phase was washed with water and brine, dried over MgSO4 and the solvent was removed in vacuo to give a yellow solid.

2.4.3 SYNTHESIS OF THE HOMOLEPTIC REFERENCE COMPLEXES

The homoleptic reference complexes were synthesized as described for the combinatorial procedures but with only one amine or boronic acid respectively. The crude products were purified by recrystallization as specified with the characterization data.

2.4.4 SEPARATION, IDENTIFICATION VIA MS AND SPECTRA

The semipreparative separation of the complex libraries was performed on an Agilent Technologies HPLC system consisting of a quaternary pump [G1311A], a vacuum degasser [G1322A], a thermostatted autosampler [G1329A], a thermostatted column compartment [G1316A], a diode-array detector (DAD) SL [G1315C] and a fluorescence detector (FLD) [G1321A] as well as an analytical scale fraction collector [G1364C]. The column used was a HIbar® 250 mm x 10mm x 5µm diol column (Merck KGaA). The crude complex libraries were resolved in an appropriate volume of DCM (1-2 mL), filtered through a 2 µm PTFE syringe-filter and used for semipreparative HPLC separation using gradient elution (hexane/THF). All absorption and emission spectra were measured online via DAD and FLD detectors. The fractions were collected automatically (peak based fraction collection).

For the identification of the compounds, the collected samples were analyzed via LC-MS. The analysis was performed on an Agilent Technologies 1200 HPLC/MS system consisting of a binary pump SL [G1312B], a degasser [G1379B], an Infinity high performance micro autosampler [G1329B] with thermostat [G1330B], a thermostatted column compartment [G1316B], an Infinity diode-array detector (DAD) [G4212B] and an accurate mass Q-TOF/MS [G6530A] with an APCI (atmospheric pressure chemical ionization) ion source. The column used was a HIbar® 250 mm x 4 mm x 5µm diol column (Merck KGaA).

2.4.5 QUANTUM YIELD ESTIMATION

The PL quantum yields were determined relative to quinine hemisulfate monohydrate in 1 N H_2SO_4 (QY = 0.55). UV measurements were carried out on a Varian Cary 50Bio UV-Vis spectrophotometer, phosphorescence measurements on a Varian Eclipse Fluorescence spectrophotometer in sealable Hellma precision cells [117.100F-QS] with silicone/PTFE coated septa. The complexes were dissolved in DCM and the solutions were degassed in the cells via vigorous argon purge through the solution prior to the measurements.

2.4.6 PHOTODEGRADATION STUDIES

The pure complexes were dissolved in varying volumes of toluene (p.a.) to give solutions of similar concentration. The volume of toluene was adjusted according to the integration area of the peaks for each complex (from the semipreparative separation). 1 mL of the resulting

solutions was transferred to a headspace vial and sealed with a silicone/PTFE septum. Two samples were prepared from each complex for the testing under atmospheric and inert conditions. In case of the photodegradation studies under inert conditions, the vials were degassed via 4 freeze-pump thaw cycles under argon. All samples were irradiated in a custom made irradiation unit (SIM GmbH, picture see supporting information). It consists of an aluminum printed circuit board with 30 400 nm LEDs, connected to a cooling unit, that ensures a constant temperature of 13 °C of the board during the irradiation. Two 15 sample chromatography trays can be placed in the unit so that each of the sample vials is centered over one LED (d = 1 cm). The total duration of irradiation was 1000 min. After 0, 200, 400, 600, 800 and 1000 min, the samples were analyzed via HPLC (analytical system, see above). The percentage of remaining emitter was determined via integration of the DAD signal at 305 nm in relation to that of an external standard (quaterphenyl in toluene, 0.026 mM).

2.4.7 SUPPORTING INFORMATION

^{1}H and ^{13}C NMR spectra as well as HR-Mass (APCI) characterization of reference complexes prepared via conventional synthesis, 3D-absorption- and emission-plots of libraries 2-4, absorption and emission spectra as well as the photodegradation plots for all compounds and a picture of the irradiation unit can be found in the appendix.

2.5 REFERENCES

[1] K. K.-W. Lo, C.-K. Chung, T. K.-M. Lee, L.-H. Lui, K. H.-K. Tsang, N. Zhu, *Inorg. Chem.* **2003**, *42*, 6886-6897.

[2] K. K.-W. Lo, D. C.-M. Ng, C.-K. Chung, *Organometallics* **2001**, *20*, 4999-5001.

[3] K. K.-W. Lo, K. Y. Zhang, S.-K. Leung, M.-C. Tang, *Angew. Chem., Int. Ed.* **2008**, *47*, 2213-2216.

[4] C. S. K. Mak, D. Pentlehner, M. Stich, O. S. Wolfbeis, W. K. Chan, H. Yersin, *Chem. Mater.* **2009**, *21*, 2173-2175.

[5] Y. You, S. Y. Park, *Adv. Mater.* **2008**, *20*, 3820-3826.

[6] W. Zhao, F. N. Castellano, *J. Phys. Chem. A* **2006**, *110*, 11440-11445.

[7] T. N. Singh-Rachford, F. N. Castellano, *Coord. Chem. Rev.* **2010**, *254*, 2560-2573.

[8] E. Baranoff, J.-H. Yum, M. Graetzel, M. K. Nazeeruddin, *J. Organomet. Chem.* **2009**, *694*, 2661-2670.

[9] B. F. DiSalle, S. Bernhard, *J. Am. Chem. Soc.* **2011**, *133*, 11819-11821.

[10] J. I. Goldsmith, W. R. Hudson, M. S. Lowry, T. H. Anderson, S. Bernhard, *J. Am. Chem. Soc.* **2005**, *127*, 7502-7510.

[11] N. Sutin, C. Creutz, E. Fujita, *Comments Inorg. Chem.* **1997**, *19*, 67-92.

[12] Y.-J. Yuan, Z.-T. Yu, X.-Y. Chen, J.-Y. Zhang, Z.-G. Zou, *Chem.--Eur. J.* **2011**, *17*, 12891-12895.

[13] K. Zeitler, *Angew. Chem., Int. Ed.* **2009**, *48*, 9785-9789.

[14] H.-W. Shih, M. N. Vander Wal, R. L. Grange, D. W. C. MacMillan, *J. Am. Chem. Soc.* **2010**, *132*, 13600-13603.

[15] A. G. Condie, J. C. González-Gómez, C. R. J. Stephenson, *J. Am. Chem. Soc.* **2010**, *132*, 1464-1465.

[16] M. A. Baldo, D. F. O'Brien, Y. You, A. Shoustikov, S. Sibley, M. E. Thompson, S. R. Forrest, *Nature* **1998**, *395*, 151-154.

[17] T. Hofbeck, H. Yersin, *Inorganic Chemistry* **2010**, *49*, 9290-9299.

[18] H. Yersin, A. F. Rausch, R. Czerwieniec, T. Hofbeck, T. Fischer, *Coord. Chem. Rev.* **2011**, *255*, 2622-2652.

[19] Y. You, S. Y. Park, *Dalton Trans.* **2009**, 1267-1282.

[20] Y. Chi, P.-T. Chou, *Chem. Soc. Rev.* **2010**, *39*, 638-655.

[21] P. T. Chou, Y. Chi, *Chem.--Eur. J.* **2007**, *13*, 380-395.

[22] E. Baranoff, S. Fantacci, F. De Angelis, X. Zhang, R. Scopelliti, M. Grätzel, M. K. Nazeeruddin, *Inorg. Chem.* **2010**, *50*, 451-462.

[23] F. De Angelis, S. Fantacci, N. Evans, C. Klein, S. M. Zakeeruddin, J.-E. Moser, K. Kalyanasundaram, H. J. Bolink, M. Grätzel, M. K. Nazeeruddin, *Inorg. Chem.* **2007**, *46*, 5989-6001.

[24] C. L. Ho, W. Y. Wong, Z. Q. Gao, C. H. Chen, K. W. Cheah, B. Yao, Z. Y. Xie, Q. Wang, D. G. Ma, L. X. Wang, X. M. Yu, H. S. Kwok, Z. Y. Lin, *Adv. Funct. Mater.* **2008**, *18*, 319-331.

[25] J. Li, P. I. Djurovich, B. D. Alleyne, M. Yousufuddin, N. N. Ho, J. C. Thomas, J. C. Peters, R. Bau, M. E. Thompson, *Inorg. Chem.* **2005**, *44*, 1713-1727.

[26] M. S. Lowry, W. R. Hudson, R. A. Pascal, S. Bernhard, *J. Am. Chem. Soc.* **2004**, *126*, 14129-14135.

[27] E. M. Gordon, R. W. Barrett, W. J. Dower, S. P. A. Fodor, M. A. Gallop, *J. Med. Chem.* **1994**, *37*, 1385-1401.

[28] C. Gennari, U. Piarulli, *Chem. Rev. (Washington, DC, U. S.)* **2003**, *103*, 3071-3100.

[29] N.-M. Hsu, W.-R. Li, *Angew. Chem., Int. Ed.* **2006**, *45*, 4138-4142.

[30] E. Baranoff, I. Jung, R. Scopelliti, E. Solari, M. Gratzel, M. K. Nazeeruddin, *Dalton Trans.* **2011**, *40*, 6860-6867.
[31] C. E. Kibbey, *Laboratory Robotics and Automation* **1997**, *9*, 309-321.
[32] L. Zeng, L. Burton, K. Yung, B. Shushan, D. B. Kassel, *J. Chromatogr., A* **1998**, *794*, 3-13.
[33] H. N. Weller, *Mol. Diversity* **1998**, *4*, 47-52.
[34] C. Adachi, M. A. Baldo, S. R. Forrest, M. E. Thompson, *Appl. Phys. Lett.* **2000**, *77*, 904-906.
[35] Y. Kawamura, K. Goushi, J. Brooks, J. J. Brown, H. Sasabe, C. Adachi, *Appl. Phys. Lett.* **2005**, *86*, 071104-071103.
[36] D. Tanaka, H. Sasabe, Y.-J. Li, S.-J. Su, T. Takeda, J. Kido, *Jpn. J. Appl. Phys.*, *46*, L10.
[37] N. Cumpstey, R. N. Bera, P. L. Burn, I. D. W. Samuel, *Macromolecules* **2005**, *38*, 9564-9570.
[38] Y. You, C.-G. An, J.-J. Kim, S. Y. Park, *The Journal of Organic Chemistry* **2007**, *72*, 6241-6246.
[39] Y. You, C.-G. An, D.-S. Lee, J.-J. Kim, S. Y. Park, *Journal of Materials Chemistry* **2006**, *16*, 4706-4713.
[40] P. Stoessel, H. Spreitzer, H. Becker, Covion Organic Semiconductors, **2002**.
[41] P. Stoessel, I. Bach, H. Spreitzer, Covion Organic Semiconductors, **2004**.
[42] P. Stoessel, H. Spreitzer, H. Becker, Covion Organic Semiconductors, **2002**.
[43] R. M. Anemian, B. Schroeder, A. H. Parham, C. d. Nonancourt, Merck Patent GmbH, **2011**.
[44] The solutions were degassed via 4 consecutive freeze-pump-thaw cycles applying a membrane vacuum pump (~10 mbar) and backfilling with argon. It should be noted that a complete, quantitative removal of oxygen is unlikely under these conditions but it should be sufficient to establish the overall trend of the influence of oxygen on the photostability of the materials.
[45] K. Ono, M. Joho, K. Saito, M. Tomura, Y. Matsushita, S. Naka, H. Okada, H. Onnagawa, *Eur. J. Inorg. Chem.* **2006**, *2006*, 3676-3683.
[46] Y. You, K. S. Kim, T. K. Ahn, D. Kim, S. Y. Park, *J. Phys. Chem. C* **2007**, *111*, 4052-4060.
[47] N. C. Giebink, B. W. D'Andrade, M. S. Weaver, J. J. Brown, S. R. Forrest, *J. Appl. Phys.* **2009**, *105*, 124514-124517.
[48] N. C. Giebink, B. W. D'Andrade, M. S. Weaver, P. B. Mackenzie, J. J. Brown, M. E. Thompson, S. R. Forrest, *J. Appl. Phys.* **2008**, *103*, 044509.
[49] R. Seifert, S. Scholz, B. Lussem, K. Leo, *Appl. Phys. Lett.* **2010**, *97*, 013308-013303.
[50] T. Sajoto, P. I. Djurovich, A. B. Tamayo, J. Oxgaard, W. A. Goddard, M. E. Thompson, *J. Am. Chem. Soc.* **2009**, *131*, 9813-9822.
[51] I. R. d. Moraes, S. Scholz, B. Lüssem, K. Leo, *Organic Electronics* **2011**, *12*, 341-347.
[52] W. Sotoyama, T. Satoh, M. Kinoshita, M. Tobise, K. Kawato, T. Ise, H. Takizawa, S. Yamashita, *Fujifilm Research and Development* **2010**, *No.055*, 24-28.
[53] R. Gao, D. G. Ho, B. Hernandez, M. Selke, D. Murphy, P. I. Djurovich, M. E. Thompson, *J. Am. Chem. Soc.* **2002**, *124*, 14828-14829.
[54] S.-y. Takizawa, R. Aboshi, S. Murata, *Photochem. Photobiol. Sci.* **2011**, *10*, 895-903.
[55] P. I. Djurovich, D. Murphy, M. E. Thompson, B. Hernandez, R. Gao, P. L. Hunt, M. Selke, *Dalton Trans.* **2007**, 3763-3770.
[56] P. Stoessel, H. Spreitzer, H. Becker, **2002**.

CHAPTER 3

3. STUDIES ON THE PHOTODEGRADATION OF RED, GREEN AND BLUE PHOSPHORESCENT OLED EMITTERS*

* Author contributions: Susanna Schmidbauer and Andreas Hohenleutner contributed equally.

3.1 INTRODUCTION

For applications like displays or lighting, organic light-emitting devices have to enable the efficient conversion of electrons into photons to ensure sufficient light output at low power consumptions. To achieve this, the use of organo-transition metal complexes as phosphorescent dopants has proved highly beneficial. While fluorescent dyes normally emit from their singlet excited states (at room temperature) and therefore can only utilize singlet excitons, phosphorescent organo-transition metal dopants emit from their triplet excited states and in addition are able to effectively convert singlet into triplet states via fast intersystem crossing . The recombination of electron – hole pairs generates singlet and triplet excitons in a ratio of 1:3 which means that the use of phosphorescent devices can give up to 4 times higher efficiencies than those based on fluorescent emitters – which is called the triplet harvesting effect.[1] However, while OLEDs with efficiencies comparable to fluorescent tube lamps have been realized,[2] the operational stability of the devices remains to be a challenge in this field. In particular, the chemical degradation of the materials during operation is still considered the major obstacle for the development of economically feasible devices. In many cases of highly efficient phosphorescent devices it is indeed likely that the luminance loss over time can be in part or even largely attributed to the deterioration of the phosphorescent dopants.[3-4] The development of highly stable phosphorescent dopants is therefore a topic of high interest (see chapter 1). Thus, investigating the mechanisms and pathways responsible for the degradation of these materials is of high importance as the insights from these studies can guide the development of new materials with enhanced stabilities. Most studies on the degradation mechanisms of materials in OLEDs in general and of the phosphorescent emitters in particular suggest the participation of excited states.[3, 5-13] This can proceed via direct instability of the excited states, or via higher lying unstable states that are accessible via annihilation reactions[14-15] or thermal population.[16] Investigations on the photodegradation of these compounds could therefore potentially provide valuable information on the processes that are responsible for the limited stability of phosphorescent OLEDs.

In a previous study we already used the photoinduced degradation of phosphorescent iridium complexes in solution as a fast screening tool for their degradation behavior and observed interesting differences and effects in correlation to the examined structures.[17] In this context, we wanted to gain a deeper understanding of the processes at work and examine whether the photostability in solution and in a solid organic matrix would show a similar behavior. We therefore selected four well known phosphorescent emitters for a detailed investigation of their

photodegradation behavior in solution and thin polymer films. To gain information on the chemical degradation mechanisms, we tried to identify formed deterioration products via liquid chromatography mass spectrometry (LC-MS) and other analytical methods where applicable.

3.2 RESULTS AND DISCUSSION

For our investigations, we chose the four iridium complexes depicted in Figure 3-1. The compounds exhibit emission in the red ($Ir(piq)_3$), green ($Ir(Me\text{-}ppy)_3$ and $Ir(ppy)_3$) and blue region ($Ir(F,CN\text{-}ppy)_3$) respectively. Especially $Ir(piq)_3$ and $Ir(ppy)_3$ are popular phosphorescent emitters and often used in devices.

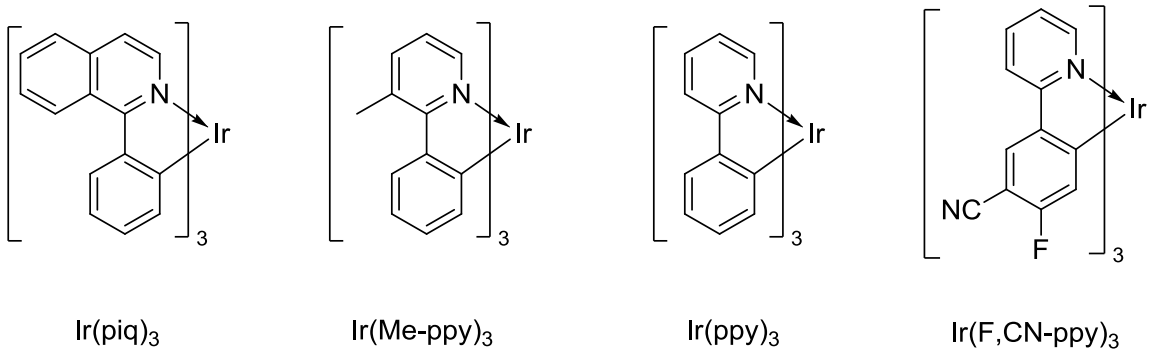

Figure 3-1: Structures of the investigated phosphorescent tris-cyclometalated iridium complexes.

For the investigation of the behavior of these compounds under continuous excitation, the samples were irradiated with light of 400 nm high power LEDs (350mW). This allows the excitation of the MLCT absorption band and further enables the irradiation through standard chromatography glass vials/ glass substrates without having to resort to quartz cuvettes. Toluene was chosen as solvent since it is a comparably inert non-coordinating solvent that is also preferably used for the processing of OLEDs from solution. To check for the solvent influence, we also performed experiments in DCM. To be able to compare the behavior in solution and solid state, we further prepared thin poly(methyl metacrylate) (PMMA) films doped with the different materials via spin coating and subjected them to irradiation under the same conditions. For the degradation studies in solution, the ratio of remaining to initial complex concentration after the different irradiation times was determined via HPLC analysis, for the solid samples via measuring the luminescence intensities of the samples. The majority of the experiments was performed at least twice and was reproducible within an estimated error

of < 10%. The degradation curves were generated using the average value of the obtained data (the results of the individual experiments are provided in the supporting information). We will first discuss general trends and observations and then elaborate on the role of halogenated solvents followed by a more detailed discussion for each of the investigated compounds behavior.

3.2.1 GENERAL OBSERVATIONS

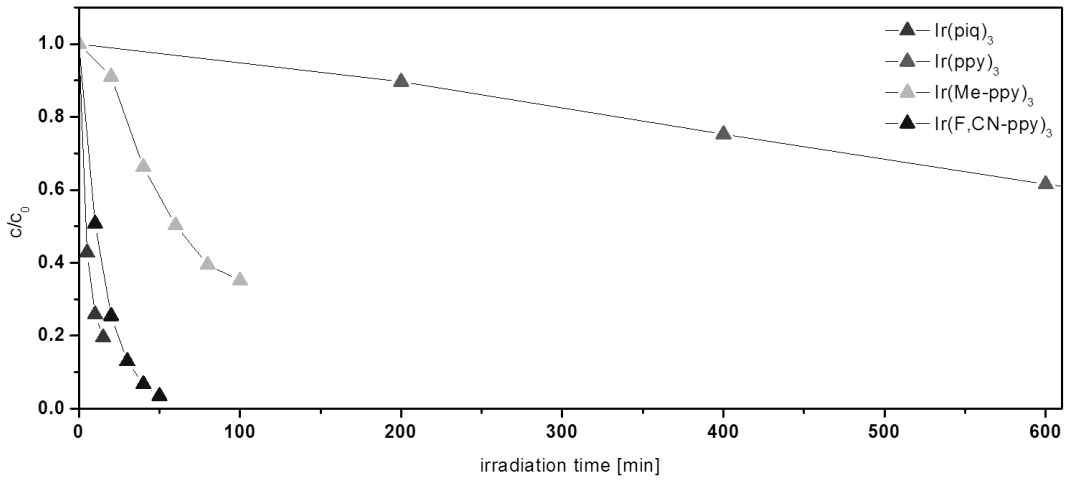

Figure 3-2: Photodegradation of the different compounds in toluene in ambient atmosphere. Plotted is the ratio between the remaining and initial concentrations for the respective compound against the irradiation time.

The rate of photodegradation shows substantial differences as can be seen in Figure 3-2, which compares the concentration decrease of the four substances in toluene at ambient conditions. While $Ir(ppy)_3$ is fairly stable, $Ir(Me\text{-}ppy)_3$ is degrading considerably faster and $Ir(piq)_3$ as well as $Ir(F,CN\text{-}ppy)_3$ exhibit an extremely fast deterioration in the course of only a few minutes. While this general trend for the stability of the different complexes ($Ir(ppy)_3$ >> $Ir(Me\text{-}ppy)_3$ > $Ir(piq)_3$/$Ir(F,CN\text{-}ppy)_3$) was found to apply to all examined conditions, the matrix can have a pronounced influence on the degradation rate. All compounds exhibit at least equal or higher stabilities in toluene compared to DCM (no reproducible results could be obtained for $Ir(F,CN\text{-}ppy)_3$ in DCM). Interestingly, deterioration in the solid PMMA matrix also follows the overall trends as observed for the experiments in solution. This may be an indicator that the processes leading to the deterioration of these compounds might indeed at least partly be the same in

solution and solid state. Figure 3-3 shows the degradation in different matrices at ambient conditions for all four compounds (note the different scale for the separate graphs).

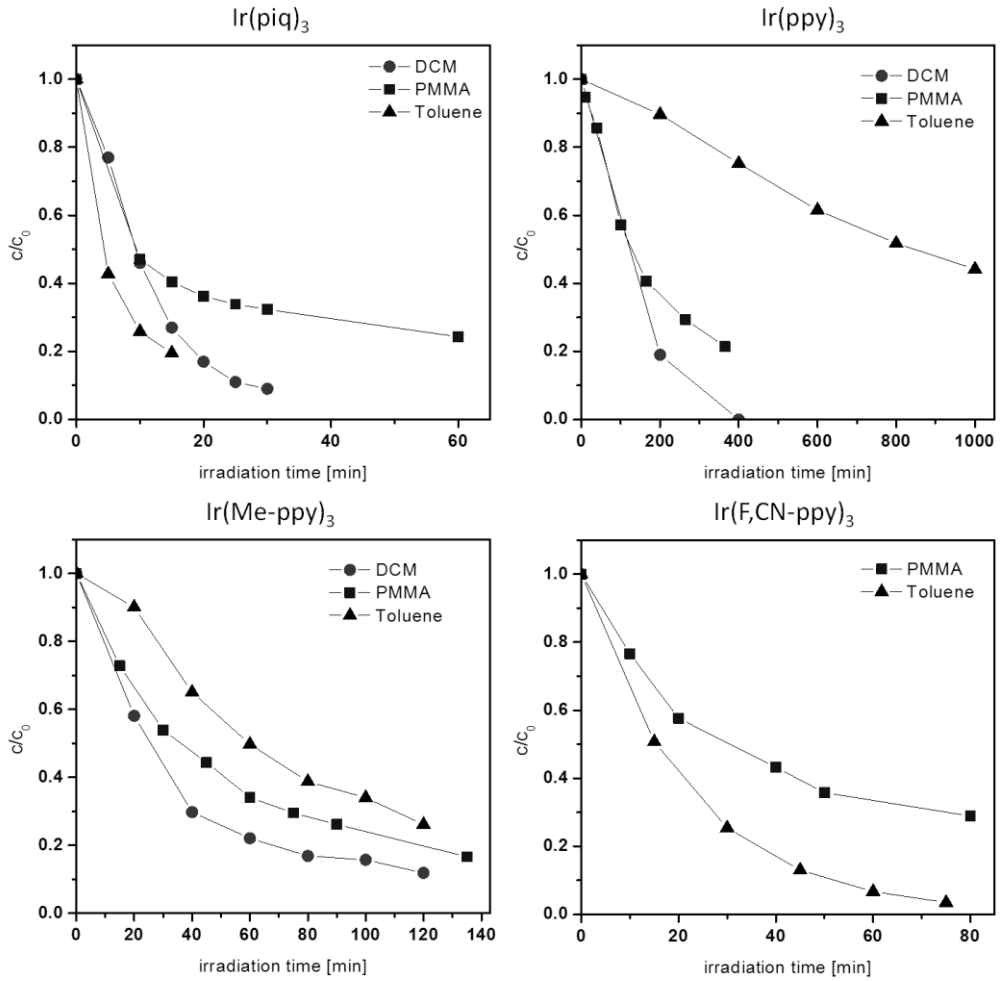

Figure 3-3: Photodegradation behavior of the iridium complexes in DCM and toluene solution and in a spin coated PMMA polymer film under ambient conditions. For measurements that were performed repeatedly, the depicted values represent the mean of all experiments.

3.2.2 THE INFLUENCE OF HALOGENATED SOLVENTS

Though halogenated solvents often provide the best solubility for this class of compounds, it is generally believed that their use is detrimental to the stability of these materials. The observed higher degradation rates of the compounds in DCM seem to support this assumption. The higher the general stability of the investigated compounds, the stronger the detrimental effect of using DCM seemed to be. While there is little to no solvent influence observable for $Ir(F,CN\text{-}ppy)_3$ and $Ir(piq)_3$, it is more pronounced for $Ir(Me\text{-}ppy)_3$ and becomes particularly striking for $Ir(ppy)_3$

with the degradation being about eight times faster in DCM compared to toluene. A possible explanation for this observation could be that solvent independent processes are responsible for the generally very low photostabilities of the red and blue emitter and the solvent effect is therefore negligible. With the overall higher stabilities of the green emitting compounds however, processes associated with DCM as the solvent become apparent. LC-MS analysis indeed revealed that the main observed degradation products of $Ir(ppy)_3$ after irradiation in DCM were chlorinated species, formed via the exchange of one or two hydrogen atoms for a chlorine substituent (Figure 3-4). This can be concluded from the m/z values as well as isotope distribution patterns. Analogous products could also be observed for $Ir(Me\text{-}ppy)_3$ though only as a side product (see below) while no indication of halogen abstraction was found for the other two complexes.

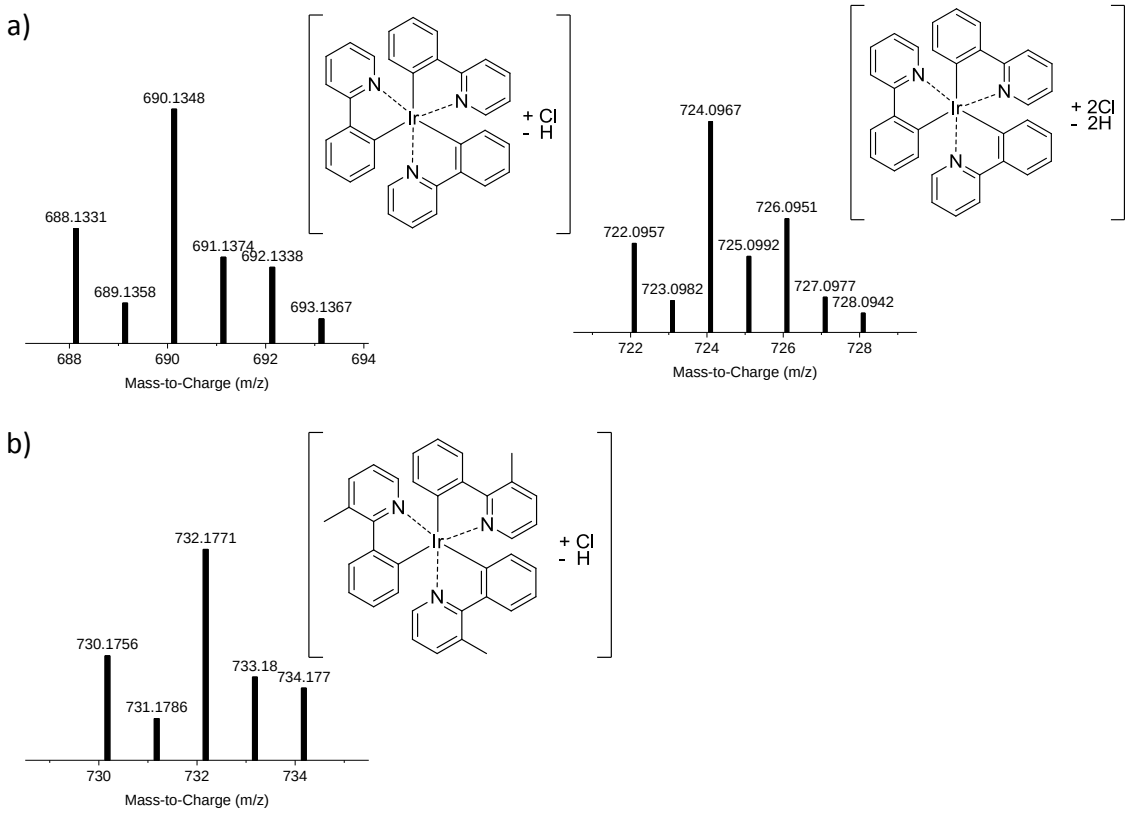

Figure 3-4: Mass spectra of the identified halogenated degradation products of a) $Ir(ppy)_3$ after 200 min of irradiation in DCM and b) $Ir(Me\text{-}ppy)_3$ after 120 min of irradiation in DCM (obtained from the LC-MS analysis of the respective samples).

3.2.3 THE INFLUENCE OF OXYGEN

As cyclometalated Ir-complexes are very efficient singlet oxygen sensitizers, we wanted to investigate the influence of oxygen on the photostability of the compounds. $^1O_2$ is known to undergo a variety of reactions with nitrogen heterocycles[18] and might thus attack the emitters, leading to the formation of a variety of deterioration products. We therefore performed the irradiation experiments in different solvents under atmospheric as well as inert conditions (freeze-pump-thaw, then argon atmosphere). All compounds were irradiated in DCM and toluene as mentioned above, but also in benzene and benzene-d6. Singlet oxygen has a significantly higher lifetime in deuterated solvents, resulting in an enhancement of processes induced by this highly reactive species. The comparison of degradation rates in benzene and benzene-d6 should therefore help to elucidate the role singlet oxygen plays in the degradation of these materials as the degradation should be faster under atmospheric conditions than under inert atmosphere and show a further increase when performed in benzene-d6.

Other processes, possibly competing with the above singlet oxygen induced degradation route can be proposed to proceed via the excited state of the emitter molecule. This might be due to instability of the excited molecule itself, via interaction of the excited molecule with its local environment or even other excited states. [16, 19-20] Supposed the molecule is not susceptible to an attack of $^1O_2$, it would be expected that the presence of oxygen in this case actually increases the photostability of the material. This is due to the very fast quenching of the excited state by O_2,[21] leading to a significantly shorter lifetime of the excited states and consequently a reduced degradation rate for processes induced via those states.

The observations from the photodegradation experiments suggest strong differences in the contribution of these two pathways for the four examined compounds. We therefore discuss the photodegradation behavior and the observed degradation products individually for each of the emitters.

The investigations in DCM under both ambient and inert conditions showed the same trend as those in benzene for all complexes. Within the range of measurement accuracy, no differences in the degradation behavior between experiments in toluene and benzene were observable. For clarity, only the results of the measurements in benzene and benzene-d6 are therefore depicted and discussed in the following part (the supporting information provides the additional experimental degradation data).

3.2.4 IR(PIQ)$_3$

As mentioned above, red emitting Ir(piq)$_3$ is one of the most unstable compounds in the series of complexes investigated here. Irradiation in benzene under atmospheric conditions led to fast degradation with only about 10% of the initial concentration after 30 min of irradiation (Figure 3-5). Under the exclusion of oxygen, however, the degradation is suppressed significantly. Therefore, reactive oxygen species are likely to be responsible for the decomposition of Ir(piq)$_3$. Experiments in deuterated benzene under atmospheric conditions support this assumption showing more than 80% decrease in the complex concentration after only 5 min of irradiation. The observation that the degradation is also considerably faster in deuterated benzene under inert conditions might be attributed to the fact that a quantitative removal of oxygen is unlikely by the employed procedure. The repeated punctuation of the septa by the injector needle of the HPLC-autosampler might further allow small quantities of oxygen to enter the sample vial. This suggests that only traces of oxygen can have a pronounced effect on the durability of the complexes.

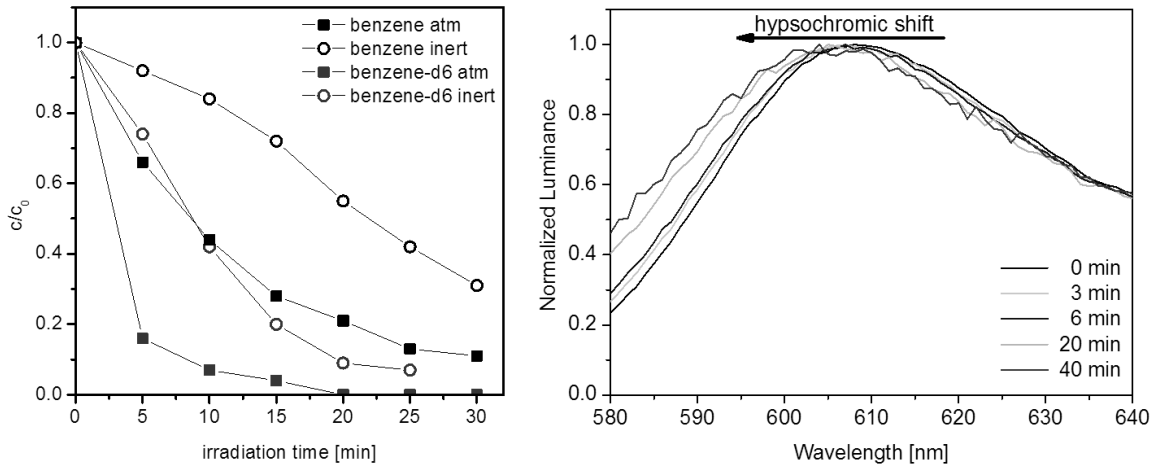

Figure 3-5. Degradation curves of Ir(piq)$_3$ in benzene and benzene-d6 under ambient and inert conditions (left). Hypsochromic shift of the phosphorescence of an Ir(piq)$_3$ doped PMMA film with increased irradiation time (right).

Incorporation of the complex in a PMMA matrix leads to similar degradation rates at the beginning of the experiment (Figure 3-3). However, after 15 -20 min of irradiation, the luminance changes decrease significantly. A possible explanation is the formation of degradation products which are still capable of phosphorescent emission, albeit at lower

luminescence quantum efficiencies. This rational is supported by comparing the normalized phosphorescence spectra after consecutive irradiation periods (Figure 3-5). A hypsochromic shift and signal broadening with increased irradiation times is observed, indicating the presence of other species contributing to the emission.

In fact, the HPLC-DAD chromatograms of the soluble samples show that the decrease of the complex signal is accompanied by the emergence of two new peaks (Figure 3-6). These degradation products can be assigned to the m/z values 811 (①) and 824 (②) respectively. Despite NMR investigations of the decomposed sample, the structure of these two products could not be elucidated so far.

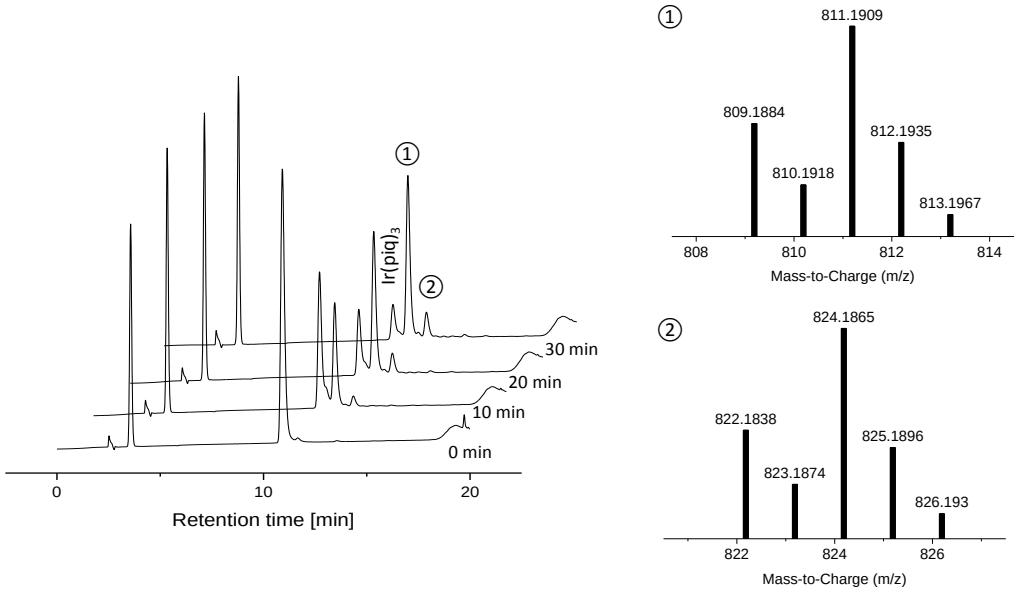

Figure 3-6. DAD chomatogram showing the formation of two main degradation products (left) and their assigned mass spectra (right).

3.2.5 IR(PPY)$_3$

In contrast, for the green emitting Ir(ppy)$_3$ the presence of oxygen in benzene has a beneficial effect on the compounds stability. This is likely due to the ability of oxygen to quench the triplet excited state of the complex, thus preventing degradation through this state (Figure 3-7). Newly formed species, substantiating the contribution of the excited state on the complexes degradation, were identified via HPLC/MS analysis: the m/z value of 501 can be assigned to a species formed by the dissociation of one phenylpyridine ligand (③, Figure 3-8). This literature known phenomenon can be explained by the population of higher lying metal-centered states leading to bond rupture.[9-10, 22-23]

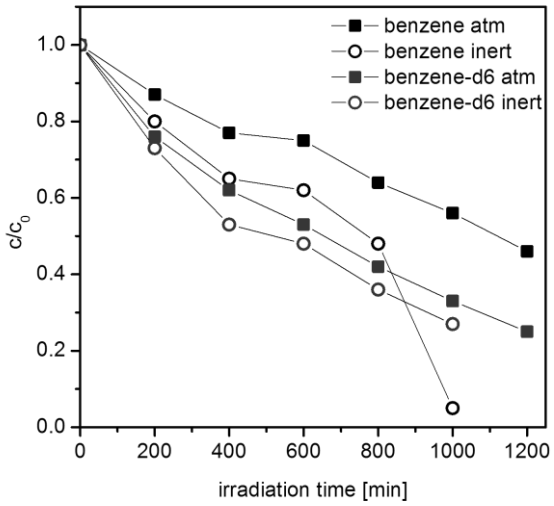

Figure 3-7. Degradation curves of Ir(ppy)$_3$ in benzene and benzene-d6 under ambient and inert conditions.

Mass spectrometric investigations revealed the formation of three additional degradation products with the m/z values 603, 632 and 686, respectively. For the latter, an oxygenated species [Ir(ppy)$_3$+2O-2H] ④ can be assumed (Figure 3-8). However, the very small amounts did not allow for additional analyses by NMR to confirm the suggested structures.

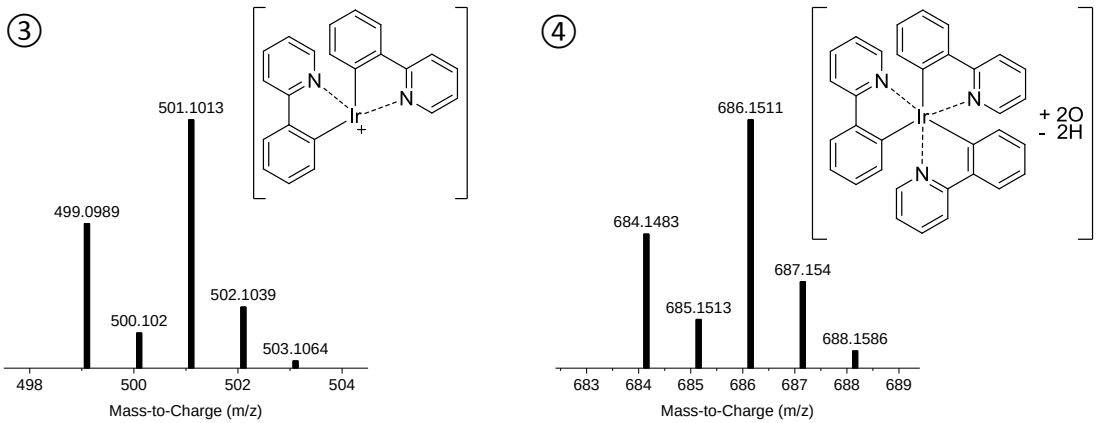

Figure 3-8: Mass spectra of two degradation products of $Ir(ppy)_3$ with the assigned structures.

3.2.6 IR(ME-PPY)$_3$

As already observed for $Ir(ppy)_3$, the methylated derivative $Ir(Me\text{-}ppy)_3$ degrades much faster under inert than under atmospheric conditions in benzene (Figure 3-9), which indicates the degradation via excited state induced processes. The same trend can be observed in benzene-d6 albeit with a significantly diminished stability.

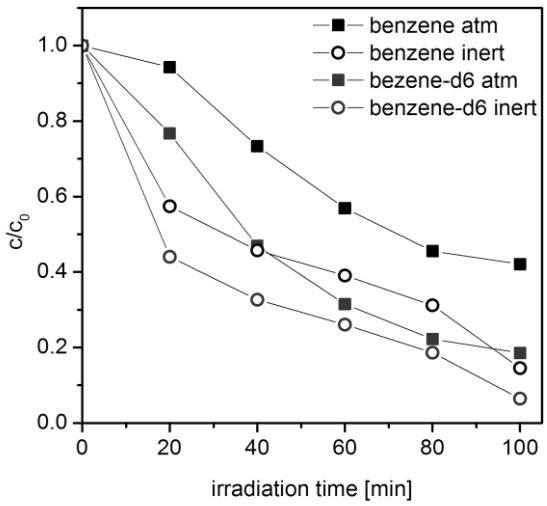

Figure 3-9. Degradation curves of $Ir(Me\text{-}ppy)_3$ in benzene and benzene-d6 under ambient and inert conditions.

According to the DAD chromatogram, the decrease of the complex signal with the irradiation time was accompanied by the formation of only one visible degradation product with a mass of 712 (MH^++14). This species was attributed to the aldehyde functionalized complex derivative

(⑤, Figure 3-10), as the carbonyl functionality was confirmed by NMR spectroscopy with a signal at 10.5 ppm as well as IR spectroscopy with a typical signal at around 1700 cm^{-1}. As it is known that singlet oxygen can oxidize methyl substituted aromatic systems to form aromatic aldehydes,[24] this proposed structure is in good agreement with the course of the degradation curve of the experiments in benzene-d6 under ambient conditions. The increased lifetime of $^1O_2$ in the deuterated solvent enhances the complex oxidation. Nonetheless, the observation that the degradation proceeds fastest under inert conditions in deuterated benzene cannot be explained with this deterioration model. As this behavior can also be observed for the green analogue $Ir(ppy)_3$ (Figure 3-7) the contribution of another, still unidentified, deterioration pathway is most likely.

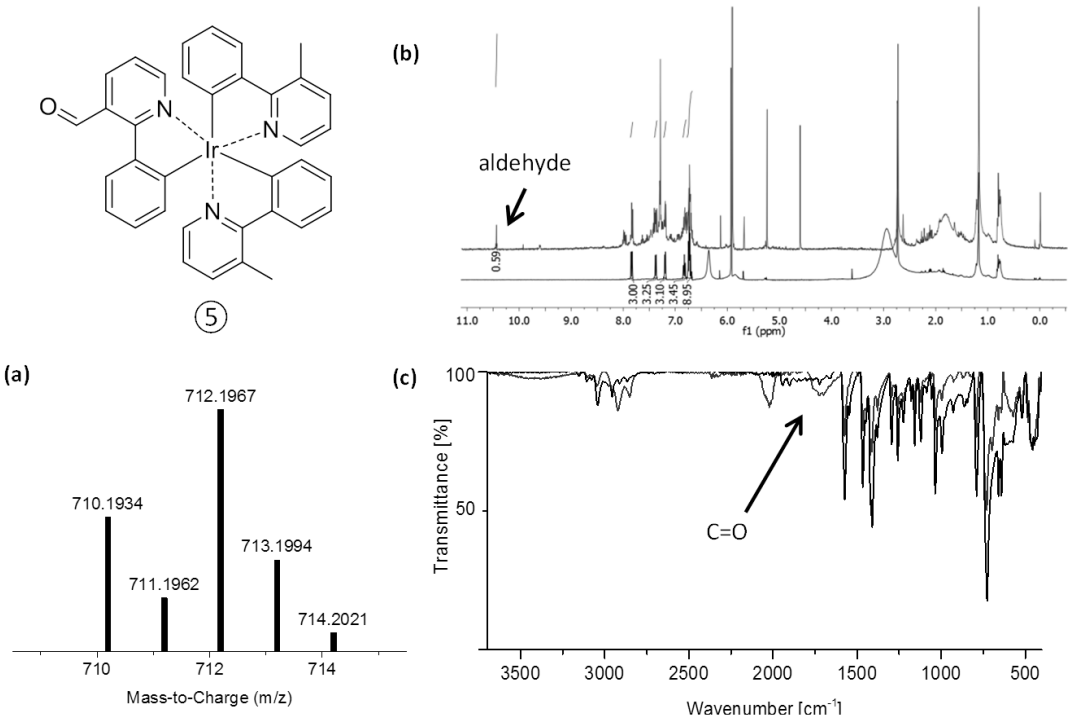

Figure 3-10. Structure of the main degradation product of $Ir(Me\text{-}ppy)_3$ as confirmed by mass spectrometry (a), NMR (b) and IR (c) spectroscopy. (b) NMR spectra of $Ir(Me\text{-}ppy)_3$ before (black) and after (red) irradiation, showing an arising aldehyde signal at 10.5 ppm. (c) IR spectra of $Ir(Me\text{-}ppy)_3$ before (black) and after (red) irradiation, showing an emerging carbonyl signal at around 1700 cm^{-1}.

3.2.7 IR(F,CN-PPY)$_3$

The degradation behavior of the blue emitting Ir(F,CN-ppy)$_3$ is more complex. The solubility of this compound in all chosen solvents was poor and the complex turned out to be very unstable in solution even without irradiation: after one day in the dark, the DAD signal of this complex decreased by half in toluene, benzene and benzene-d6. Therefore, the reproducibility of the experiments was not satisfying. Reliable results were only achieved for the measurements in toluene under atmospheric conditions, with an estimated error of ~ 10% (Figure 3-11). The experiment in benzene and benzene-d6 under ambient conditions showed similar degradation behavior. Under inert conditions, no reliable dataset could be obtained.

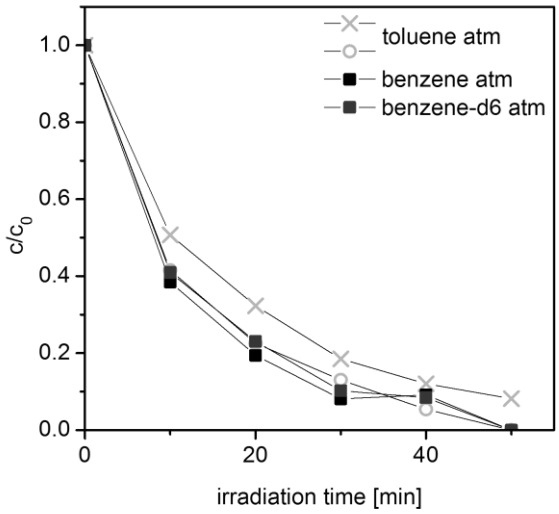

Figure 3-11. Degradation curves of Ir(F,CN-ppy)$_3$ in benzene and benzene-d6 and toluene under ambient conditions.

Expected degradation products like species formed by fluorine cleavage, which were reported previously for blue emitting iridium analogues,[25-26] could not be observed. This might be due to the generally poor ionization of the complex. Only small traces of a degradation product with m/z =816 were detected (⑥, Figure 3-12), which may correspond to a double oxidized derivative [Ir(F,CN-ppy)$_3$ +2O].

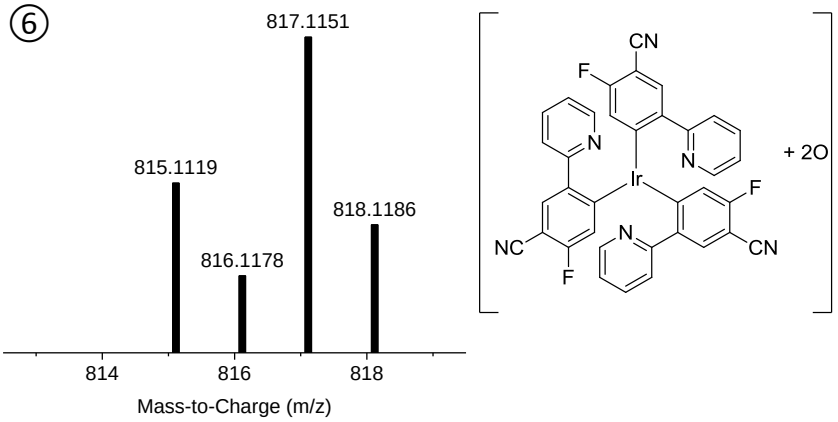

Figure 3-12. Mass spectrum of the detected degradation product of Ir(F,CN-ppy)$_3$, which matches a twofold oxidized derivative with regard to its m/z value and the corresponding isotope pattern.

3.3 CONCLUSIONS

In conclusion, we have investigated the degradation behavior of four well established iridium emitters. The general stability of these complexes in solution and thin solid films follows the trend Ir(ppy)$_3$ > Ir(Me-ppy)$_3$ > Ir(piq)$_3$ (~ Ir(F,CN-ppy)$_3$). Irradiation of the samples in different solvents and under atmospheric as well as inert conditions allowed us to suggest several pathways that can contribute to the deterioration of these compounds.

DCM as a representative of halogenated solvents has a detrimental influence on the stability of the compounds. The fast deterioration in this solvent and the identification of chlorinated species after the irradiation experiments for Ir(ppy)$_3$ and Ir(Me-ppy)$_3$ support the general notion that halogenated solvents should be avoided for these complexes when possible.

Utilizing the enhanced lifetime of $^1O_2$ in deuterated solvents, we showed that the emitters can be very susceptible to singlet oxygen induced degradation depending on their structure. This pathway was identified as the predominant degradation mechanism for the red emitting Ir(piq)$_3$. Ir(Me-ppy)$_3$ also showed sensitivity towards reactive oxygen species and an oxidized deterioration product could be identified after irradiation. The very fast degradation under the influence of oxygen and light emphasizes the necessity to process the devices and handle and store the materials under inert atmosphere and the exclusion of light whenever possible.

While the mechanisms for these reactions can be manifold and the exact structural identification of specific products is very difficult, the results suggest a strong contribution of degradation via the excited state. These processes are likely also the ones that are most relevant for the operational degradation of these compounds in OLEDs. We could for example observe the dissociation of one phenylpyridine ligand for $Ir(ppy)_3$, a product that has been identified in aged OLEDs as well.[7]

However, the photodegradation of these materials is complex and likely caused not only by one but many different mechanisms. Observations indicating the contribution of the excited states, singlet oxygen, and possibly other unidentified pathways to the degradation of $Ir(Me\text{-}ppy)_3$ show that the different mechanisms are competing for this emitter.

The results from this study furthermore show how even small changes in the ligand structure can have a huge impact not only on the rate but also on the mechanisms of their degradation. The comparison between $Ir(ppy)_3$ and $Ir(Me\text{-}ppy)_3$ is particularly striking as they only differ in one methyl group. Knowledge on the mechanisms and products may contribute to understand degradation processes occurring during device operation but also to avoid adverse conditions such as halogenated solvents, light or oxygen during preparation, storage and handling of these materials. This can prevent the formation of degradation products that might be detrimental to the stability of organic light emitting devices.

3.4 EXPERIMENTAL PART

The complexes were provided by Merck KGaA. The solvents were purchased from Merck KGaA, Acros and Sigma Aldrich and were used as received without further purification. Toluene and benzene were used in p.a. quality. DCM, THF and hexane were LiChrosolv solvents *Photodegradation studies of the liquid samples:* The complexes were dissolved in the appropriate solvent (50 µM). 1 mL of the resulting solution was transferred to a headspace vial and sealed with a silicone/PTFE septum. Two samples were prepared from each complex for the testing under atmospheric and inert conditions. In case of the photodegradation studies under inert conditions, the vials were degassed via 3 consecutive freeze-pump thaw cycles under argon. All samples were irradiated in a custom made irradiation unit (SIM GmbH). It consists of an aluminum printed circuit board with 30 400 nm LEDs (350mW, Edison Edixeon 3W Emitter, [LT-1467]), connected to a cooling unit, that ensures a constant temperature of 20 °C of the board during the irradiation. Two 15 sample chromatography trays can be placed in the unit so that each of the sample vials is centered over one LED (d = 1 cm). The irradiation intervals were chosen individually for each complex according to the overall lifetime. After each irradiation cycle, the samples were analyzed via HPLC (see below). The remaining emitter concentration was determined via integration of the DAD signal at 305 nm in relation to that of an external standard (quaterphenyl in toluene, 0.026 mM). For each investigated compound the measurements in toluene under atmospheric conditions were performed at least twice to check for the accuracy of the measurement (< 10%, see supporting information).

Analysis of the liquid samples and identification of degradation products: The analysis was performed on an Agilent Technologies 1200 HPLC/MS system consisting of a binary pump SL [G1312B], a degasser [G1379B], an *Infinity* high performance micro autosampler [G1329B] with thermostat [G1330B], a thermostatted column compartment [G1316B], an *Infinity* diode-array detector (DAD) [G4212B] and an accurate mass Q-TOF/MS [G6530A] with an APCI (atmospheric pressure chemical ionization) ion source. The column used was a HIbar® 250 mm x 4 mm x 5µm diol column (Merck KGaA). For NMR and IR investigations, the solvent (toluene) was removed from the irradiated sample in a nitrogen stream. NMR spectra of the in deuterated tetrachloroethane (TCE-d2) were recorded on a Bruker Avance 400 (400.13 MHz for 1H and 100.03 MHz for 13C) spectrometer. IR spectra of the solid samples were recorded on a BIO-RAD Excalibur IR spectrometer.

Photodegradation studies of the PMMA substrates: PMMA and the complex (0.17 wt%) were dissolved in DCM and spin coated on a glass substrate. The films were irradiated as described for the liquid samples. The analysis of the PMMA substrates was performed on a *HORIBA Scientific* Fluoromax-4 spectrofluorometer using a solid sample holder, which ensures an accurate positioning of the substrate for the measurement. The c/c_0-values were determined via the ratio of the integrated phosphorescence spectra after irradiation to its initial value. All measurements were performed twice to check for the accuracy of the measurement (< 5%, see supporting information).

3.5 REFERENCES:

[1] M. A. Baldo, D. F. O'Brien, Y. You, A. Shoustikov, S. Sibley, M. E. Thompson, S. R. Forrest, *Nature* **1998**, *395*, 151-154.

[2] S. Reineke, F. Lindner, G. Schwartz, N. Seidler, K. Walzer, B. Lussem, K. Leo, *Nature* **2009**, *459*, 234-238.

[3] D. Y. Kondakov, W. C. Lenhart, W. F. Nichols, *J. Appl. Phys.* **2007**, *101*, 024512-024517.

[4] H. Z. Siboni, H. Aziz, *Appl. Phys. Lett.* **2012**, *101*, 063502-063504.

[5] D. Y. Kondakov, T. D. Pawlik, W. F. Nichols, W. C. Lenhart, *Journal of the Society for Information Display* **2008**, *16*, 37-46.

[6] I. R. de Moraes, S. Scholz, B. Lüssem, K. Leo, *Organic Electronics* **2012**, *13*, 1900-1907.

[7] I. R. de Moraes, S. Scholz, B. r. Lüssem, K. Leo, *Appl. Phys. Lett.* **2011**, *99*, 053302.

[8] R. Meerheim, S. Scholz, S. Olthof, G. Schwartz, S. Reineke, K. Walzer, K. Leo, *J. Appl. Phys.* **2008**, *104*, 014510-014518.

[9] I. R. d. Moraes, S. Scholz, B. Lüssem, K. Leo, *Organic Electronics* **2011**, *12*, 341-347.

[10] S. Scholz, C. Corten, K. Walzer, D. Kuckling, K. Leo, *Organic Electronics* **2007**, *8*, 709-717.

[11] S. Scholz, R. Meerheim, K. Walzer, K. Leo*, Vol. 6999*, 1 ed. (Eds.: P. L. Heremans, M. Muccini, E. A. Meulenkamp), SPIE, Strasbourg, France, **2008**, pp. 69991B-69910.

[12] S. Scholz, K. Walzer, K. Leo, *Adv. Funct. Mater.* **2008**, *18*, 2541-2547.

[13] S. Winter, S. Reineke, K. Walzer, K. Leo*, Vol. 6999*, 1 ed. (Eds.: P. L. Heremans, M. Muccini, E. A. Meulenkamp), SPIE, Strasbourg, France, **2008**, pp. 69992N-69998.

[14] N. C. Giebink, B. W. D'Andrade, M. S. Weaver, P. B. Mackenzie, J. J. Brown, M. E. Thompson, S. R. Forrest, *J. Appl. Phys.* **2008**, *103*, 044509.

[15] N. C. Giebink, B. W. D'Andrade, M. S. Weaver, J. J. Brown, S. R. Forrest, *J. Appl. Phys.* **2009**, *105*, 124514-124517.

[16] T. Sajoto, P. I. Djurovich, A. B. Tamayo, J. Oxgaard, W. A. Goddard, M. E. Thompson, *J. Am. Chem. Soc.* **2009**, *131*, 9813-9822.

[17] A. Hohenleutner, S. Schmidbauer, R. Vasold, D. Joosten, P. Stoessel, H. Buchholz, B. König, *Adv. Funct. Mater.* **2012**, n/a-n/a.

[18] M. V. George, V. Bhat, *Chem. Rev. (Washington, DC, U. S.)* **1979**, *79*, 447-478.

[19] N. C. Giebink, B. W. D'Andrade, M. S. Weaver, P. B. Mackenzie, J. J. Brown, M. E. Thompson, S. R. Forrest, *J. Appl. Phys.* **2008**, *103*, 044509.

[20] M. A. Baldo, C. Adachi, S. R. Forrest, *Phys. Rev. B* **2000**, *62*, 10967-10977.

[21] H. Yersin, A. F. Rausch, R. Czerwieniec, T. Hofbeck, T. Fischer, *Coord. Chem. Rev.* **2011**, *255*, 2622-2652.

[22] I. R. de Moraes, S. Scholz, B. Lussem, K. Leo, *Appl. Phys. Lett.* **2011**, *99*, 053302-053303.

[23] S. Scholz, R. Meerheim, B. Lussem, K. Leo, *Appl. Phys. Lett.* **2009**, *94*, 043314-043313.

[24] A. G. Griesbeck, M. Cho, *Org. Lett.* **2007**, *9*, 611-613.

[25] V. Sivasubramaniam, F. Brodkorb, S. Hanning, H. P. Loebl, V. van Elsbergen, H. Boerner, U. Scherf, M. Kreyenschmidt, *J. Fluorine Chem.* **2009**, *130*, 640-649.

[26] R. Seifert, I. Rabelo de Moraes, S. Scholz, M. C. Gather, B. Lüssem, K. Leo, *Organic Electronics* **2013**, *14*, 115-123.

CHAPTER 4

4. NEW IRIDIUM PHOTOCATALYSTS WITH INCREASED REDUCTIVE POWER IN THE EXCITED STATE*

* Theoretical calculations by Christian Ehrenreich (Merck KGaA Darmstadt). Cyclic voltammetry data of the quenchers **3-8** were obtained by Maria Cherevatskaya and Durga Prasad Hari. Excited state lifetime and photoluminescence quantum yield for compound **2** was measured by Markus Leitl (group of Prof. Dr. Hartmut Yersin, University of Regensburg). All other experiments (synthesis, cyclic voltammetry, UV-Vis and Fluorescence spectroscopy, Stern-Volmer quenching experiments) as well as analysis and interpretation of the data was performed by Andreas Hohenleutner.

4.1 INTRODUCTION

Harnessing the energy of light to drive organic transformations has been a long standing ideal for the scientific community[1] and there are reports of photochemically induced organic transformations dating back as far as a century.[2] Nevertheless, it was only recently that the emerging field of visible-light photoredox catalysis has excited widespread interest and recognition with synthetic chemists.[3-6] Photosensitizers that absorb light in the visible region and readily donate or accept an electron in their excited states enable the activation of a broad range of substrates for synthetic transformations. The employed photosensitizers can be organic dyes,[7] organo-transition metal complexes and even inorganic or organic semiconductors.[8] Upon absorption of visible light, the photocatalyst in its excited state can either accept an electron from another molecule (reductive quenching) to give the reduced form of the sensitizer or transfer an electron to another molecule (oxidative quenching) yielding the oxidized sensitizer (see Figure 4-1).

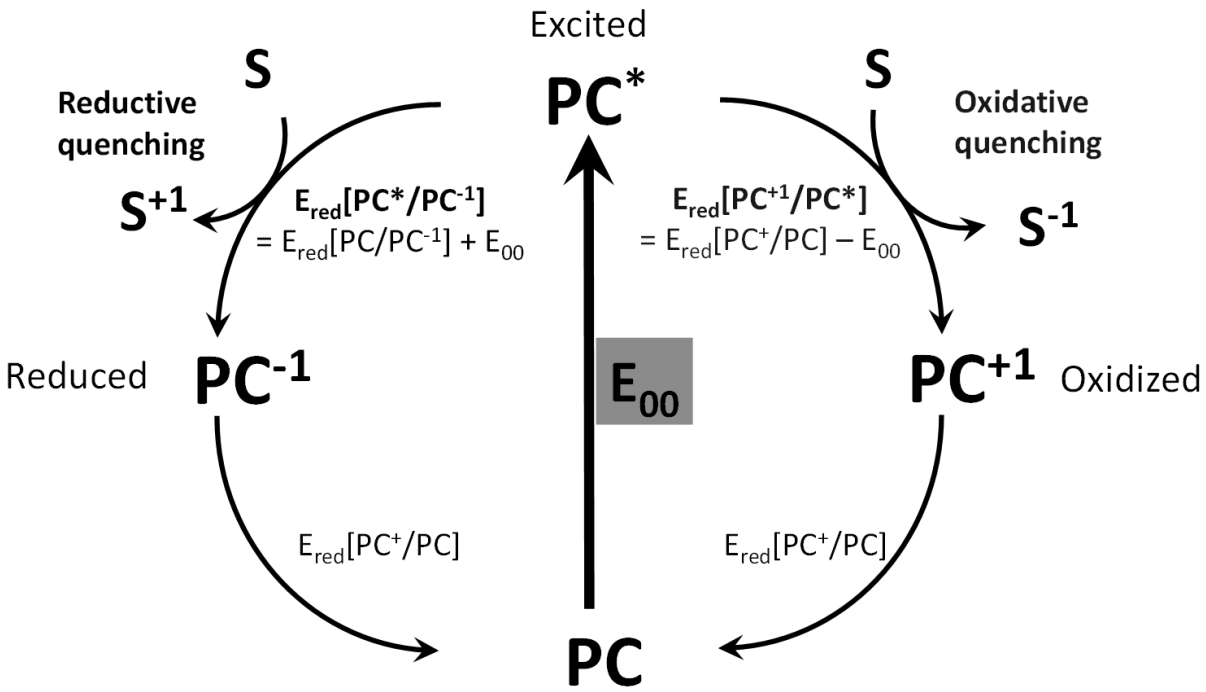

Figure 4-1: Schematic representation of oxidative and reductive quenching cycles of a photocatalyst. The arrow directions do not represent the direction of the corresponding potentials but rather the progression of the reaction.

The reductive/oxidative power of a photocatalyst in its excited state is determined by the energy difference between the photocatalytically active excited state and the reduced/oxidized form of the sensitizer. The excited state reduction and oxidation potentials can thus be estimated using the oxidation or reduction potentials in the ground state and the $E_{0.0}$ energy according to:[9]

$$E_{red}[PC^*/PC^{-1}] = E_{red}[PC/PC^{-1}] + E_{0,0} \text{ (reductive quenching)}$$

$$\text{and} \quad E_{red}[PC^{+1}/PC^*] = E_{red}[PC^{+}/PC] - E_{0,0} \text{ (oxidative quenching)}$$

$E_{0.0}$ is the zero-zero transition energy and can be estimated by using the maximum emission energy of the compound. It should be noted however, that significant errors are to be expected when using this approximation for organic dyes: The emission from these compounds usually occurs from the singlet excited state while the electron transfer occurs mostly via the triplet state, which can be significantly lower in energy.

Especially transition metal complexes have been extensively used as photoredox catalysts as they offer several advantages: First and foremost, the photophysical properties of these compounds have been extensively studied,[10-12] allowing for a better understanding of their behavior in photochemical transformations. Another desired property is their absorption at higher energies compared to the most commonly employed organic dyes. The reductive or oxidative power of the excited photocatalyst scales directly with the energy of the $E_{0,0}$ transition and the activation of challenging substrates is thus only possible with sufficiently high excitation energies. In addition, since electron transfer occurs from the triplet state, for a high performance photocatalyst a high triplet yield is imperative. Transition metal complexes exhibit a large spin orbit coupling leading to a very efficient inter system crossing, thus increasing the fraction of excitation events that lead to formation of the desired triplet states.[11]

Iridium complexes in particular exhibit very high reductive power in their excited state and have been successfully employed for the activation of challenging substrates such as benzyl, alkyl and aryl halides for oxidative quenching reactions. Furthermore, by careful modification of the ligand structure, it is possible to tune the HOMO/LUMO and emission energies in this class of compounds.[13] Figure 4-2 shows calculated HOMO and LUMO orbitals for $Ir(ppy)_3$ (a popular OLED emitter that has recently also found applications as a high reductive power photocatalyst[14-15]). It is to the best of our knowledge the compound with the highest reductive power that has been applied as a sensitizer in photoredox catalysis to date.

Although choosing a catalyst with appropriate photoredox properties has in several cases enabled the conversion of otherwise unreactive substrates,[14-15] these studies all used known and available complexes. The aim of this study was to design a new iridium based photocatalyst with specifically tailored photoredox properties for use in oxidative quenching photoredox catalysis. A sensitizer with an increased reductive power in the excited state could open up the possibility of performing photocatalytic transformations with challenging non-activated substrates that are not accessible with photocatalysts available today.

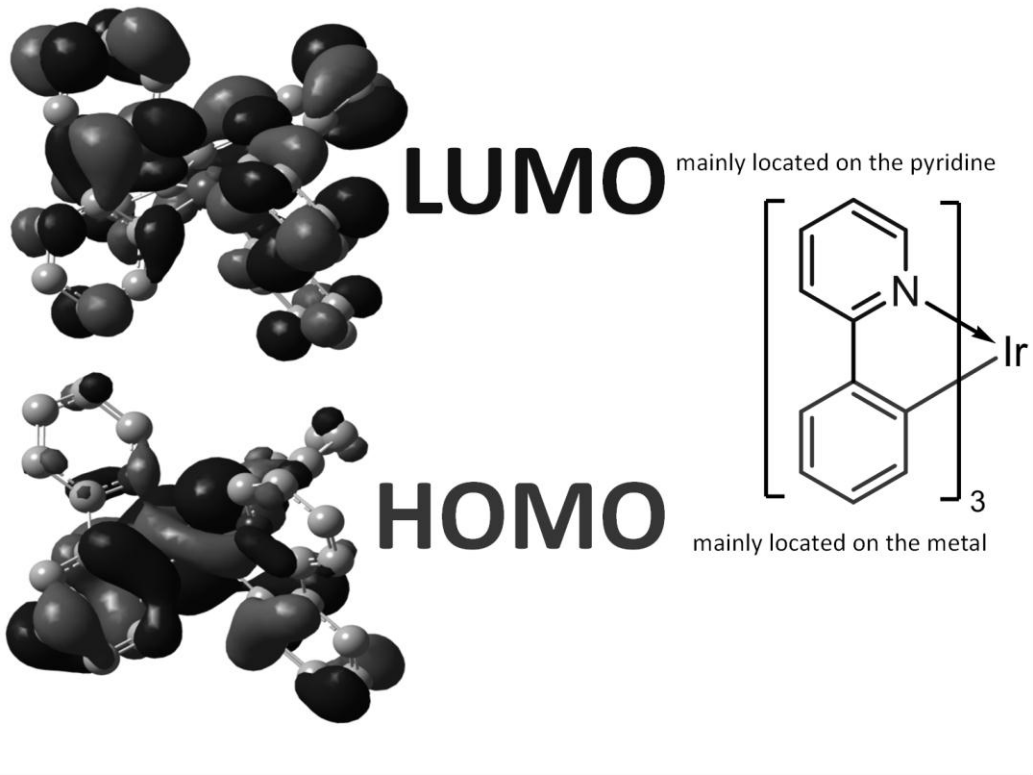

Figure 4-2: Calculated HOMO (top) and LUMO (bottom) orbitals of $Ir(ppy)_3$.

While the HOMO is mainly located on the metal and the phenyl ring of the cyclometallated ligand, the LUMO is located on the ligand and particularly on the pyridine ring. Substitution on the phenyl part of the ligand, especially para to the Ir-C bond changes the electron donation to the metal via the metal-carbon bond. This affects mainly the metal centered HOMO of the complex. Alterations on the pyridine ring on the other hand have a stronger impact on the energy of the LUMO since the LUMO is ligand centered and mostly located on the pyridine. The

orbital distribution also illustrates the strong MLCT character with contributions from ligand centered (LC) transitions.

4.2 RESULTS AND DISCUSSION

We expected that the introduction of a strongly electron donating group on the pyridine ring of the ligand in para position to the nitrogen atom should significantly lift the LUMO energy and thus increase the reductive power of the complex in the excited state. To judge the impact of such a modification, time dependent density functional theory (TD-DFT) calculations were performed on the geometry optimized structures of $Ir(ppy)_3$ and compound **1**. The obtained energy levels were corrected by a linear function based on empirical data (provided by Merck KgaA). The results showed that the introduction of the dimethyl amino group not only results in the expected higher LUMO energies but also increases the HOMO energies (see table 1). The more positive LUMO energies translate into a lower oxidation potential and should therefore additionally increase the excited state reduction potential.

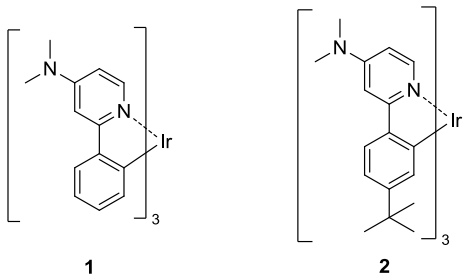

Figure 4-3: Structures of **1** and **2**.

Compound **1** was synthesized according to scheme 1 via a substitution reaction of 2,4-dibromopyridine with dimethyl amine in ethanol followed by a Suzuki-Miyaura coupling with phenylboronic acid and subsequent cyclometallation with the metal precursor $Ir(acac)_3$. The product was obtained as a yellowish-green precipitate but proved to be insoluble in all commonly used laboratory solvents. Although the solubility was not sufficient to obtain NMR spectra of the compound, the identity of **1** could be supported via high resolution mass spectroscopy and the detailed photophysical characterization (see chaper 5).

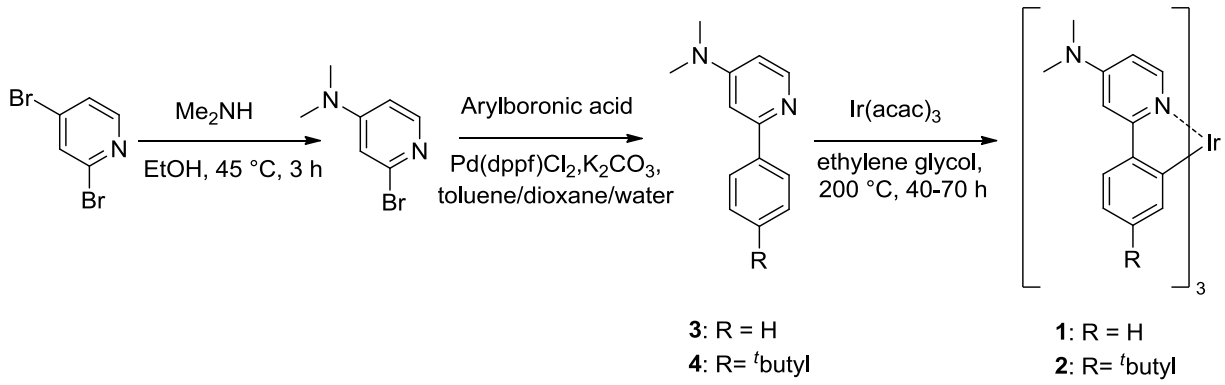

Scheme 4-1: Synthesis of compounds **1** and **2**.

To increase the solubility of the complex, compound **2** was synthesized following the same synthetic pathway. The ^{t}butyl group in the 4'-position of the phenyl ring indeed increased the solubility substantially. DFT calculations were also performed on **2** and suggest that the electronic influence of the ^{t}butyl group in this position does not have a significant impact on the energy levels of the HOMO and LUMO in this compound and should therefore also not have any negative impact on the photoredox properties. Table 4-1 summarizes the calculated values of the HOMO and LUMO energies for $Ir(ppy)_3$, **1** and **2**.

Table 4-1: HOMO and LUMO energy levels obtained via time dependent DFT calculations.

	$HOMO_{calculated}$	$LUMO_{calculated}$
$Ir(ppy)_3$	-4.95 eV	-1.25 eV
Compound **1**	-4.46 eV	-0.68 eV
Compound **2**	-4.46 eV	-0.68 eV

Data were obtained using Gaussian 09W. For computational details on the calculations see the experimental section

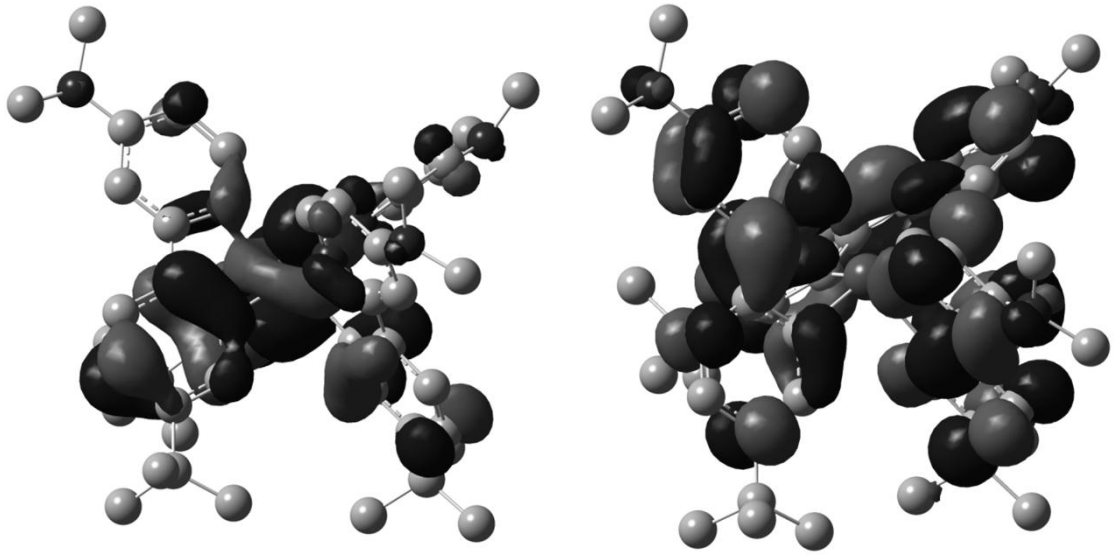

Figure 4-4: HOMO (left) and LUMO (right) orbitals of compound **2.**

The complex exhibits strong phosphorescence with a peak at 510 nm at room temperature in a deaerated DCM solution. The strong LC absorption band at 265 nm and the MLCT band at ~385 nm are both slightly shifted to higher energies compared to the unsubstituted $Ir(ppy)_3$. Cyclic voltammetry measurements were performed to determine the oxidation and reduction potentials of the compound in order to calculate the reductive power of the complex in the excited state. Compound **2** showed a reversible oxidation at a half wave potential of -2.56 V and two reversible reductions at -2.56 V and -2.80 V vs. SCE (in DMF).

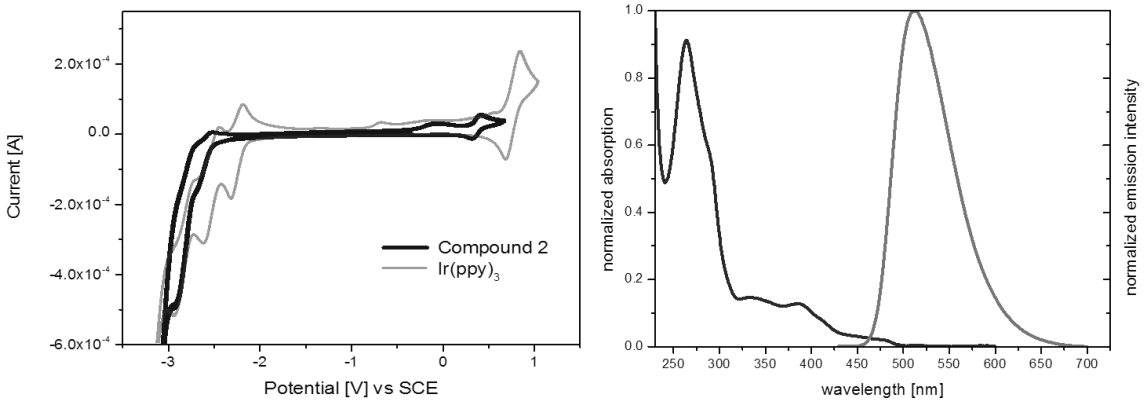

Figure 4-5: Left: Cyclic voltammograms of $Ir(ppy)_3$ (grey) and compound **2** (blue) measured in DMF. Right: Absorption (red) as well as emission spectrum (green) of **2** in DCM at room temperature.

The next step in evaluating the potential of the new photocatalyst was to perform Stern-Volmer quenching studies with the new compound as well as with two already known and well characterized iridium complexes. Table 4-2 gives an overview on electrochemical data, derived energy levels and excited state reduction potentials as well as decay times of the three complexes.

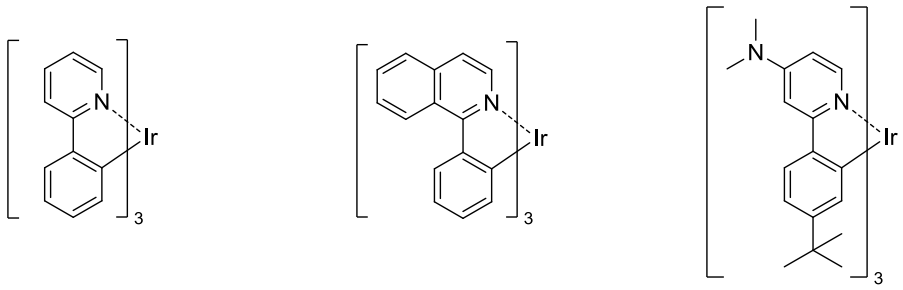

$Ir(ppy)_3$ $Ir(piq)_3$ **2**

Figure 4-6: Structures of the investigated Iridium complexes.

Table 4-2: Comparison of the ox/red-potentials, energy levels, reductive power in the excited state and decay times of **2** with $Ir(ppy)_3$ and $Ir(piq)_3$.

	$E_{1/2}$ (Ox) (vs SCE)[a]	*$E_{1/2}$ (Red) (vs SCE)[a]*	*E (HOMO)[b]*	*E (LUMO)[b]*	*Emission*	*$E_{1/2}(C^*/C^+)$ (vs SCE) [c]*	*decay time[d]*
Ir(ppy)3	***0.77 V***	***-2.19 V***	***-5.17 eV***	***-2.21 eV***	***2.42 eV***	***-1.65***	***1.6 (1.4)[11]***
2	***0.42 V***	***-2.56 V***	***-4.82 eV***	***-1.84 eV***	***2.43 eV***	***-2.01***	***0.76 (0.82)***
Ir(piq)3	***0.59 V***	***-1.5 V***	***-4.99 eV***	***-2.91 eV***	***2.00 eV***	***-1.41***	***1.3(1.25)[11]***

[a]determined via cyclic voltammetry. [b]calculated via: E(HOMO/LUMO) = -(4.4 + $E_{1/2\ ox/red}$). [c]calculated via $E_{1/2}(C^*/C^+) = E_{1/2\ ox} - \Delta E$ (Emission). [d]**2** and $Ir(ppy)_3$ were measured in 2-Me-THF, $Ir(piq)_3$ in CH_2Cl_2 – the values in brackets were measured in a spincoated PMMA polymer matrix thin film.

The phosphorescence quenching of these catalysts by substrates with different reduction potentials was studied in order to establish a correlation between the properties of the photocatalyst and the rate of electron transfer. The bimolecular electron transfer process deactivates the excited state and thus leads to a quenching of luminescence intensity which is proportional to the concentration of the electron acceptor (quencher) present.

It can be described by the Stern-Volmer equation (1) where **I** and $\mathbf{I_0}$ are the emission intensities before and after addition of the quencher, $\mathbf{k_q}$ is the quenching constant and **[Q]** the concentration of the quenching species. The quenching constant $\mathbf{k_Q}$ can be expressed as $\boldsymbol{\tau k_2}$ – the product of the mean lifetime of the photoexcited state (decay time) and the rate constant for the bimolecular quenching process (the rate constant of electron transfer from the catalyst to the substrate).

$$I_0/I = 1 + k_Q[Q] = 1 + \tau k_2[Q] \qquad (1)$$

The different quenchers that were employed are depicted in Figure 4-7. The reduction potentials of the different compounds range from -0.30 V to -2.05 V vs. SCE (in DMF) due to the different electronic influence of the substituents. The more electron withdrawing the substitution of the aromatic ring, the easier the reduction of these compounds. Figure 4-8 exemplarily depicts the Stern-Volmer plot for the quenching of the three different catalysts with para-CN-benzyl bromide.

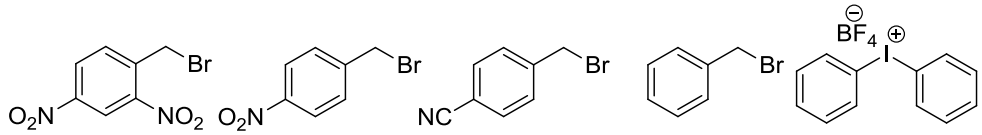

5 -0.30 V **6** -1.07 V **7** -1.70 V **8** -2.05 V **9** -1.0 V

Figure 4-7: Structures and their respective reduction potentials vs. (SCE) of the employed quenchers in the Stern-Volmer quenching studies with the different photocatalysts.

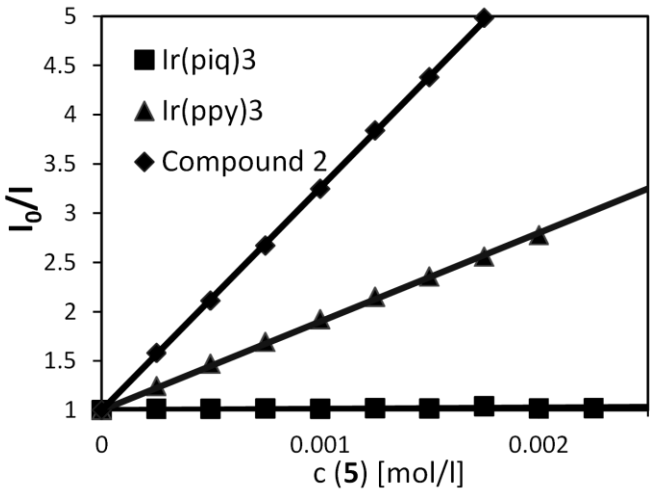

Figure 4-8: Stern-Volmer quenching plot for the phosphorescence quenching of $Ir(ppy)_3$, $Ir(piq)_3$, and **2** with 4-cyanobenzyl bromide.

Table 4-3 shows the determined quenching constants for the investigated catalyst-quencher combinations. According to Marcus theory of electron transfer, the electron transfer rate constant should scale with $-\Delta G_{ET}$ (the Gibbs free energy for the transfer of an electron from the catalyst to the substrate) which is true for the particular case of quencher **7** for example (Figure 4-8).[16-17] But even though **2** has a significantly higher reductive power in the excited state and ΔG_{ET} is therefore more negative, the observed quenching constant is often greater for $Ir(ppy)_3$ in comparison with **2**. The reason for this becomes obvious when keeping in mind that the quenching always competes with radiative and other non-radiative processes. The low excited state lifetime of only 0.76 μs ($Ir(ppy)_3$: 1.6 μs) thus leads to lower overall quenching rates.

Indeed, when looking at the pure rate constants for the electron transfer step (see Table 4-4), compound **2** exhibits significantly higher rates for almost all employed quenchers.

Table 4-3: Determined Stern-Volmer quenching constants.

	K_Q [mol^{-1}]				
Catalyst	***5***	***6***	***7***	***8***	***9***
Ir(piq)3	4.98E+03	3.15E+03	no quenching	no quenching	6.24E+01
Ir(ppy)3	1.43E+04	9.52E+03	9.00E+02	2.50E+01	9.49E+02
2	5.98E+03	6.67E+03	2.26E+03	5.36E+02	1.36E+03

The values for k_q were obtained as the slope of a linear regression fit for I_0/I as a function of the quenchers concentration with a fixed intercept of 1.

Table 4-4: Rate constants for the electron transfer calculated via $k_2 = k_Q/\tau$.

	$K_2\ [s^{-1}]$				
Catalyst	***5***	***6***	***7***	***8***	***9***
Ir(piq)3	3.83E+09	2.42E+09	No quenching	No quenching	4.80E+07
Ir(ppy)3	8.94E+09	5.95E+09	5.63E+08	1.56E+07	5.93E+08
2	7.87E+09	8.78E+09	2.97E+09	7.05E+08	1.79E+09

Marcus theory predicts that the electron transfer rates are the highest for a free energy change that is approximately equal to reorganization energy ($\lambda = -\Delta G_{ET}$) where λ is the energy necessary for distorting the acceptor and its surroundings (solvent reorganization) enough to reach the equilibrium state of the donor (see Figure 4-9). For $\lambda > -\Delta G_{ET}$, the rates increase with the driving force of the reaction (normal region) while for very large free energy changes ($\lambda < -\Delta G_{ET}$) the electron transfer rates decrease with the driving force. This counterintuitive phenomenon is called the Marcus inverted region.[16-17]

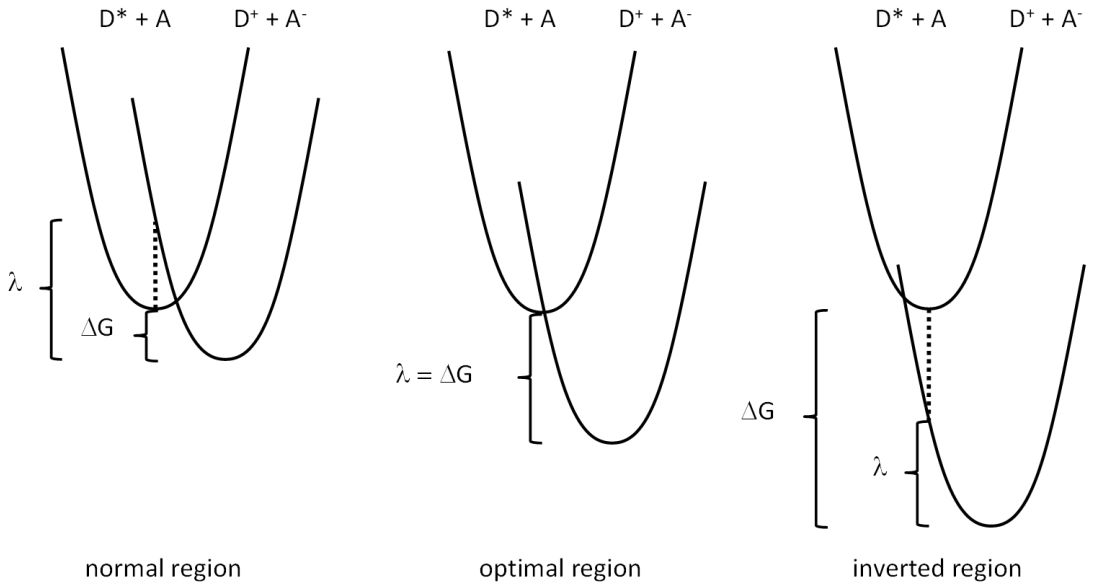

Figure 4-9: Normal ($\lambda > -\Delta G_{ET}$), optimal ($\lambda = -\Delta G_{ET}$) and inverted ($\lambda < -\Delta G_{ET}$) regions as predicted by Marcus theory of electron transfer.

This means that when plotting the rate constants for electron transfer against $-\Delta G_{ET}$, a "bell-shaped" curve would be expected with the rates first increasing, then reaching a maximum at $\lambda = -\Delta G_{ET}$ and finally decreasing at very large driving forces (inverted region). Figure 4-10

shows the different electron transfer rate constants of the investigated quenchers as a function of the respective estimated ΔG_{ET} values. There are several noteworthy observations to be made when looking at the data:

In general, the data of the investigated benzyl bromides seems to follow exactly the behavior predicted by Marcus theory with a steep increase in the electron transfer rates in the ΔG_{ET} range from 0 to -0.5 eV followed by a "plateau" between -0.5 and -1 eV that would correspond to the "normal" and "optimal" region respectively. There is even a drop of the rates for the combination of **2** and 2,4-dinitro benzyl bromide **3** at ΔG_{ET} = -1.71 eV that might already lie in the inverted region. It should be noted that though the trends are quite obvious, the values might contain significant errors due to inaccuracies in the determination of electrochemical potentials (and thus ΔG_{ET}) or the quenching studies. This might also be the reason while quenching (though very low) could also be observed for slightly positive ΔG_{ET} values.

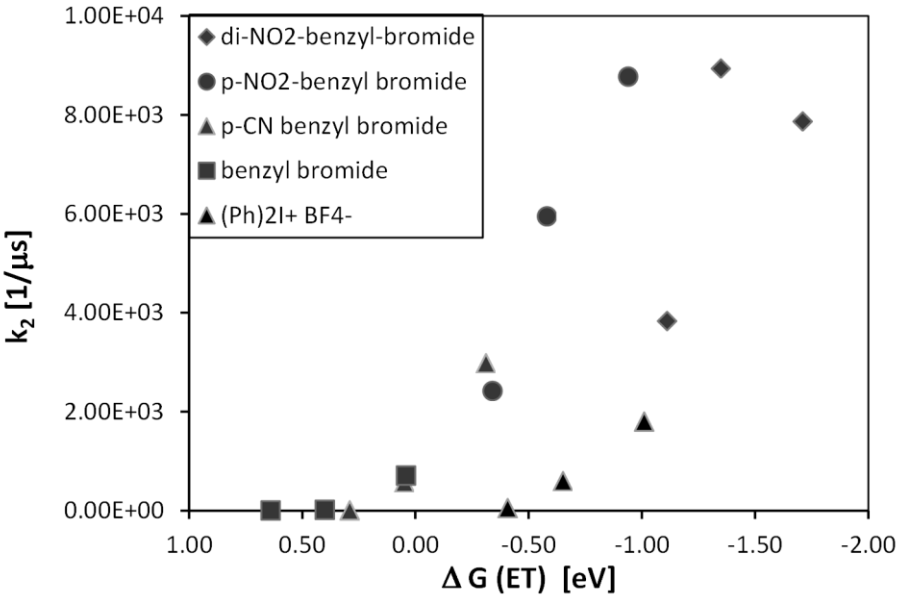

Figure 4-10: The different electron transfer rate constants of the investigated quenchers as a function of the respective estimated ΔG_{ET}.

Table 4-5: Gibbs free energies for the electron transfer between the investigated catalyst/quencher combinations.

	Gibbs free energy ΔG_{ET} [eV]				
Catalyst	***5***	***6***	***7***	***8***	***9***
Ir(piq)3	-1.11	-0.34	0.29	0.64	-0.41
Ir(ppy)3	-1.35	-0.58	0.05	0.40	-0.65
2	-1.71	-0.94	-0.31	0.04	-1.01

Calculated as described in[9].

Another interesting observation is made when comparing the data of the benzyl bromides (red in Figure 4-10) with the ones of quencher **7** (black): there is a significant offset for these points, indicating that the optimal region for this compound lies at considerably higher ΔG_{ET} values. Quenchers **3**-**6** are structurally very similar compounds (they are all benzyl bromides) and are therefore expected to exhibit similar reorganization energies. The diphenyl iodonium tetrafluoroborate salt **7** has a distinctly different structure. This should also reflect on its reorganization energy which, as implied by the obtained data, seems to be notably higher. This emphasizes that even though the free energy change for a given photoinduced electron transfer reaction might be known, the rate of electron transfer also depends heavily on the structural properties of the acceptor, namely its reorganization energy – a property that is much harder to predict accurately.

4.3 CONCLUSIONS

In conclusion, we synthesized and characterized a new photocatalyst with enhanced reductive power in the excited state. Luminescence quenching experiments were performed for a series of different quenchers and confirmed the higher activity of the new compound towards less activated substrates. The new photocatalyst or future analogues might thus allow for the conversion of hitherto inaccessible substrates and broaden the synthetic applicability of photoredox catalysis.

While we could prove the concept of modifying the photoredox properties via tailored ligand structures, the short excited state lifetime of the sensitizer is detrimental to the efficiency of the photoinduced electron transfer step. For further optimization of photocatalytic performances, it would therefore be favorable to develop sensitizers with lower radiative as well as non-

radiative rates. One possible approach in this direction could be to lower the MLCT character of the radiative transition.[11, 18]

The obtained data also suggests a profound influence of the quencher type on the electron transfer rates. Since the structure of the targeted substrate has a big impact on the reorganization energies, it should not be overlooked when trying to determine the right choice of photoredox catalyst for a given reaction.

4.4 EXPERIMENTAL PART

4.4.1 GENERAL INFORMATION

For details regarding the synthesis of **1** and **2** please see the next chapter. 2-Bromo, 4-(*N*,*N*)-dimethylamino pyridine, as well as compound **4** were reported previously although they were synthesized via different procedures.[19]

4.4.2 DFT CALCULATIONS

All calculations were performed using the Gaussian 09W program package.

The geometries of **1** and **2** were optimized via Hartree Fock and LANL2MB basis sets were used for all atoms. Energies were computed via TD-DFT using the B3PW91 exchange correlation functional. In all calculations, a LANL2DZ basis set was employed for the iridium atom, in which a relativistic effective core potential (ECP) on Ir replaces the inner core electrons, leaving the outer core 5s2 5p6 and 5d6 as valence electrons of the iridium center. The 6-31G* basis set was used for all remaining atoms.

4.4.3 QUENCHING EXPERIMENTS

A solution of the respective sensitizer in 1 mL of DMSO in a quartz cuvette equipped with a silicone/PTFE septum was thoroughly degassed via rigorous bubbling with argon for 10 min. After measuring the phosphorescence intensity (integration of the emission peak) of the sample, a 0.25 M solution of the respective quencher in DMSO was added stepwise via a Hamilton syringe (typically in 1 μL amounts) the relative high concentration and low addition volumes were to make sure that dilution effects could be ignored. After each addition, the cuvette was shaken for a few seconds to ensure proper mixing and the phosphorescence

intensity determined again. The values for k_q were obtained as the slope of a linear regression fit for I_0/I as a function of the quenchers concentration with a fixed intercept of 1.

4.4.4 CYCLIC VOLTAMMETRY EXPERIMENTS

Measurements were carried out with a glassy carbon working electrode, a platinum counter electrode and a silver or platinum wire pseudo reference electrode. All compounds were measured in DMF with tetrabutyl ammonium tetrafluoroborate as the supporting electrolyte and the solvent was degassed by vigorous argon bubbling prior to the measurements. All experiments were performed under argon atmosphere. Ferrocene was used as an internal reference for determining the reduction and oxidation potentials.

4.5 REFERENCES

[1] N. S. Lewis, *Science* **2007**, *315*, 798-801.
[2] G. Ciamician, *Science* **1912**, *36*, 385-394.
[3] K. Zeitler, *Angew. Chem., Int. Ed.* **2009**, *48*, 9785-9789.
[4] J. M. R. Narayanam, C. R. J. Stephenson, *Chem. Soc. Rev.* **2011**, *40*, 102-113.
[5] J. W. Tucker, C. R. J. Stephenson, *The Journal of Organic Chemistry* **2012**, *77*, 1617-1622.
[6] T. P. Yoon, M. A. Ischay, J. Du, *Nat Chem* **2010**, *2*, 527-532.
[7] M. Neumann, S. Füldner, B. König, K. Zeitler, *Angew. Chem., Int. Ed.* **2011**, *50*, 951-954.
[8] M. Cherevatskaya, M. Neumann, S. Füldner, C. Harlander, S. Kümmel, S. Dankesreiter, A. Pfitzner, K. Zeitler, B. König, *Angew. Chem., Int. Ed.* **2012**, *51*, 4062-4066.
[9] G. Grampp, *Berichte der Bunsengesellschaft für physikalische Chemie* **1994**, *98*, 1349-1349.
[10] T. Hofbeck, H. Yersin, *Inorg. Chem. (Washington, DC, U. S.)* **2010**, *49*, 9290-9299.
[11] H. Yersin, A. F. Rausch, R. Czerwieniec, T. Hofbeck, T. Fischer, *Coord. Chem. Rev.* **2011**, *255*, 2622-2652.
[12] E. Baranoff, J.-H. Yum, M. Graetzel, M. K. Nazeeruddin, *J. Organomet. Chem.* **2009**, *694*, 2661-2670.
[13] L. Flamigni, A. Barbieri, C. Sabatini, B. Ventura, F. Barigelletti, **2007**, *281*, 143-203.
[14] H.-W. Shih, M. N. Vander Wal, R. L. Grange, D. W. C. MacMillan, *J. Am. Chem. Soc.* **2010**, *132*, 13600-13603.
[15] J. D. Nguyen, E. M. D'Amato, J. M. R. Narayanam, C. R. J. Stephenson, *Nat Chem* **2012**, *4*, 854-859.
[16] G. J. Kavarnos, N. J. Turro, *Chem. Rev. (Washington, DC, U. S.)* **1986**, *86*, 401-449.
[17] R. A. Marcus, *Annu. Rev. Phys. Chem.* **1964**, *15*, 155-196.
[18] H. Yersin, A. F. Rausch, R. Czerwieniec, in *Physics of Organic Semiconductors* (Eds.: C. Adachi, R. Holmes, W. Bruetting), Wiley-VCH, **2012**, p. 371.
[19] F. De Angelis, S. Fantacci, N. Evans, C. Klein, S. M. Zakeeruddin, J.-E. Moser, K. Kalyanasundaram, H. J. Bolink, M. Grätzel, M. K. Nazeeruddin, *Inorg. Chem.* **2007**, *46*, 5989-6001.

CHAPTER 5

5. TUNING RADIATIVE RATES AND QUENCHING EFFECTS IN PHOSPHORESCENT IRIDIUM COMPLEXES VIA STRUCTURAL MODIFICATIONS*

* Theoretical calculations by Christian Ehrenreich (Merck KGaA Darmstadt) and Andreas Hohenleutner. Photophysical characterization (spectra, decay times, quantum yield measurements) by Markus Leitl (group of Prof. Dr. Hartmut Yersin, University of Regensburg). All other experiments by Andreas Hohenleutner. Analysis and interpretation of the data by Andreas Hohenleutner with help of Markus Leitl and Prof. Hartmut Yersin. Andreas Hohenleutner wrote the manuscript.

5.1 INTRODUCTION

Phosphorescent transition metal complexes are an extensively investigated class of compounds mainly due to their interesting photophysical properties and various applications ranging from sensing and biological labeling over photocatalysis to organic electronics. Their most prominent application is their use as phosphorescent emitters in organic electroluminescent devices.[1-4] Since excitons in organic light emitting devices are formed via recombination of electrons and holes, which both have spins, their recombination leads to a statistical distribution of 75% triplet and 25% singlet excitons. Normal organic molecules can only emit from their singlet excited states as radiative decay from the excited triplet is a spin forbidden process. 75% of the formed excitons in an electroluminescent device are therefore lost. In transition metal complexes however, the heavy metal atom causes a strong spin-orbit coupling that induces a certain singlet character of the emitting triplet and thus renders the transition from the triplet excited state to the singlet ground state distinctly allowed. It also enables efficient intersystem crossing from singlet excited states into triplets and thus can collect all formed excitons in the emitting triplet excited state. This phenomenon has been labeled the “triplet harvesting” effect and has enabled internal quantum efficiencies in organic light-emitting diodes approaching the theoretical limit of 100%.[5-6] Especially iridium complexes have received a lot of attention in this regard for the last decade due to their favorable properties.[1, 3-4, 7] To achieve highly efficient phosphorescence from electroluminescent devices, the emitter should exhibit a high photoluminescence quantum efficiency to enable the efficient conversion of the formed excitons to photons. Another desirable property is a short excited state lifetime of the emitting compound which leads to a shorter residence of excited states in the device and thus decreases the exciton density in the emitting layer. Excited state quenching processes like exciton-polaron or exciton-exciton annihilation are detrimental to the efficiency of OLEDs. Especially at high current densities, efficiency roll-off becomes a problem which can be due to those quenching effects or simply to a “saturation” of available emitter sites with excited states. Furthermore, a range of chemical degradation processes is believed to involve the participation of potentially unstable excited states (see chapter 2). Consequently, a short luminescence decay time at high quantum efficiencies is extremely desirable for efficient and stable electroluminescence.

The quantum efficiency Φ_{PL} and decay time τ of a given compound is governed by the competition of radiative and non-radiative rates (k_r, k_{nr}) according to:[8]

$$\phi_{PL} = \frac{k_r}{k_r + k_{nr}} = \tau k_r \quad (1)$$

This makes it obvious that for a given non-radiative rate, enhancing the radiative rate will lead to a higher quantum yield as well as a shorter excited state lifetime.

While predicting and tuning electrochemical properties and emission colors by varying ligand substitution patterns for tris-cyclometalated iridium complexes is relatively easy and has been extensively investigated over the last years, the influence of structural modifications on the balance of radiative and non-radiative rates is less straightforward. Establishing structure-property relationships for controlling radiative rates in this class of compounds is therefore highly desirable.

In our efforts to prepare a photocatalyst with a high reductive power in its excited state (see chapter 4) we noticed the strikingly short emission decay time of 0.76 μs for **1,** a tris-cyclometalated iridium complex based on the widely used green phosphorescent emitter $Ir(ppy)_3$. Together with its high ϕ_{PL} value of 0.74 these are very interesting properties for applications in organic light-emitting devices and lead us to investigate the origin of this significantly enhanced radiative rate. We therefore prepared a number of structurally related compounds, systematically varying the substituents on the cyclometalated ligand and examined them spectroscopically and via DFT calculations.

5.2 RESULTS AND DISCUSSION

5.2.1 SYNTHESIS

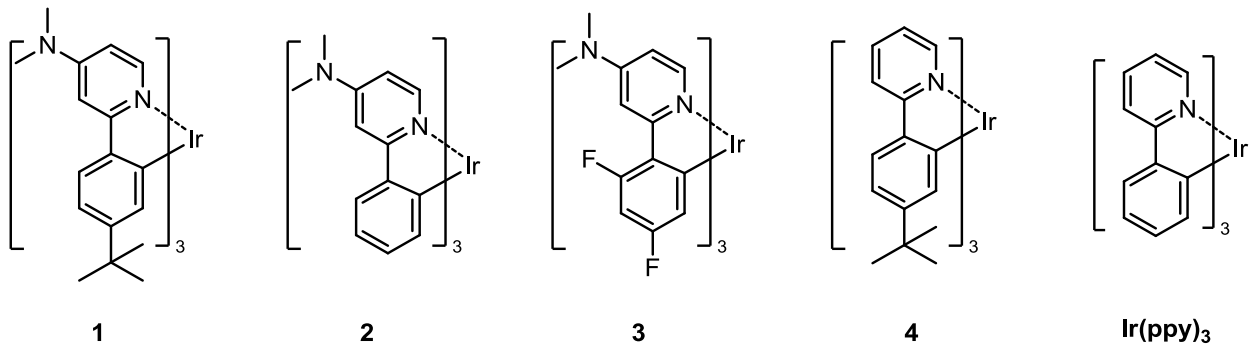

Figure 5-1: Structure of the four synthesized iridium complexes (Compounds 1-4) and $Ir(ppy)_3$.

Figure 5-1 depicts the structure of the synthesized phosphorescent iridium complexes as well as $Ir(ppy)_3$,which we used as a reference for the photophysical and computational study since it is one of the most popular and well examined examples for the use of iridium complexes in OLEDs. By varying the substitution pattern, we hoped to elucidate the origin of the enhanced radiative rates and whether we could find this phenomenon for other compounds as well.

The ligands for preparing the Iridium complexes where synthesized via Suzuki-Miyaura coupling of 2-promopyridines with the corresponding boronic acids and could be obtained in good to very good yields. The following cyclometalation step was performed in ethylene glycol using $Ir(acac)_3$ as the metal precursor and afforded the complexes in yields of 64-93%.

Compound **2** and **3** exhibited a very low solubility in all tested solvents while compound **1** and **4** showed comparatively good solubility in several common laboratory solvents (such as DCM, $CHCl_3$, DMF and THF). This can probably be ascribed to the effect of the bulky ^{t}butyl groups. While the solubility of compound **2** and **3** was too low for standard analytical techniques their identity is supported via high resolution mass spectrometry as well as by their characteristic photophysical properties (see below). Even though compound **4** has been reported before, we decided to reinvestigate its photophysical properties as the available information is very limited.[9]

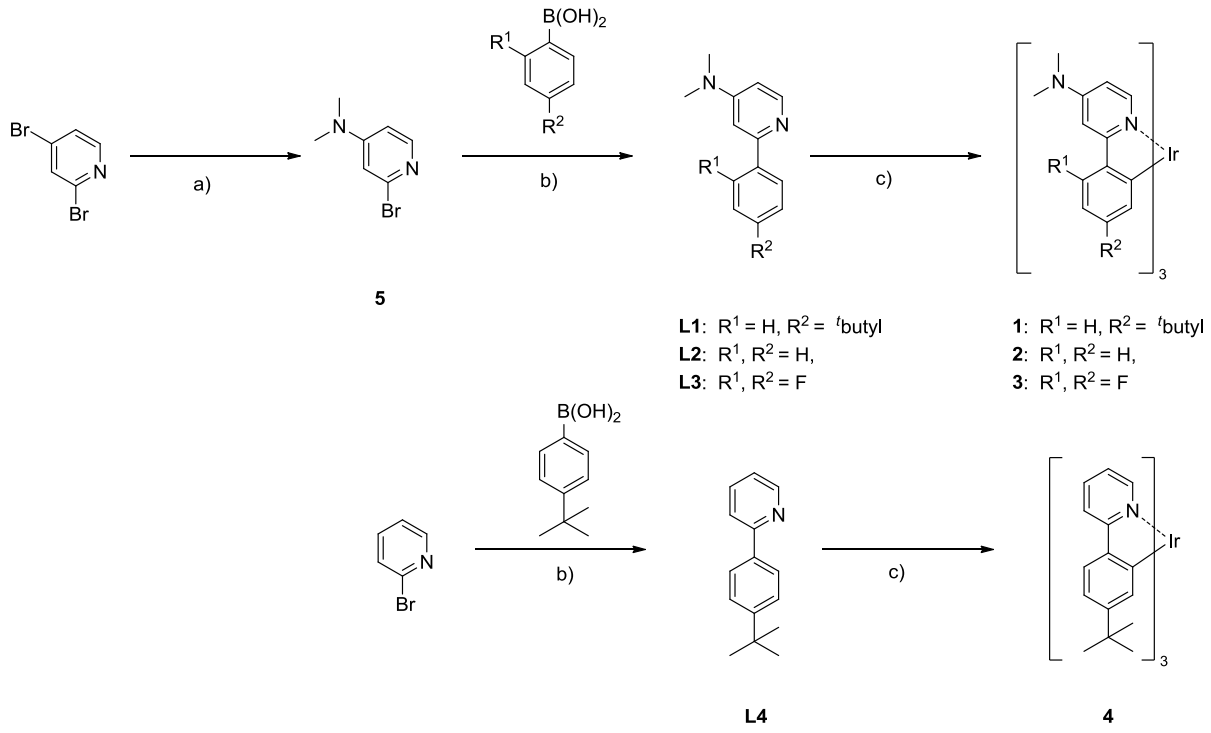

Scheme 5-1: Synthesis of the cyclometalated iridium complexes**1**-**4**. Reaction conditions: a) $N(Me)_2H$, EtOH, 50 °C, 3-4 h. b) Boronic acid, $Pd(dppf)Cl_2*CH_2Cl_2$, K_2CO_3,H_2O/dioxane/toluene, 100°C, overnight. c)$Ir(acac)_3$, ethylene glycol, 200° C, 15-48 h.

5.2.2 PHOTOPHYSICAL INVESTIGATIONS

The four compounds all exhibited absorption characteristics in line with what is expected for this class of compounds and were assigned accordingly. [8, 10] Figure 5-2 exemplarily shows the absorption spectrum of compound **1** in dichloromethane at ambient temperature. The intense band below 300 nm can be assigned to spin allowed ligand centered π–π* transitions while the broad unresolved region from 320 nm to ~450 nm are associated with ^{1}MLCT states (d–π* transitions).

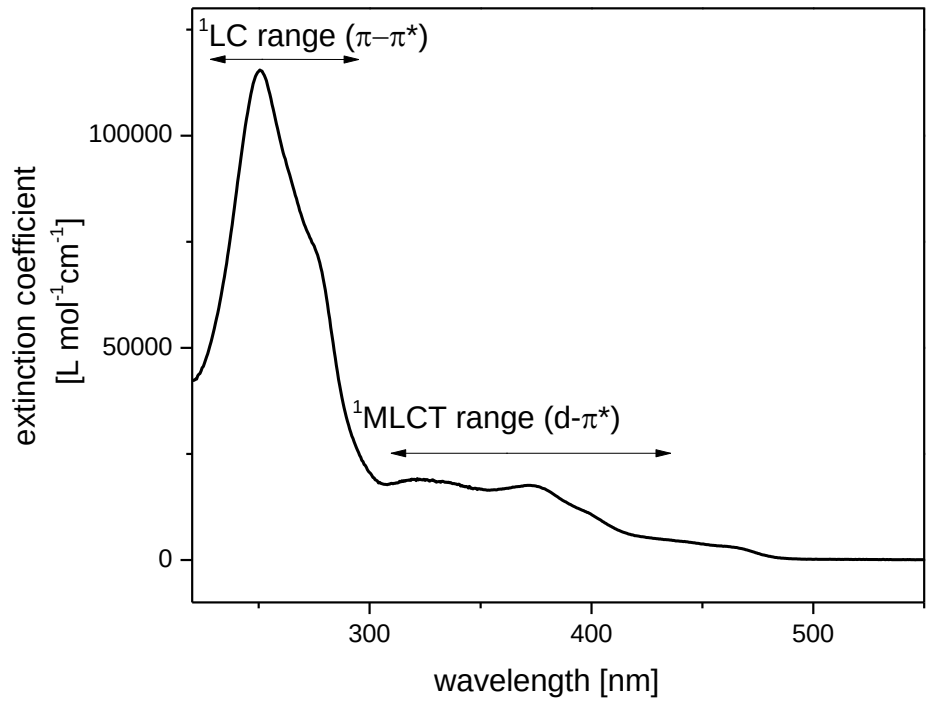

Figure 5-2: Absorption spectrum of compound **1** in CH_2Cl_2 at ambient temperature. Assignment of the ranges for the different transitions should only be taken as guidelines.

All compounds were strongly phosphorescent in deaerated solutions at room temperature with green emission for complexes **1**, **2** and **4** and a sky-blue emission for complex **3**. The emission of all investigated compounds was strongly quenched by oxygen as phosphorescent iridium complexes are highly efficient singlet oxygen sensitizers.[11-13] Figure 5-3 shows the normalized emission spectra of the four compounds measured at ambient temperature and 77 K respectively.

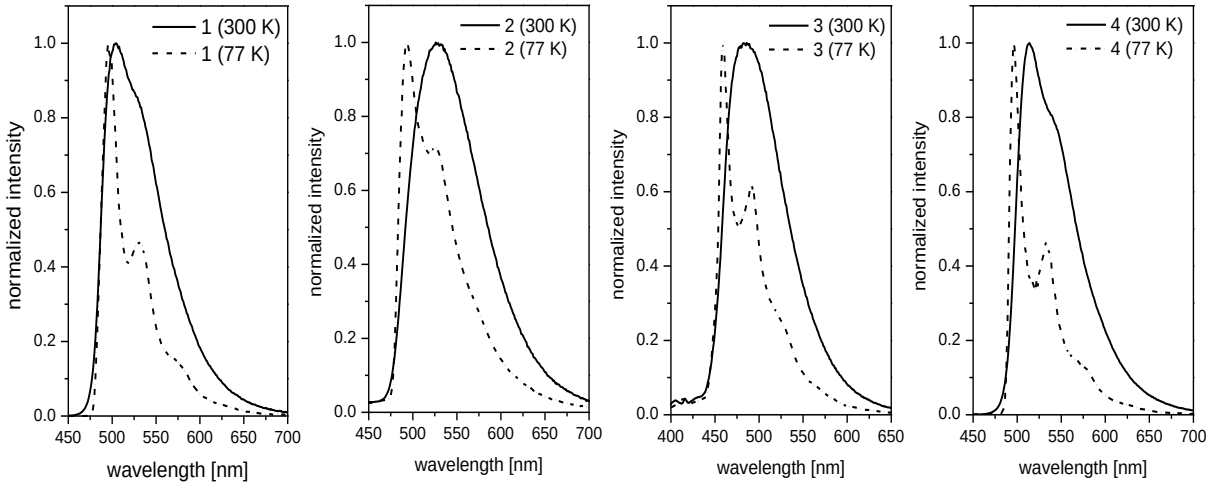

Figure 5-3: Normalized emission spectra of compounds **1**-**4** measured at 77 K and 300 K in solution. **1**, **3** and **4** were measured in Me-THF, **2** in Acetonitrile.

All compounds show relatively broad, unresolved emission at ambient temperature. When cooled down to 77 K, the emission spectra are more resolved with a sharp, dominant peak accompanied by one or more peaks at lower energies. These additional maxima can be attributed to vibrational satellites of ground state modes.[8, 10] Table 5-1 summarizes the emission characteristics of the investigated compounds including ϕ_{PL}, emission maxima and decay times at ambient temperature and 77 K as well as the rate constants for the radiative and non-radiative decay. The latter can be calculated from the decay times and ϕ_{PL} values using formula (1). As far as the solubility permitted, the compounds were characterized in a suitable solvent as well as doped into a spincoated polymer film (PMMA).

Table 5-1: Emission maxima and decay times at ambient temperature and 77 K, photoluminescence quantum yields and the determined radiative/ nonradiative rate constants at ambient temperature for the examined compounds as well as for $Ir(ppy)_3$ as a reference compound.

			77 K		300 K			
		ϕ_{PL}(300K)	λ_{MAX} [nm]	τ [µs]	λ_{MAX} [nm]	τ [µs]	k_r(300 K)	k_{nr}(300 K)
1	MeTHF	0.74	495	4	504	0.76	9.74E+05	3.42E+05
	PMMA	0.82	n.d.	n.d.	n.d.	0.85	9.65E+05	2.12E+05
2	AcCN	n.d.[a]	495	3.4	527	1.22	n.d.[a]	n.d.[a]
3	MeTHF	0.84	459	2.08	484	1.02	8.24E+05	1.57E+05
	PMMA	0.81	469	2.37	478	0.85	9.53E+05	2.24E+05
4	MeTHF	0.93	497	4.91	514	1.56	5.96E+05	4.49E+04
	PMMA	0.93	510	5.71	511	1.54	6.04E+05	4.55E+04
$Ir(ppy)_3$[b]	THF	0.90	491	4	508	1.6	6.06E+05	1.88E+04
	PMMA	0.3	503	5	508	1.4	6.86E+05	2.86E+04

a) No reliable values could be obtained due to the poor solubility of the compound. b) Values taken from[8].

All compounds show efficient phosphorescence emission with high photoluminescence quantum yields (75-93 %) and high radiative rates. Note that due to its bad solubility, it was not possible to obtain a reliable value for the photoluminescence quantum yield of **2**. While the decay time for **4** is very similar to the one observed for $Ir(ppy)_3$,[8] all other compounds exhibit a significantly shorter decay time which at the high ϕ_{PL} values also translate into higher radiative rates. This suggests that the faster radiative decay is caused by the introduction of the dimethylamino group para to the pyridine nitrogen of the ligand. The observed radiative decay times are to the best of our knowledge among the shortest radiative decay times ever observed for phosphorescent iridium complexes and thus make the compounds highly interesting for OLED applications. The ^{t}butyl group at the 4'-position of the phenyl ring does not seem to have a significant influence apart from a slight bathochromic shift of the emission maximum.

Another interesting observation could be made for the phosphorescence efficiencies of the bulk materials: While the photoluminescence quantum efficiency of $Ir(ppy)_3$ is only 0.03 as a powder under nitrogen atmosphere, it is 0.18 under the same conditions for compound **1** with the values for **2**, **3** and **4** lying in between (see Table 5-2).

Table 5-2: Photoluminescence quantum yields for **1-4** as well as $Ir(ppy)_3$ in the solid state(powder).

Compound	ϕ_{PL}(powder, 300 K)[a)]
1	0.18
2	0.08
3	0.07
4	0.09
$Ir(ppy)_2$	0.3

a)measured under nitrogen atmosphere

The crystal structure of $Ir(ppy)_3$ which was elucidated by Yersin *et al.* shows a "shifted π stack type interlocking of adjacent molecules" (Figure 5-4).[15] It is conceivable that these interactions lead to a very efficient energy transfer between neighboring molecules in the bulk material and thus contribute significantly to the phosphorescence quenching of the material in the solid phase. This can happen either via triplet-triplet annihilation of two excited states in close proximity or via fast energy transfer to defect sites that act as luminescence quenchers.[16-17] The steric hindrance induced by the bulky dimethylamino and ^{t}butyl groups of **1** are likely to prevent these stacking interactions in the crystal and thus also reduce phosphorescence quenching effects. The fact that the quantum yield increases with increasing steric demand of the substituents (**2**, **3** and **4**, which each only possess one of the bulky groups show intermediate values, while **1** exhibits the highest ϕ_{PL}) supports this assumption.

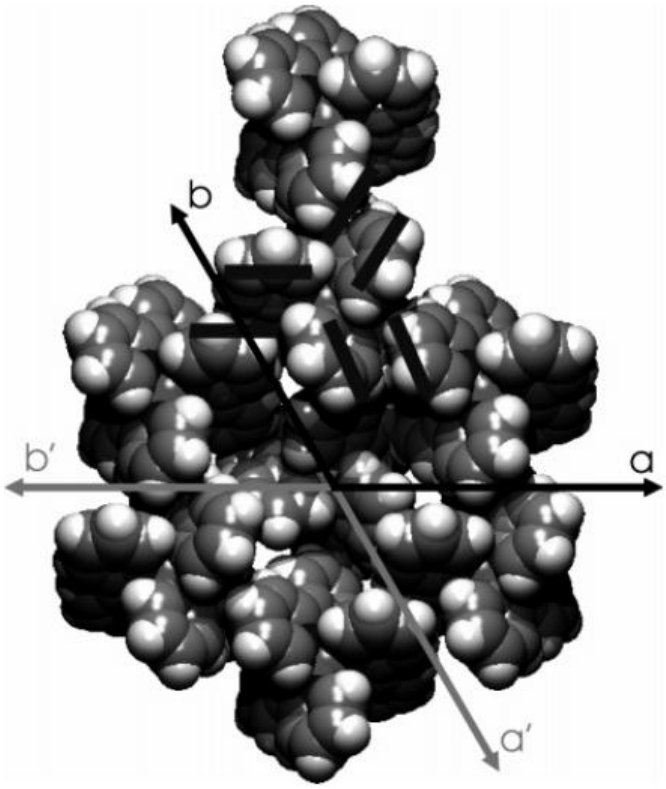

Figure 5-4: Space-filling packing diagram of molecular layers in *fac* -Ir(ppy) 3 . Axes of both twin domains are shown. The "shifted π-stack"-type interlocking of adjacent molecules is indicated by parallel bars. Reprinted with permission from J. Breu, P. Stössel, S. Schrader, A. Starukhin, W. J. Finkenzeller, H. Yersin, *Chem. Mater.* **2005**, *17*, 1745-1752. Copyright 2005 American Chemical Society.

5.2.3 DENSITY FUNCTIONAL THEORY CALCULATIONS

To gain a better understanding of the influence of the dimethylamino group on the properties of the compounds, we performed TD-DFT evaluations on the Hartree-Fock optimized ground state geometries of complex **1**, and $Ir(ppy)_3$. As depicted in Figure 5-5, the electron donating effect of the dimethylamino group causes a rise of both HOMO and LUMO energies compared to $Ir(ppy)_3$. This also explains why the emission energy does not shift significantly with the introduction of the group. The result is in good qualitative agreement with the HOMO and LUMO levels that were obtained via cyclic voltammetry (see chapter 4).

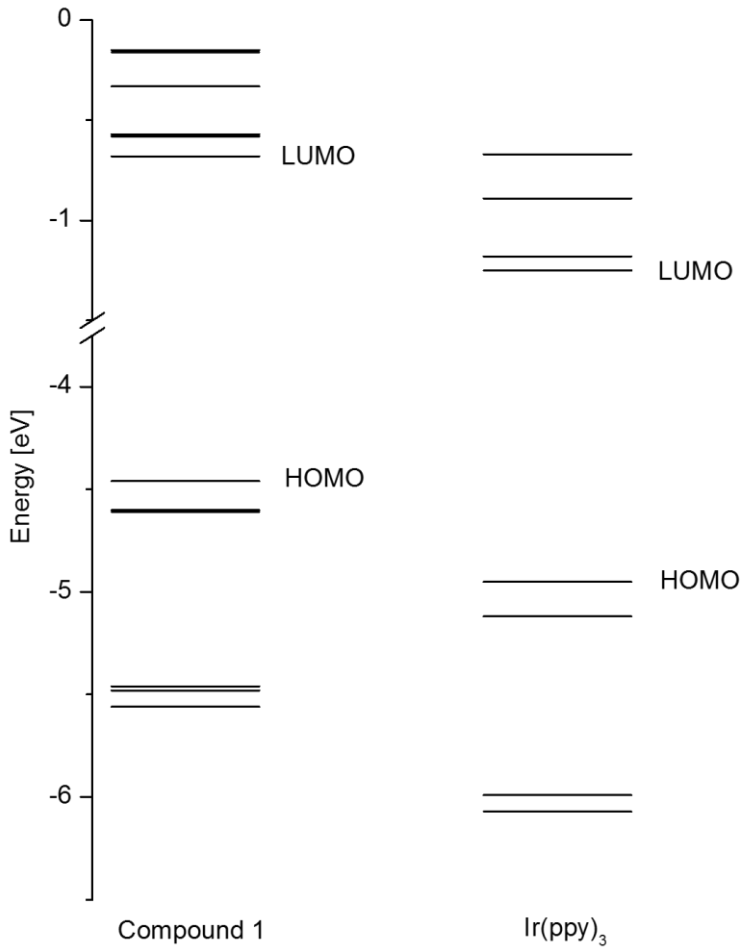

Figure 5-5: Molecular orbital (MO) energy levels for Compound **1** and $Ir(ppy)_3$. Values for the MO energies were obtained via the theoretical calculations.

As the radiative transition from the lowest excited state (a triplet state) to the ground state (a singlet state) is a spin forbidden process, efficient spin-orbit coupling (SOC) is necessary to induce the required singlet character for radiative transition to the ground state. Efficient SOC can only take place if the two coupling states are of significant MLCT character, only between singlet and triplet states, and only if the singlet and triplet result from different d orbitals of the metal. This essentially means that a given emitting triplet T_1 will only couple to higher lying ^{1}MLCT states ($^1MLCT_2$, $^1MLCT_3$, $^1MLCT_4$, …), not to $^1MLCT_1$, ^{1}LC states or other triplets.[18-20] In a quantitative description, the radiative rate can be expressed by equation (2) that is resulting from second order perturbation theory.[20] $\langle S_m|H_{SO}|T_1(i)\rangle$ describes the spin-orbit coupling between the emitting triplet substrate i (i = I, II, III) and a higher lying singlet state S_m,

$E[T_1]$-$E[S_m]$ is the energy difference between these two coupling states and $\langle S_0|er|S_m\rangle$ is the transition dipole moment for the transition from the ground state S_0 to the mixing higher lying Singlet S_m.

$$k_r(i) = \frac{64\pi^4 v^{-3}}{3hc^3} \cdot \sum_m \left| \frac{\langle Sm|H_{SO}|T_1(i)\rangle}{E[T_1]-E[S_m]} \right|^2 \cdot |\langle S_0|er|S_m\rangle|^2 \quad (2)$$

The square of the transition dipole moment gives the probability for this transition and is therefore proportional to the oscillator strength or the extinction coefficient of the transition. In other words, the radiative rate should increase with a smaller energy splitting between the emitting triplet and the coupling higher lying singlets as well as with an increasing oscillator strength/extinction coefficient of the corresponding ^{1}MLCT transitions.

Table 5-3 shows the calculated oscillator strengths of the four lowest singlet excited states for compound **1** and $Ir(ppy)_3$. The significantly higher oscillator strengths for **1** in comparison with $Ir(ppy)_3$ could provide the explanation for the observed higher radiative rates.

Table 5-3: Calculated oscillator strengths for the 4 lowest excited states for compound **1** and $Ir(ppy)_3$.

Compound	Transition	Oscillator strength
compound **1**	S_0 -> S_1	0.0091
	S_0 -> S_2	0.0024
	S_0 -> S_3	0.0026
	S_0 -> S_4	0.0373
$Ir(ppy)_3$	S_0 -> S_1	0.0031
	S_0 -> S_2	0.0013
	S_0 -> S_3	0.0013
	S_0 -> S_4	0.0140

However, since in transition metal compounds, the results for ground state as well as excited state calculations can be very different when using Hartree-Fock compared to DFT methods,[21] the obtained results should be treated with an appropriate degree of skepticism. Therefore, we compared the measured extinction coefficients of the ^{1}MLCT region for complex **2** and $Ir(ppy)_3$ as depicted in Figure 5-6 and indeed found the values to be significantly higher for compound **2**. Together with the results from the theoretical calculations, this provides strong evidence that the origin of the increased radiative rates lies with the stronger singlet metal-to-ligand charge transfer transitions.

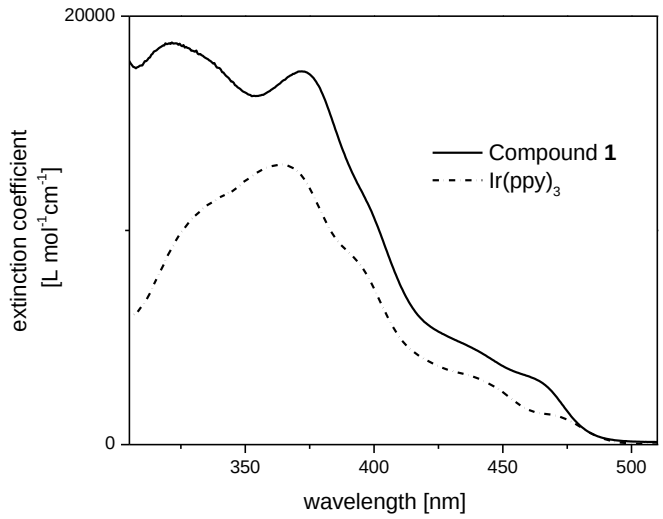

Figure 5-6: Extinction coefficient in the ^{1}MLCT region plotted against the wavelength for **1** and $Ir(ppy)_3$.

5.3 CONCLUSIONS

In conclusion, we prepared a number of new, highly phosphorescent tris-cyclometalated iridium complexes and investigated their photopysical properties. Some of the investigated compounds showed strongly enhanced radiative rates that are to the best of our knowledge some of the highest ever reported for iridium complexes. By systematically varying the substitution pattern of the compounds, we could elucidate that the introduction of a strongly electron donating dimethylamino group is responsible for this rate enhancement. Considerations on the spin orbit coupling routes for these compounds and strong evidence provided by theoretical calculations and photophysical measurements suggest that the electronic origin for the fast radiative decay lies with the enhanced strength of higher lying ^{1}MLCT transitions that are contributing to the singlet character of the emissive state. The high radiative rates lead to short excited state lifetimes which are highly desirable for applications in organic light emitting diodes as they can lead to a reduced "efficiency roll-off" as well as decreased likelihood of exciton induced degradation reactions.

We also observed that the increased bulkiness of the ligands can reduce solid state quenching effects for these compounds. This could potentially allow for higher phosphorescent dopant concentrations in the emitting layer and thus help avoiding saturation effects at higher current densities.

The fast and efficient emission together with the reduced susceptibility to solid state photoluminescence quenching are therefore very promising features for their application in organic light-emitting diodes. Further detailed investigations on the connection between the structural modification and the enhanced ^{1}MLCT transitions will show how the new findings can be utilized for the development of new highly efficient phosphorescent emitters.

5.4 EXPERIMENTAL PART

5.4.1 GENERAL INFORMATION

All NMR spectra were recorded on a Bruker Avance 400 MHz spectrometer at 300 K or Bruker Avance 300 MHz spectrometer. Chemical shifts are reported in δ [ppm] relative to an internal standard (solvent residual peak). Coupling constants are reported in Hertz [Hz]. Characterization of the signals: s = singulet, d = dublet, t = triplet, q = quartet, m = multiplet, bs = broad singulet, dd = dublet of dublet. Integration is directly proportional to the number of the protons. Characterization of the ^{13}C- NMR signals (determined by 135°- DEPT- NMR): (+) for CH_3 or CH, (-) for CH_2 and (C_{quat}) for quarternary C- atoms. The used solvents are indicated for each spectrum. Mass spectra were recorded using EI-, CI-, FAB- (via xenon gas) APCI or ESI ionistaion techniques. All reagents were obtained from commercial suppliers and used without further purification unless otherwise specified. If necessary, solvents were dried accorded to standard techniques. Standard Schlenk techniques were applied to guarantee inert N_2 or Ar atmosphere if needed. Reaction monitoring via TLC was performed using silica gel coated aluminium plates (Merck 60F^{254} Silicagel, 0,2 mm). The visualization was done by UV light at 254 nm or 366 nm. For preparative column chromatography Merck Geduran SI 60 (70- 230 grain diameter) and Macherey-Nagel 60M (0,04 - 0,063 mm, 230 - 400 grain diameter) silica gel was used.

7, **L2**, **L3**, **3** and **L4** were reported previously although they were synthesized via different procedures.[22]

5.4.2 Synthetic procedures

2-Bromo, 4-(N,N)-dimethylamino pyridine

2,4-Dibromopyridine (2.37 g, 10 mmol) and a solution of 33% dimethylamine in ethanol (10 mL) were combined in a crimp-top vial, sealed and heated to 50 °C for 4 h. The solvent was removed *in vacuo* and the residue purified via column chromatography (ethyl acetate/ hexanes; 30-70%) to give a white solid (1.4 g, 69 mmol, 69%). Analytical data in accordance with literature.[22]

^{1}H NMR (400 MHz, $CDCl_3$) δ 7.92 (d, *J* = 6.0 Hz, 1H), 6.62 (d, *J* = 2.4 Hz, 1H), 6.42 (dd, *J* = 6.0, 2.4 Hz, 1H), 2.98 (s, 6H).

^{13}C NMR (101 MHz, $CDCl_3$) δ 155.79, 149.30, 143.11, 109.25, 106.22, 39.26.

General procedure A: preparation of the ligands via Suzuki-Miyaura coupling:

2-Bromo, 4-(*N,N*)-dimethylamino pyridine (503 mg, 2.5 mmol), the corresponding boronic acid (1.5 eq), K_2CO_3 (1.04 g, 7.5 mmol) and $PdCl_2(dppf)Cl_2*CH_2Cl_2$ (102 mg, 0.125 mmol) were combined in a crimp top vial, sealed and flushed with nitrogen. Degassed solvents (water: 5 mL; dioxane: 5 mL, toluene: 5 mL) were added via a syringe and the solution was stirred at 95 °C in an aluminium heating block. After cooling down to room temperature, the mixture was filtered, washed with water (2 x 20 mL) and extracted with 2 M HCl (3 x 20 mL). The aqueous phase was then brought to pH 8 with a concentrated solution of KOH. After extraction with CH_2Cl_2 (3 x 20 mL), the combined organic phases were dried and the solvents removed *in vacuo*. The crude product was purified via flash column chromatography using CH_2Cl_2/MeOH 1-10 % as the eluent. The pure products were obtained as colorless viscous oils that solidified slowly upon standing.

*2-(4-(tert-Butyl)phenyl)-N,N-dimethylpyridin-4-amine **L1**:*

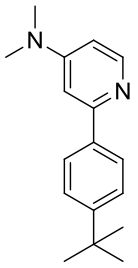

Chemical Formula: $C_{17}H_{22}N_2$
Molecular Weight: 254.37

Prepared according to general procedure **A**. Colorless solid: 1.05 g (4.1 mmol, 83%).

MP: 98 °C.

^{1}H NMR (400 MHz, $CDCl_3$) δ = 8.31 (d, *J* = 6.1, 1H), 7.93 – 7.81 (m, 2H), 7.54 – 7.41 (m, 2H), 6.87 (d, *J* = 2.6, 1H), 6.48 (dd, *J* = 6.1, 2.6, 1H), 3.06 (s, 6H), 1.35 (s, 9H).

^{13}C NMR (101 MHz, $CDCl_3$) δ = 157.08(q), 155.33(q), 152.04(q), 148.49(+), 136.728(q), 126.81(+), 125.60(+), 105.22(+), 103.43(+), 39.38(+), 34.68(q), 31.33(+).

APCI-HR-MS (Q-TOF): found: m/z: 255.187 (100%) (M+H)+, calc. m/z: 255.186

*N,N-Dimethyl-2-phenylpyridin-4-amine **L2**:[22]*

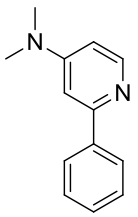

Chemical Formula: $C_{13}H_{14}N_2$
Molecular Weight: 198.26

Prepared according to general procedure **A**. Colorless solid: 489 mg (2.46 mmol, 90 %). Analytical data is in accordance with literature.[22]

^{1}H NMR (300 MHz, $CDCl_3$) δ = 8.30 (d, *J*=6.1, 3H), 7.91 (dd, *J*=8.0, 1.5, 7H), 7.58 – 7.30 (m, 12H), 6.86 (d, *J*=2.5, 3H), 6.48 (dd, *J*=6.1, 2.6, 3H), 3.06 (s, 18H).

2-(2,4-Difluorophenyl)-N,N-dimethylpyridin-4-amine) ***L4****:*[22]

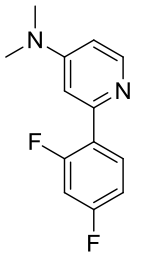

Chemical Formula: $C_{13}H_{12}F_2N_2$
Molecular Weight: 234.24

Prepared according to general procedure **A**. Colorless solid: 1.05 g (4.1 mmol, 83%). Analytical data is in accordance with literature.[22]

^{1}H NMR (400 MHz, $CDCl_3$): δ= 8.32 (d, *J* = 6.0 Hz, 1H), 7.92 (td, *J* = 8.8, 6.7 Hz, 1H), 7.00 – 6.83 (m, 3H), 6.49 (dd, *J* = 6.0, 2.6 Hz, 1H), 3.04 – 3.04 (m, 3H).

^{13}C NMR (101 MHz, $CDCl_3$): δ= 154.9 (q), 150.7 (q), 148.0 (+), 140.2 (q), 135.17 (+), 132.6 (q), 130.5 (q), 130.0 (+), 129.0 (+), 107.0 ($+_r$), 104.9 (+), 39.3 (+).

General procedure for the cyclometallation of the ligands with Ir(acac)$_3$

$Ir(acac)_3$ (1 eq), the respective ligand (5-6 eq) and ethylene glycol (3 mL) were mixed in a crimp top vial, sealed and degassed via rigorous bubbling with argon for 1 h. The mixture was heated to 200 °C for 3 days. To the dark green suspension were added 10 mL of 2 M HCl and the mixture was stirred for 2 min. The green precipitate was filtered of, washed with water and MeOH and dried in a nitrogen stream. In our experience the purity of the ligand is crucial for the successful cyclometalation. If the ligand is not sufficiently pure, the reaction often turns into a brown-black slurry and the product can only be isolated in bad yields and purity or not at all.

fac- tris[2-(4-(tert-Butyl)phenyl)-N,N-dimethylpyridin-4-amine]iridium(III) ***1****:*

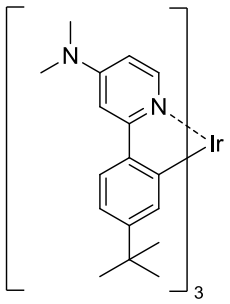

Chemical Formula: $C_{51}H_{63}IrN_6$
Molecular Weight: 952.30

The resulting fine green powder was redissolved in a small amount of CH_2Cl_2 and precipitated by addition of MeOH to yield the sufficiently pure product as yellowish green crystals (370 mg, 0.38 mmol, 64%). For the photophysical characterization, the complex was recrystallized once from CH_2Cl_2/ethanol upon which it was obtained as yellowish green crystal needles.

^{1}H NMR (400 MHz, CD_2Cl_2) δ = 7.46 (d, *J* = 8.2, 3H), 7.30 (d, *J* = 6.5, 3H), 7.03 (d, *J* = 2.7, 3H), 6.95 (d, *J* = 2.1, 3H), 6.82 (dd, *J* = 8.2, 2.2, 3H), 6.25 (dd, *J* = 6.5, 2.7, 3H), 3.04 (s, 18H), 1.08 (s, 27H).

^{13}C NMR (101 MHz, CD_2Cl_2) δ = 166.43(q), 163.03(q), 154.68(q), 151.21(q), 146.94(+), 142.70 (q), 134.45(+), 122.70(+), 116.03(+), 105.54(+), 100.69(+), 39.63(+), 34.52(q), 31.63(+).

APCI-HR-MS (Q-TOF): found: m/z: 953.480 (100%) (M+H)+, calc. m/z: 954.482.

fac- tris[N,N-Dimethyl-2-phenylpyridin-4-amine]iridium(III) ***2****:*

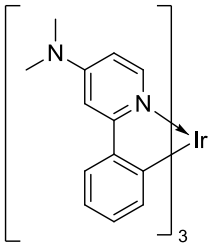

Chemical Formula: $C_{39}H_{39}IrN_6$
Molecular Weight: 783.98

Obtained as green powder (123 mg, 0.16 mmol, 87%). Solubility did not permit analysis via standard analytical techniques.

APCI-HR-MS (Q-TOF): found: m/z: 785.292 (100%) (M+H)+, calc. m/z: 785.294.

fac-tris[2-(4'-tert-Butylphenyl)pyridine]iridium (III) ***3:***[9]

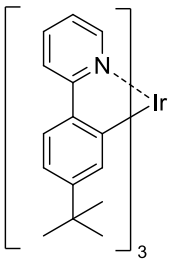

Chemical Formula: $C_{45}H_{48}IrN_3$
Molecular Weight: 823.10

The resulting precipitate was redissolved in a small amount of CH_2Cl_2 and precipitated by addition of MeOH to yield the pure product as green powder (85 mg, 0.10 mmol, 72%). The compound has been reported before.[9]

^{1}H NMR (400 MHz, $C_2Cl_4D_2$) δ = 7.74 (d, *J*=8.3, 3H), 7.59 – 7.48 (m, 6H), 7.46 (d, *J*=8.3, 3H), 6.91 – 6.81 (m, 6H), 6.78 (d, *J*=2.0, 3H), 1.02 (s, 27H).

^{13}C NMR (101 MHz, $C_2Cl_4D_2$) δ = 167.59, 161.16, 152.37, 146.98, 141.28, 136.29, 134.73, 123.96, 121.98, 119.05, 117.31, 34.74, 31.81.

fac-tris[2-(2,4-Difluorophenyl)-N,N-dimethylpyridin-4-amine]iridium(III) ***4:***

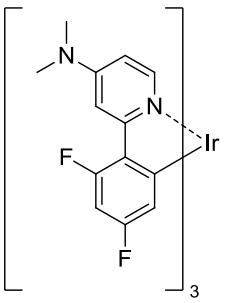

Chemical Formula: $C_{39}H_{33}F_6IrN_6$
Molecular Weight: 891.93

Obtained as green powder (250 mg, 0.28 mmol, 93%). Solubility did not permit analysis via standard analytical techniques.

APCI-HR-MS (Q-TOF): found: m/z: 893.233 (100%) (M+H)+, calc. m/z: 893.230.

5.4.3 DFT CALCULATIONS

All calculations were performed using the Gaussian 09W program package.

The ground state geometries of **1** and **2** were optimized via Hartree Fock and LANL2MB basis sets were used for all atoms. Energies were computed via TD-DFT using the B3PW91 exchange correlation functional. In all calculations, a LANL2DZ basis set was employed for the iridium atom, in which a relativistic effective core potential (ECP) on Ir replaces the inner core electrons, leaving the outer core 5s2 5p6 and 5d6 as valence electrons of the iridium center. The 6-31G* basis set was used for all remaining atoms.

5.4.4 SPECTROSCOPY

For absorption spectra, a Varian Cary 300 double beam spectrometer was used. Emission and excitation spectra at 77 K and ambient temperature were measured with a Fluorolog 3-22 (Horiba Jobin Yvon) spectrophotometer. The solid state measurements were carried out under nitrogen atmosphere. Solutions were degassed via several freeze pump thaw cycles prior to the measurements. For measurements at 77 K the sample was placed in a dewar containing liquid nitrogen during the measurement. A pulsed diode laser (PicoQuant PDL 800-B) with an excitation wavelength of ~375 nm and a pulse width of about 500 ps was used as the excitation source for emission decay measurements. Decay times were registered using a FAST Comtec multichannel PCI card with a time resolution of 250 ps.

5.4.5 QUANTUM YIELD MEASUREMENTS

The Quantum yields were determined using an absolute method applying an integrating sphere (Labsphere with Spectralon inner surface coating) with a Hamamatsu Photonics quantum yield measurement system(C9920-02).

5.5 REFERENCES

[1] C. Ulbricht, B. Beyer, C. Friebe, A. Winter, U. S. Schubert, *Adv. Mater.* **2009**, *21*, 4418-4441.

[2] E. Baranoff, J.-H. Yum, M. Graetzel, M. K. Nazeeruddin, *J. Organomet. Chem.* **2009**, *694*, 2661-2670.

[3] Y. You, S. Y. Park, *Dalton Trans.* **2009**, 1267-1282.

[4] P. T. Chou, Y. Chi, *Chem.--Eur. J.* **2007**, *13*, 380-395.

[5] Y. Kawamura, K. Goushi, J. Brooks, J. J. Brown, H. Sasabe, C. Adachi, *Appl. Phys. Lett.* **2005**, *86*, 071104-071103.

[6] M. A. Baldo, D. F. O'Brien, Y. You, A. Shoustikov, S. Sibley, M. E. Thompson, S. R. Forrest, *Nature* **1998**, *395*, 151-154.

[7] S. Kappaun, C. Slugovc, E. List, *Int. J. Mol. Sci.***2008**, *9*, 1527-1547.

[8] H. Yersin, A. F. Rausch, R. Czerwieniec, T. Hofbeck, T. Fischer, *Coord. Chem. Rev.* **2011**, *255*, 2622-2652.

[9] W. Zhu, C. Liu, L. Su, W. Yang, M. Yuan, Y. Cao, *J Mat. Chem.* **2003**, *13*, 50-55.

[10] T. Hofbeck, H. Yersin, *Inorg. Chem. (Washington, DC, U. S.)* **2010**, *49*, 9290-9299.

[11] S. Y. Takizawa, R. Aboshi, S. Murata, *Photochem. Photobiol. Sci.* **2011**, *10*, 895-903.

[12] P. I. Djurovich, D. Murphy, M. E. Thompson, B. Hernandez, R. Gao, P. L. Hunt, M. Selke, *Dalton Trans.* **2007**, 3763-3770.

[13] R. Gao, D. G. Ho, B. Hernandez, M. Selke, D. Murphy, P. I. Djurovich, M. E. Thompson, *J. Am. Chem. Soc.* **2002**, *124*, 14828-14829.

[14] T. Sajoto, P. I. Djurovich, A. B. Tamayo, J. Oxgaard, W. A. Goddard, M. E. Thompson, *J. Am. Chem. Soc.* **2009**, *131*, 9813-9822.

[15] J. Breu, P. Stössel, S. Schrader, A. Starukhin, W. J. Finkenzeller, H. Yersin, *Chem. Mater.* **2005**, *17*, 1745-1752.

[16] F. Laquai, Y. S. Park, J. J. Kim, T. Basche, *Macromol. Rapid Commun.* **2009**, *30*, 1203-1231.

[17] M. A. Baldo, C. Adachi, S. R. Forrest, *Phys. Rev. B* **2000**, *62*, 10967-10977.

[18] K. Nozaki, *J. Chin. Chem. Soc. (Taipei, Taiwan)* **2006**, *53*, 101-112.

[19] A. R. G. Smith, M. J. Riley, P. L. Burn, I. R. Gentle, S. C. Lo, B. J. Powell, *Inorg. Chem.* **2012**, *51*, 2821-2831.

[20] H. Yersin, A. F. Rausch, R. Czerwieniec, in *Physics of Organic Semiconductors* (Eds.: C. Adachi, R. Holmes, W. Bruetting), Wiley-VCH, **2012**, p. 371.

[21] F. D. Angelis, L. Belpassi, S. Fantacci, *J. Mol. Struct.: THEOCHEM* **2009**, *914*, 74-86.

[22] F. De Angelis, S. Fantacci, N. Evans, C. Klein, S. M. Zakeeruddin, J.-E. Moser, K. Kalyanasundaram, H. J. Bolink, M. Grätzel, M. K. Nazeeruddin, *Inorg. Chem.* **2007**, *46*, 5989-6001.

6. Summary

This thesis focuses on novel approaches for improving the performance of phosphorescent iridium complexes for applications in organic light-emitting diodes (OLEDs) and photocatalysis. **Chapter 1** provides an overview on the intrinsic degradation of materials in OLEDs by reviewing recent advances in the elucidation of the underlying chemical degradation mechanisms. First, the possible reasons for defect formation together with the most common and important methods to investigate those processes are covered. Next, the reactions and their products for the different types of materials present in a device are discussed. The commonalities in the occurring mechanisms are summarized, and structural features and moieties that can be detrimental to operational stability are identified. Some of the resulting implications on the development of new materials are presented and backed by concrete examples from literature.

In **chapter 2** the combinatorial synthesis and screening of phosphorescent iridium complexes as solution processable emitters for OLEDs are reported. Employing a combinatorial post modification strategy combined with a chromatographic separation and screening enables the rapid synthesis and characterization of potential new OLED emitters. Absorption and emission spectra that were obtained directly from the chromatographic separation allowed a fast assessment of the photophysical properties. This led us to find intriguing dual emission properties for some of the heteroleptic compounds. The determination of phosphorescence quantum yields in a separate experiment further illustrated the antagonistic relationship between molecular flexibility and phosphorescence efficiency. The preservation of the rigidity near the emitting center was identified as a promising new design principle for realizing soluble and highly efficient emitters. Subsequent photodegradation experiments in solution provided first hints on the complexity of this topic. Nevertheless, interesting trends were found and compounds with increased stabilities could be identified.

Aiming for a better understanding of the processes at work, four well known phosphorescent emitters were selected for a more detailed investigation of their photodegradation behavior (**chapter 3**). Irradiation of the samples in different solvents under atmospheric and inert conditions together with the analysis of the formed degradation products allowed us to identify several distinct pathways that can contribute to the deterioration of these compounds. Chemical reactions with halogenated solvents, susceptibility to degradation via singlet oxygen and the

degradation via the excited state of the molecules can all contribute to the limited photostability of the complexes. The photodegradation of these materials is complex and often caused by not one but several competing mechanisms whose influence is not always clearly distinguishable. The results from this study furthermore show how even small changes in the ligand structure can have a huge impact on the rate and mechanisms of their degradation.

Chapter 4 deals with the synthesis and characterization of a new photocatalyst with enhanced reductive power in the excited state. Luminescence quenching experiments were performed for a series of different quencher/sensitizer-combinations. The observed quenching constants showed a very good agreement with Marcus theory of electron transfer and confirmed the higher activity of the new compound towards less activated substrates. Thus the concept of modifying the excited state photoredox properties via tailored ligand structures could be proved. The results also emphasized the profound effect that the excited state lifetime of the sensitizer as well as the structure of the quencher can have on the electron transfer rates.

The newly synthesized iridium complex exhibits an unusually short excited state lifetime. In combination with its high photoluminescence quantum yield this is highly desirable for applications as phosphorescent emitters in OLEDs. This led us to investigate the structural origin of the photophysical properties in **chapter 5**. By systematically varying the substitution pattern of the compounds, the introduction of a strongly electron donating dimethylamino group was found to be responsible for a significant enhancement of the radiative rate in these compounds. The observed radiative rates are to the best of our knowledge some of the highest ever reported for iridium complexes. Considerations on the spin-orbit coupling routes for these compounds supported by strong evidence provided by theoretical calculations and photophysical measurements suggest that the electronic origin for the fast radiative decay lies with stronger S_0 to higher lying ^{1}MLCT transitions in these compounds. It was also found that the increased bulkiness of the ligands can reduce the strong solid state quenching that is observed for the widely used $Ir(ppy)_3$. These features make these compounds favorable as phosphorescent emitters in OLEDs.

In conclusion, this thesis presents new concepts and paradigms for the design of phosphorescent iridium complexes. The implications of this work are especially relevant for the development of new Materials with applications in organic light-emitting devices or photocatalysis.

7. Zusammenfassung

Diese Arbeit beschäftigt sich mit neuen Ansätzen zur Verbesserung der Eigenschaften von phosphoreszenten Iridium Komplexen für die Anwendung in Organischen Leuchtdioden (OLEDs) sowie in der Photokatalyse. **Kapitel 1** bietet eine Übersicht zum Thema der intrinsischen Degradation von OLED Materialien, in der aktuelle Fortschritte bei der Aufklärung der zugrundeliegenden chemischen Degradationsmechanismen behandelt werden. Zuerst werden die möglichen Gründe für die Bildung von Defekten aufgezeigt und die wichtigsten und meistverwendeten Methoden für ihre Untersuchung vorgestellt. Anschließend werden bekannte Abbaureaktionen sowie entstehende Degradationsprodukte für verschiedene OLED Materialien diskutiert. Es werden Gemeinsamkeiten und Unterschiede der auftretenden Mechanismen besprochen. Des Weiteren werden bestimmte strukturelle Eigenschaften und Gruppen identifiziert, welche sich nachteilig auf die Lebensdauer auswirken können. Anhand konkreter Literaturbeispiele wird die Bedeutung dieser aufgeklärten Prozesse für die Entwicklung neuer langlebiger Materialien anhand konkreter Literaturbeispiele erläutert.

In **Kapitel 2** wird eine Methode für die schnelle kombinatorische Synthese und ein zugehöriges Evaluierungsverfahren für löslich prozessierbare phosphoreszente OLED Emitter vorgestellt. Die kombinatorische Synthesestrategie für die nachträgliche Modifikation der Iridium Komplexe in Kombination mit einem eigens entwickelten Trenn- und Screeningverfahren erlaubt die effiziente Darstellung und Charakterisierung von umfangreicheren Substanzbibliotheken. Absorptions- und Emissionsspektren, die im Zuge der chromatographischen Trennung erhalten wurden, ermöglichen zudem eine schnelle Beurteilung der photophysikalischen Eigenschaften. Auf diese Weise konnten interessante duale Emissionseigenschaften einiger Verbindungen festgestellt werden. Eine Abschätzung der Phosphoreszenz-Quantenausbeuten in einem separaten Experiment ermöglichte aufschlussreiche Einblicke in den Zusammenhang zwischen struktureller Flexibilität und Emissionseffizienz. Die Bewahrung der Rigidität nahe dem emittierenden Zentrum konnte als vielversprechende Richtlinie für die Entwicklung neuer hocheffizienter, löslicher Emitter identifiziert werden. Bei anschließend durchgeführten Belichtungsversuchen konnten trotz der hohen Komplexität des Degradationverhaltens interessante Trends beobachtet und Verbindungen mit erhöhten Stabilitäten identifiziert werden.

Um ein besseres Verständnis der ablaufenden Prozesse zu ermöglichen, wurden vier bekannte und gut untersuchte Emitter ausgewählt und ihr Degradationsverhalten in **Kapitel 3** eingehender untersucht. Die Belichtung der Substanzen in verschiedenen Lösungsmitteln und unter unterschiedlichen Bedingungen (atmosphärisch/inert) erlaubte die Identifizierung mehrerer verschiedener Degradationswege. Chemische Reaktionen mit den Lösungsmitteln können ebenso zu begrenzter Photostabilität beitragen wie der Abbau durch reaktiven Singulett-Sauerstoff oder die Degradation über angeregte Zustände. Die Photodegradation der untersuchten Verbindungen ist komplex und oft von mehreren miteinander konkurrierenden Mechanismen geprägt, deren Beitrag nicht immer klar voneinander abzugrenzen ist. Interessant war vor allem der starke Einfluss, den selbst scheinbar kleine Veränderungen der Molekülstruktur auf Mechanismus und Geschwindigkeit der Degradation haben können.

Kapitel 4 befasst sich mit der Darstellung und Charakterisierung eines neuartigen Photokatalysators mit stärkerer Reduktionskraft im angeregten Zustand. Mittels Lumineszenz-Quenching Experimenten wurde der Elektronentransfer zwischen verschiedenen Photokatalysatoren und Substratmolekülen untersucht. Die erhaltenen Raten zeigten eine gute Übereinstimmung mit der Marcus-Theorie des Elektronentransfers und bestätigten die höhere Aktivität der neuen Substanz gegenüber weniger aktivierten Substraten. Die Ergebnisse der Untersuchungen zeigten darüber hinaus den starken Einfluss der Lebensdauer des angeregten Zustandes sowie der Struktur des Quenchers auf die Geschwindigkeit des Elektronentransfers.

Eine ungewöhnlich kurze Emissionslebensdauer bei gleichzeitig hoher Quantenausbeute macht diesen neuen Iridium Komplex zu einem hochinteressanten Emitter für die Anwendungen in OLEDs. Dies veranlasste uns, die strukturellen Ursachen für dieses Verhalten in **Kapitel 5** genauer zu untersuchen. Durch die systematische Variation des Substitutionsmusters in einer Reihe von neu synthetisierten Verbindungen konnten die deutlich erhöhten radiativen Raten auf den Einfluss einer stark Elektronen schiebenden Dimethylamino-Gruppe zurückgeführt werden. Die erhaltenen radiativen Raten gehören nach unserem Kenntnisstand zu den höchsten für Iridium Komplexe bisher berichteten. Theoretischen Berechnungen in Kombination mit photophysikalischen Messungen lassen unter Berücksichtigung der Spin-Bahn-Wechselwirkungen auf stärkere Übergänge von S_0 zu höheren ^{1}MLCT Zuständen als elektronische Ursache schließen. Es wurde außerdem gezeigt, dass der erhöhte sterische Anspruch der Liganden die starke Phosphoreszenzlöschung im Festkörper deutlich mindert. Diese Kombination aus vorteilhaften Eigenschaften könnte zu effizienteren und/oder langlebigeren organischen Leuchtdioden führen.

Zusammenfassend zeigt diese Arbeit neue Konzepte und Ansätze für die Entwicklung von phosphoreszenten Iridium Komplexen auf. Die gewonnenen Erkenntnisse besitzen besondere Relevanz im Hinblick auf die Entwicklung neuer Materialien für Anwendungen in organischen Leuchtdioden oder der Photokatalyse.

APPENDIX

8. APPENDIX

8.1 SUPPORTING INFORMATION FOR CHAPTER 2

8.1.1 3D-ABSORPTION- AND EMISSION-PLOTS OF LIBRARY 1, 3 AND 4.

X-axis: retention time [min]; y-axis: wavelength [nm]; z-axis: absorption intensity [mAU] / emission intensity [LU]. The colors do not represent colors as perceived by the eye.

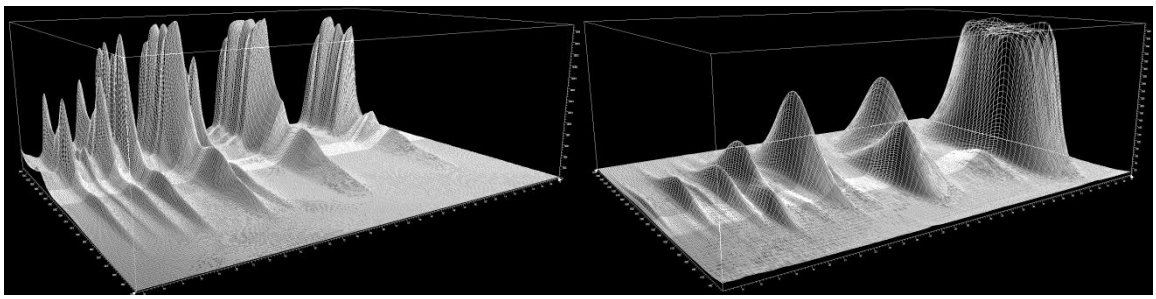

3D plots of library 1. Left: absorbance; right: emission.

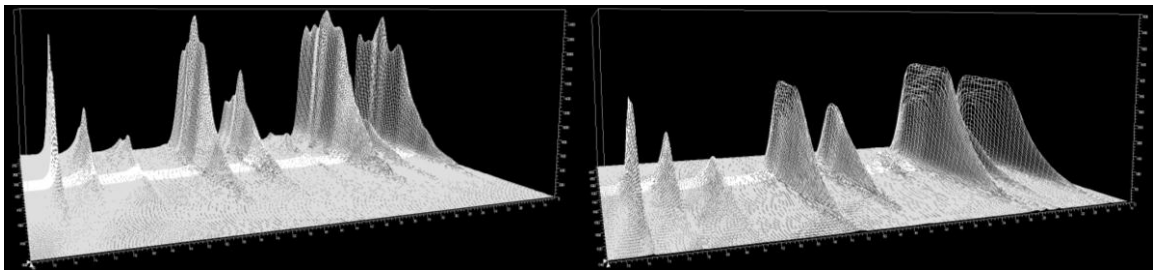

3D plots of library 3. Left: absorbance; right: emission.

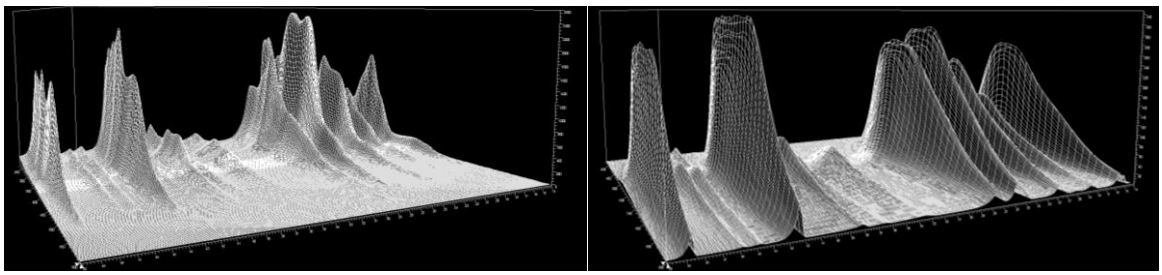

3D plots of library 4. Left: absorbance; right: emission.

8.1.2 ABSORPTION AND EMISSION SPECTRA

Normalized absorption and emission spectra of library 1:

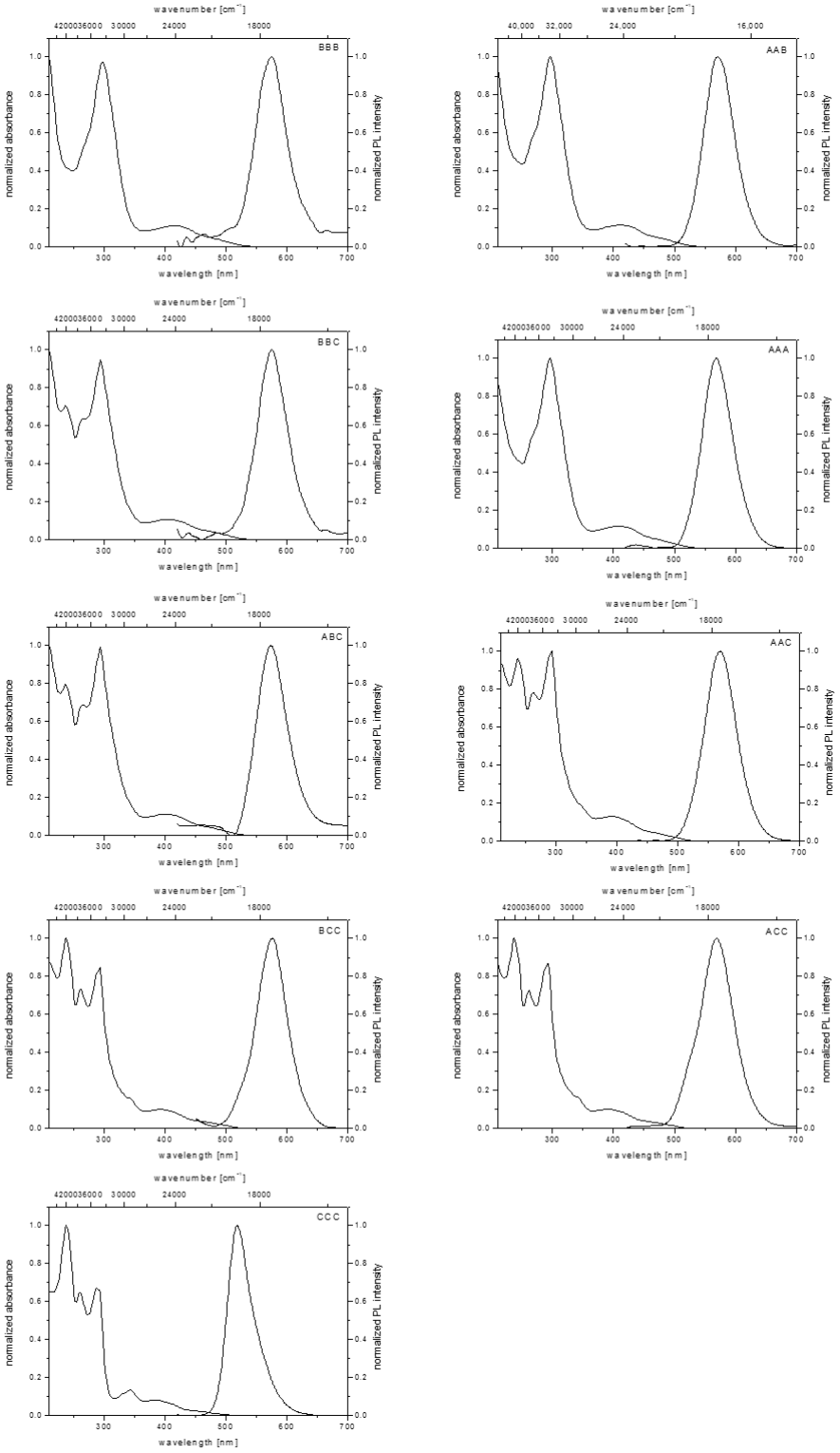

Normalized absorption and emission spectra of complex library 2:

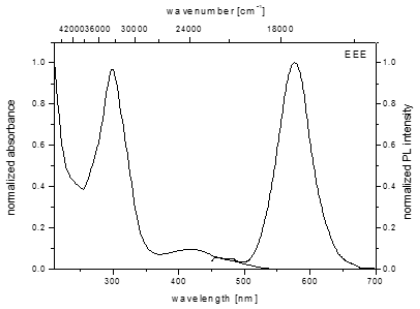

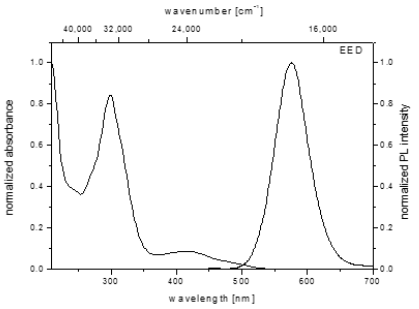

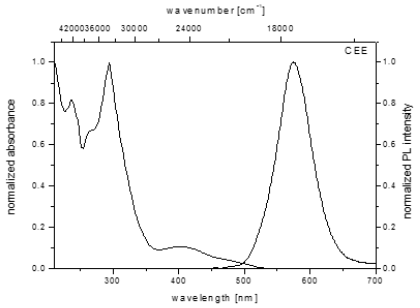

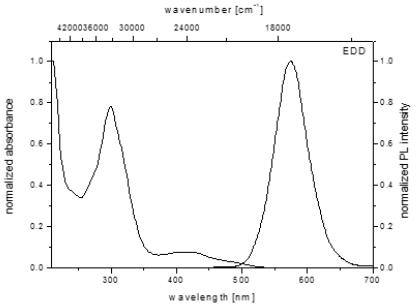

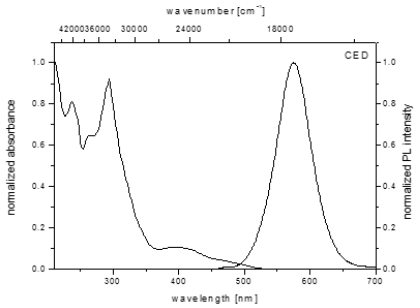

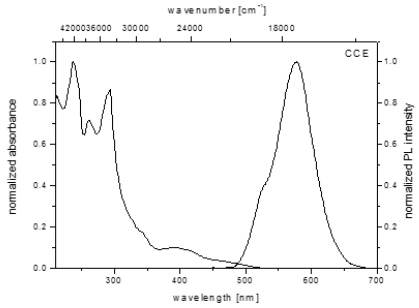

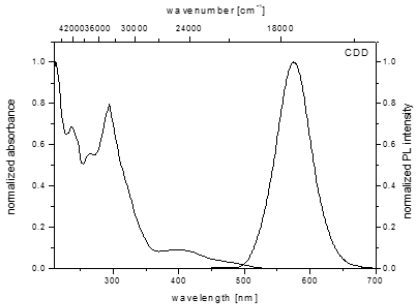

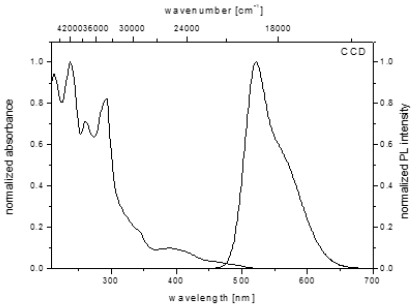

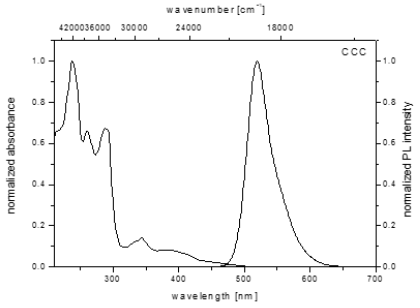

Normalized absorption and emission spectra of library 3:

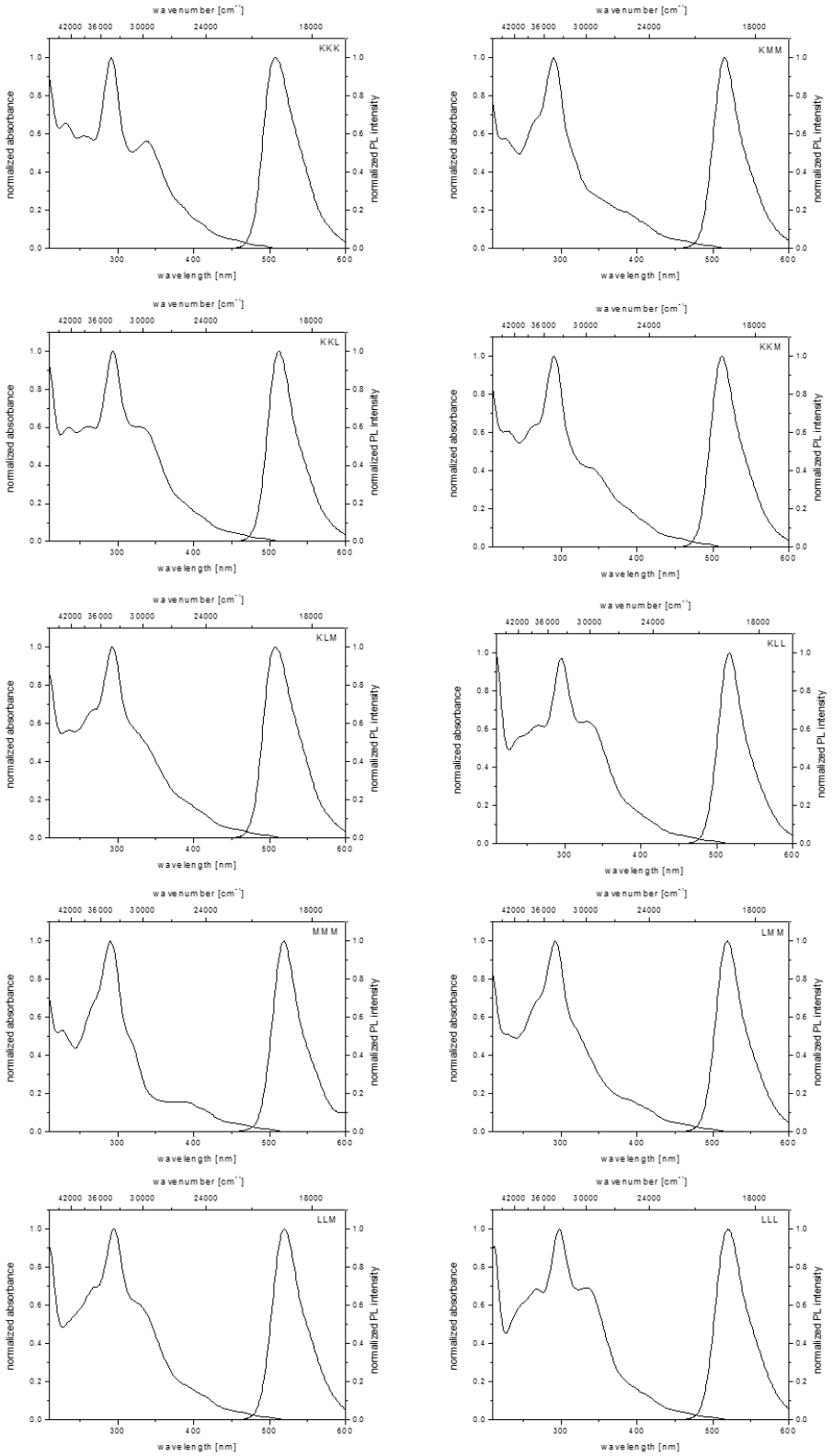

Normalized absorption and emission spectra of library 4:

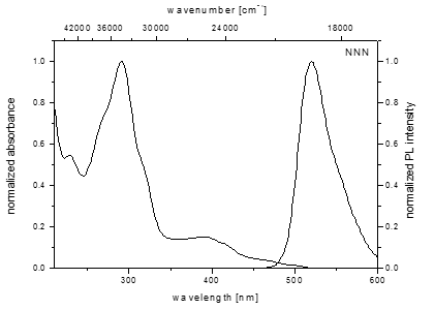

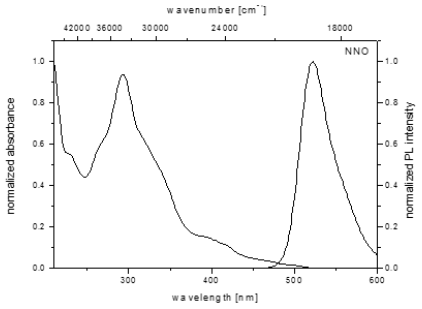

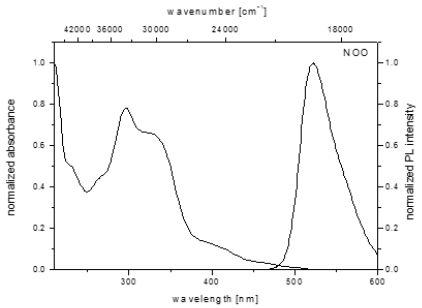

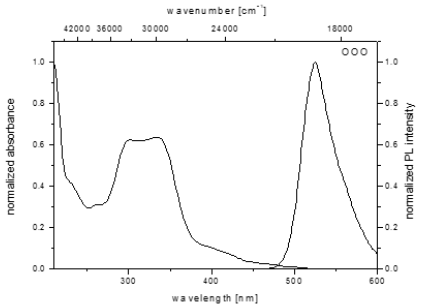

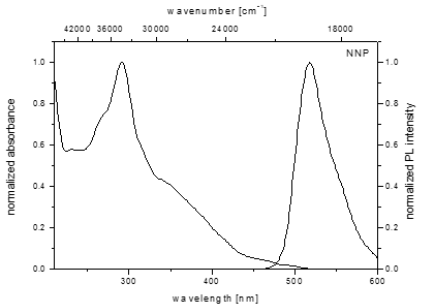

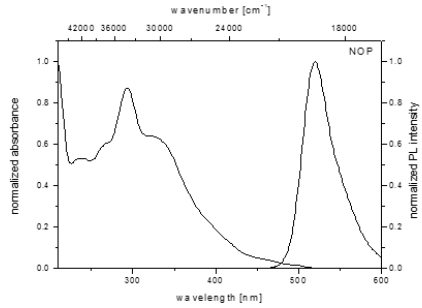

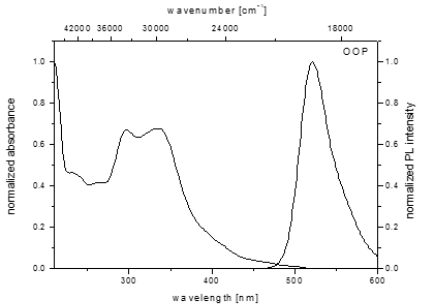

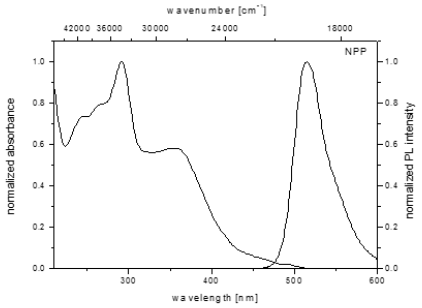

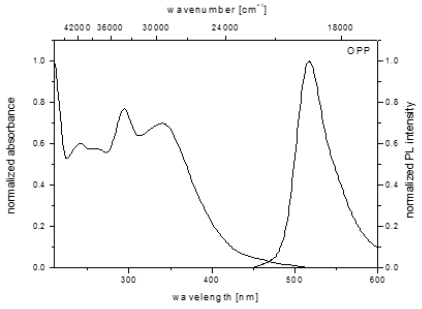

8.1.3 1.3 PHOTODEGRADATION PLOTS

X-axis: irradiation time with 400 nm LEDs [min]; y-axis: ratio C/C^0, whereas C^0 is the initial emitter-concentration and C is the emitter concentration after irradiation; estimated through the integrated DAD signals of the HPLC-setup.

Photodegradation plots of library 1:

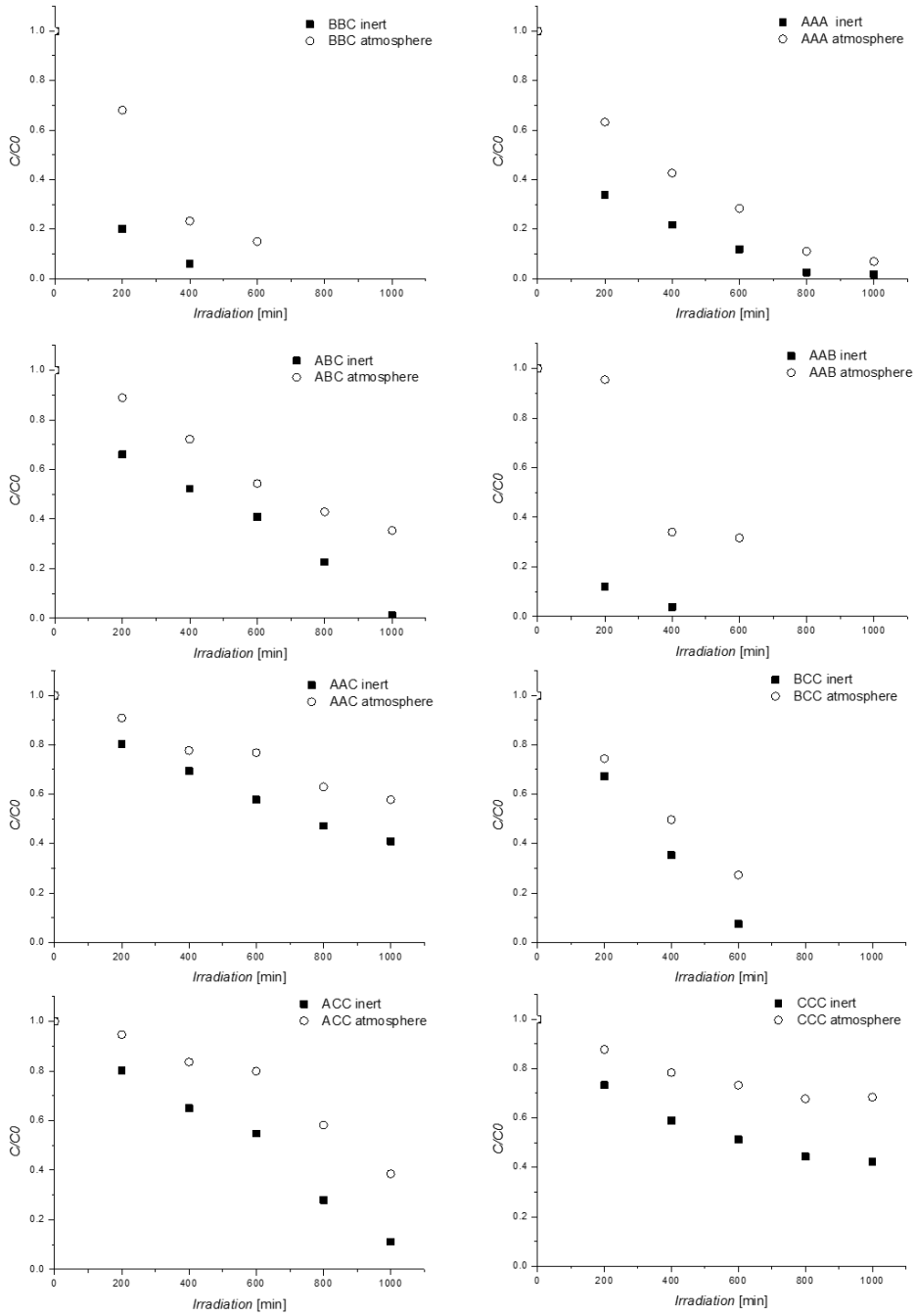

Photodegradation plots of library 2:

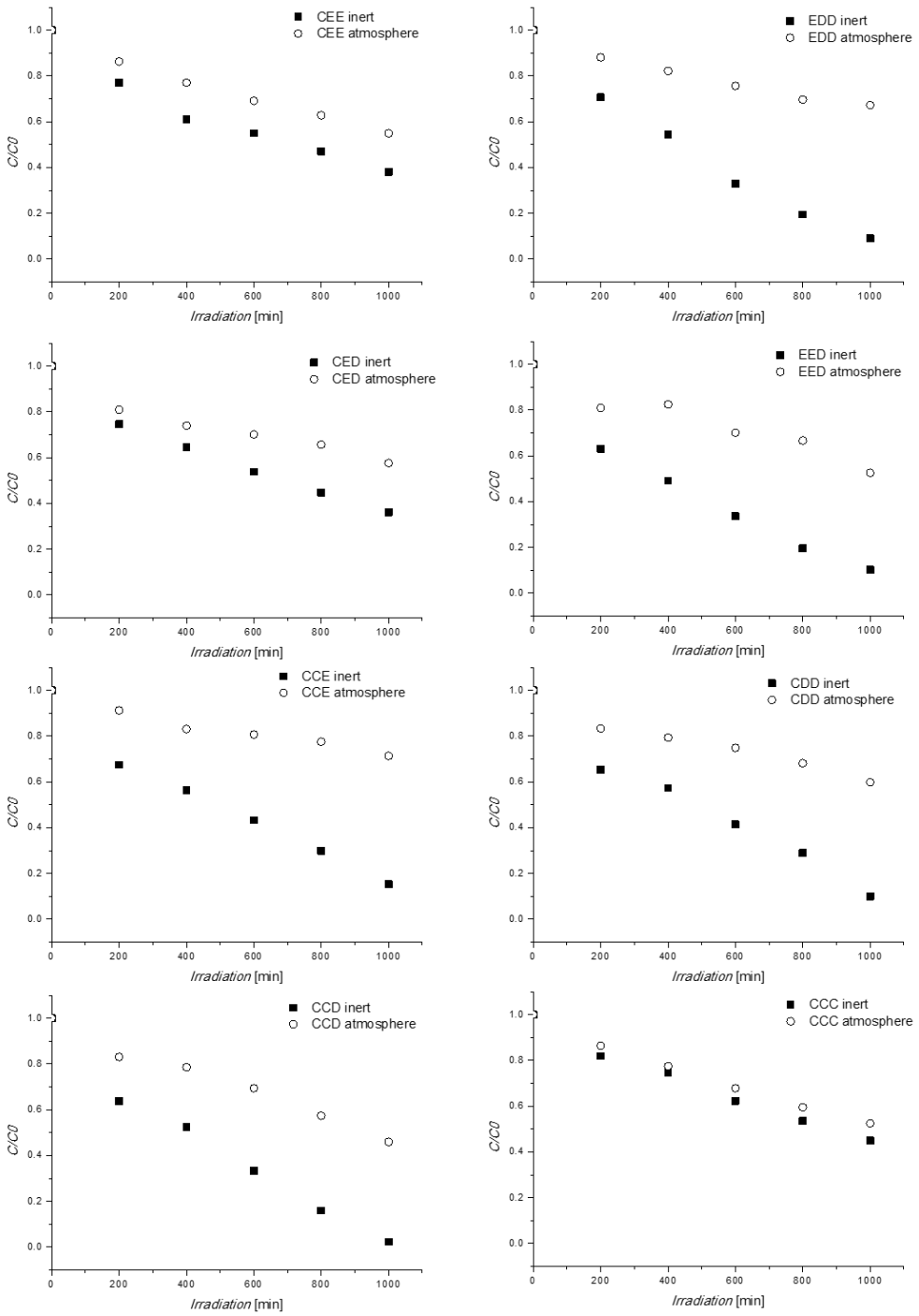

Photodegradation plots of complex library 3:

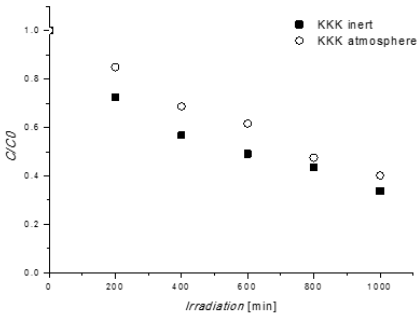

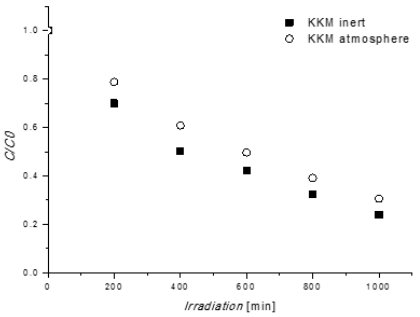

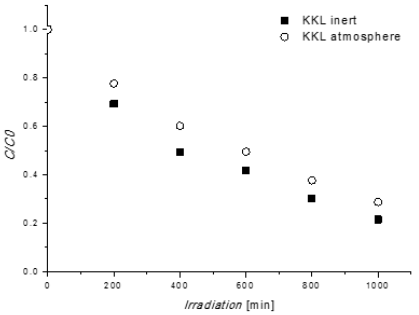

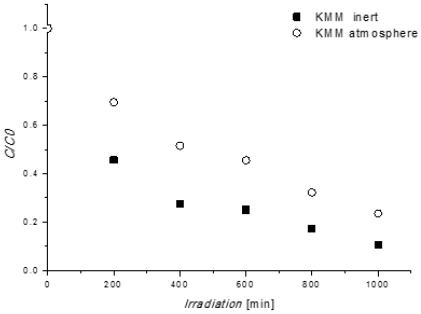

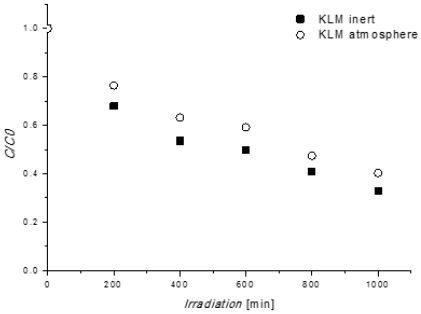

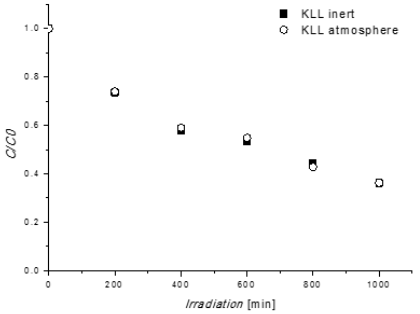

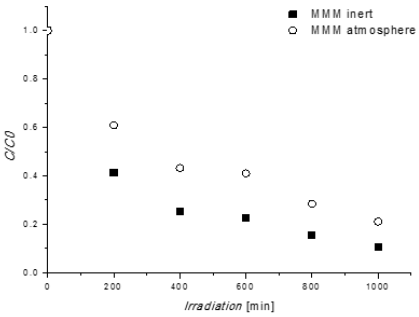

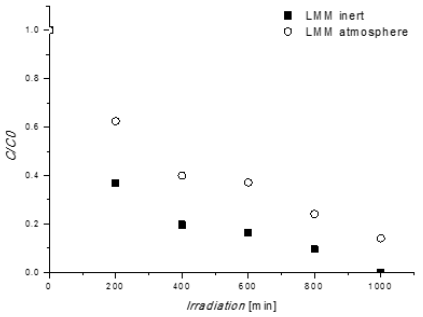

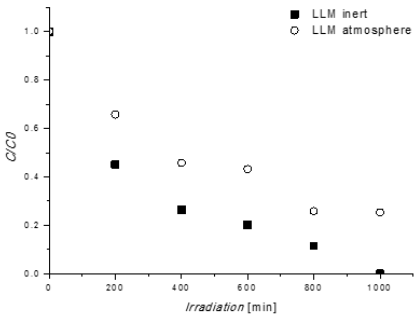

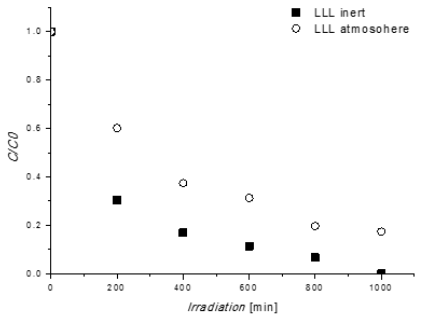

Photodegradation plots of complex library 4:

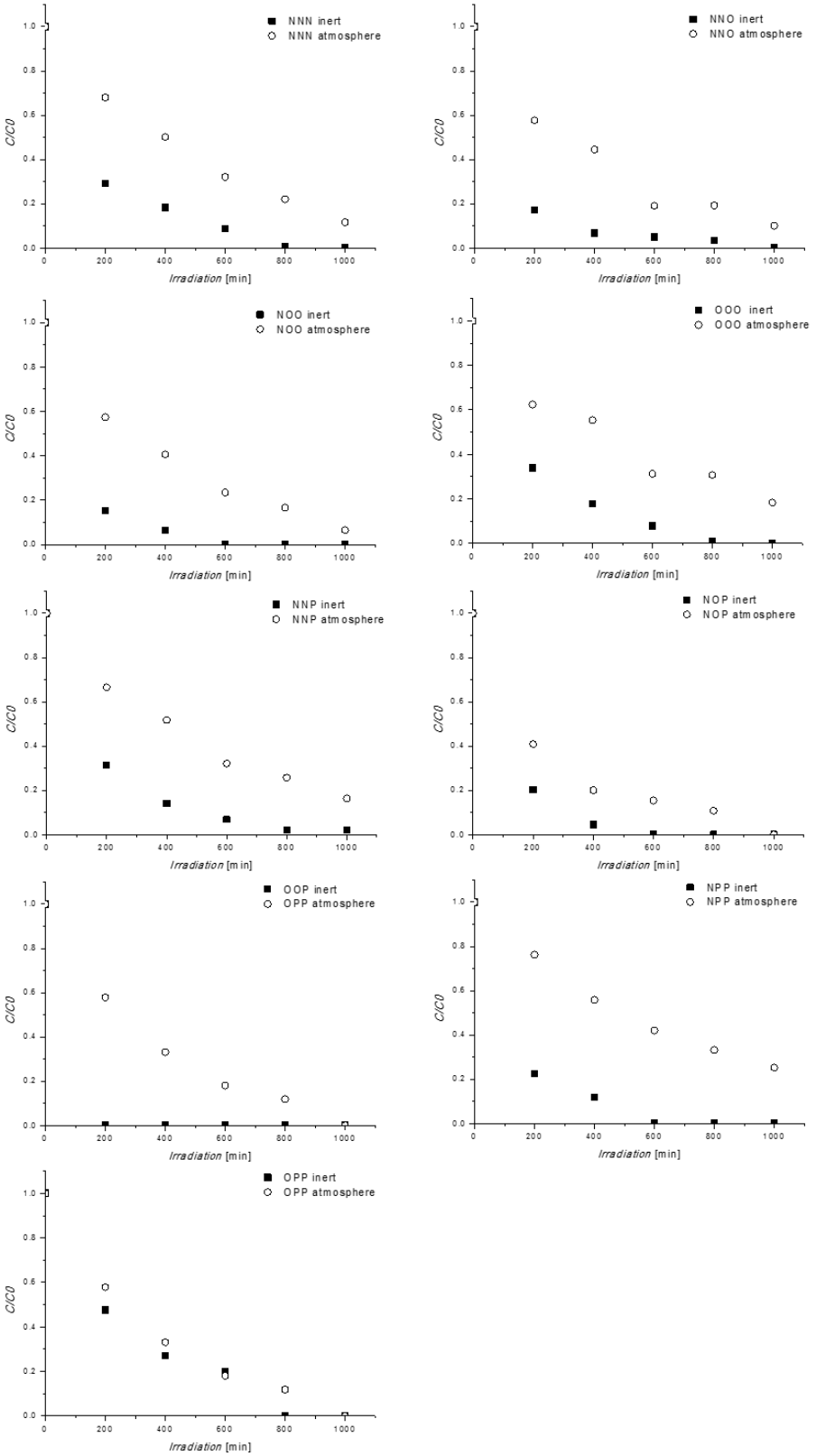

8.1.4 1.4 PICTURE OF THE IRRADIATION UNIT

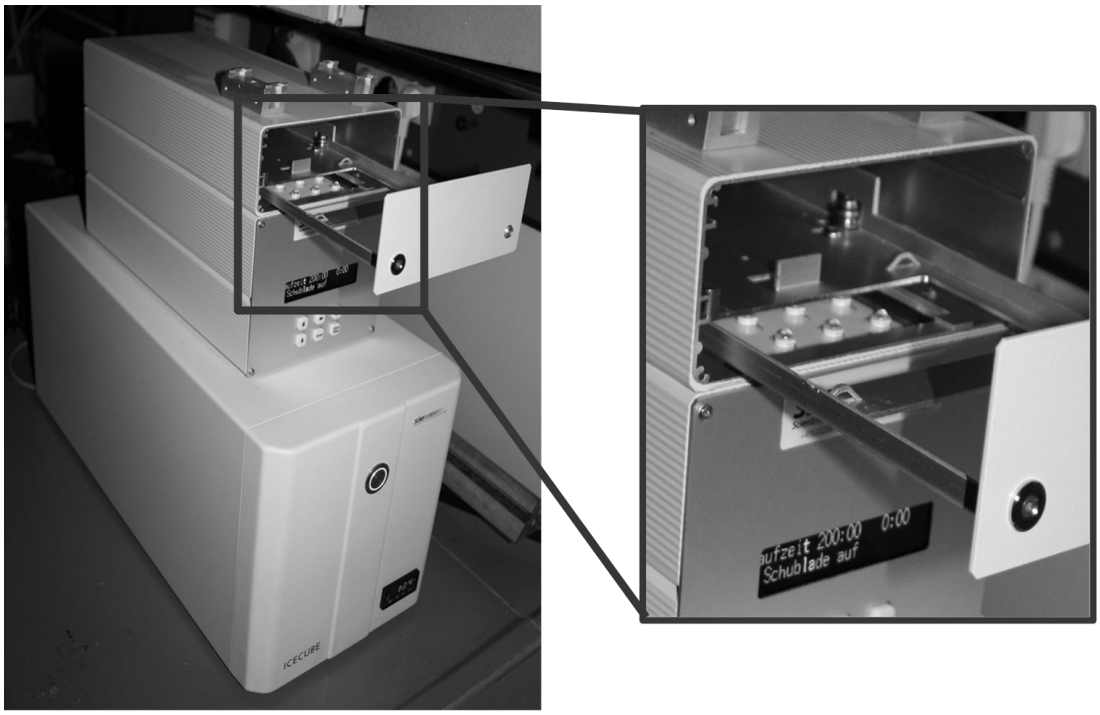

8.1.5 CHARACTERIZATION OF THE HOMOLEPTIC REFERENCE COMPLEXES

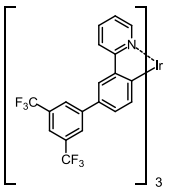

Complex **KKK**

The crude product was recrystallized from toluene/ethanol. Yellow solid. 89 mg (0.069 mmol, 63 %).

^{1}H NMR (400 MHz, $C_2Cl_4D_2$, δ): 8.06 – 7.96 (m, 9H), 7.82 (d, *J*=1.6, 3H), 7.73 – 7.64 (m, 6H), 7.52 (d, *J*=5.0, 3H), 7.07 (dd, *J*=8.0, 1.8, 3H), 6.96 (dd, *J*=14.8, 7.2, 6H), 6.96 (dd, *J*=14.8, 7.2, 6H).**^{13}C NMR** (101 MHz, $C_2Cl_4D_2$, δ): 166.08, 163.20, 147.62, 145.49, 144.68, 138.48, 137.22, 132.17, 130.14, 128.92, 128.06, 126.69, 125.34, 123.42, 122.63, 122.57, 119.92, 119.86. **HRMS** (APCI, *m/z*): $[M + H]^+$ calcd for $C_{57}H_{30}F_{18}IrN_3$, 1292.1859; found: 1292.1890.

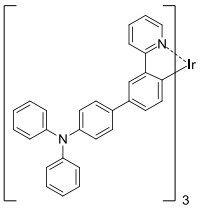

*Complex **OOO***

The crude product was recrystallized from THF/2-propanol. Yellow solid. 102 mg (0.074 mmol, 67 %). **^{1}H NMR** (400 MHz, $C_2Cl_4D_2$, δ): 7.97 – 7.90 (m, 3H), 7.83 (s, 3H), 7.63 – 7.56 (m, 3H), 7.51 – 7.45 (m, 9H), 7.21 – 7.14 (m, 12H), 7.10 – 7.01 (m, 21H), 6.96 – 6.86 (m, 12H). **^{13}C NMR** (101 MHz, $C_2Cl_4D_2$, δ): 166.67, 160.88, 148.12, 147.50, 146.39, 145.01, 138.09, 136.84, 136.50, 131.89, 129.70, 128.43, 127.16, 125.28, 124.58, 124.38, 122.99, 122.16, 119.53. **HRMS** (APCI, *m/z*)**:** $[M + H]^+$ calcd for $C_{87}H_{63}IrN_6$, 1385.4825; found: 1385.4839.

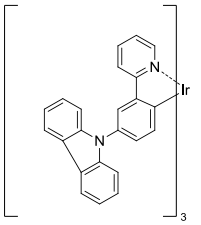

Complex **CCC**

The crude product was recrystallized from THF/2-propanol. Yellow solid: 90 mg (0.078 mmol, 78 %). **^{1}H NMR** (400 MHz, $C_2Cl_4D_2$, δ) 8.20 – 8.09 (m, 6H), 7.80 (d, *J* = 1.9 Hz, 3H), 7.73 (d, *J* = 8.3 Hz, 3H), 7.62 (d, *J* = 5.3 Hz, 3H), 7.59 – 7.53 (m, 3H), 7.49 – 7.27 (m, 15H), 7.27 – 7.22 (m, 6H), 7.14 (dd, *J* = 8.0, 2.1 Hz, 3H), 7.04 – 6.98 (m, 3H). **^{13}C NMR** (101 MHz, $C_2Cl_4D_2$, δ) 165.96, 160.56, 147.60, 145.83, 141.82, 138.62, 137.19, 130.51, 129.32, 126.34, 123.44, 123.27, 123.22, 120.70, 119.98, 119.82, 110.54. **HRMS** (APCI, *m/z*): $[M+H]^+$ calcd for $C_{69}H_{45}IrN_6$: 1151.3414; found: 1151.3442.

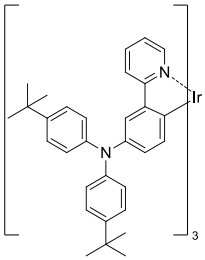

Complex EEE

The crude product was recrystallized from THF/MeOH. Orange solid: 97 mg (0.068 mmol, 68 %). **^{1}H NMR** (400 MHz, C2Cl4D2, δ) 7.56 – 7.34 (m, 12H), 7.14 (d, J = 8.6 Hz, 12H), 6.94 (d, J = 8.6 Hz, 15H), 6.84 – 6.70 (m, 6H), 1.27 (s, 54H). **^{13}C NMR** (101 MHz, C2Cl4D2, δ) 166.34, 157.21, 147.39, 146.05, 145.40, 143.90, 140.44, 137.96, 136.55, 129.89, 126.15, 123.67, 122.67, 121.90, 119.69, 34.45, 31.95. **HRMS** (APCI, m/z): [M+H]+ calcd for $C_{87}H_{87}IrN_6$: 1493.7643; found: 1493.7676.

8.2 Supporting Information for Chapter 3

Reproducibility of the degradation studies in toluene under ambient conditions:

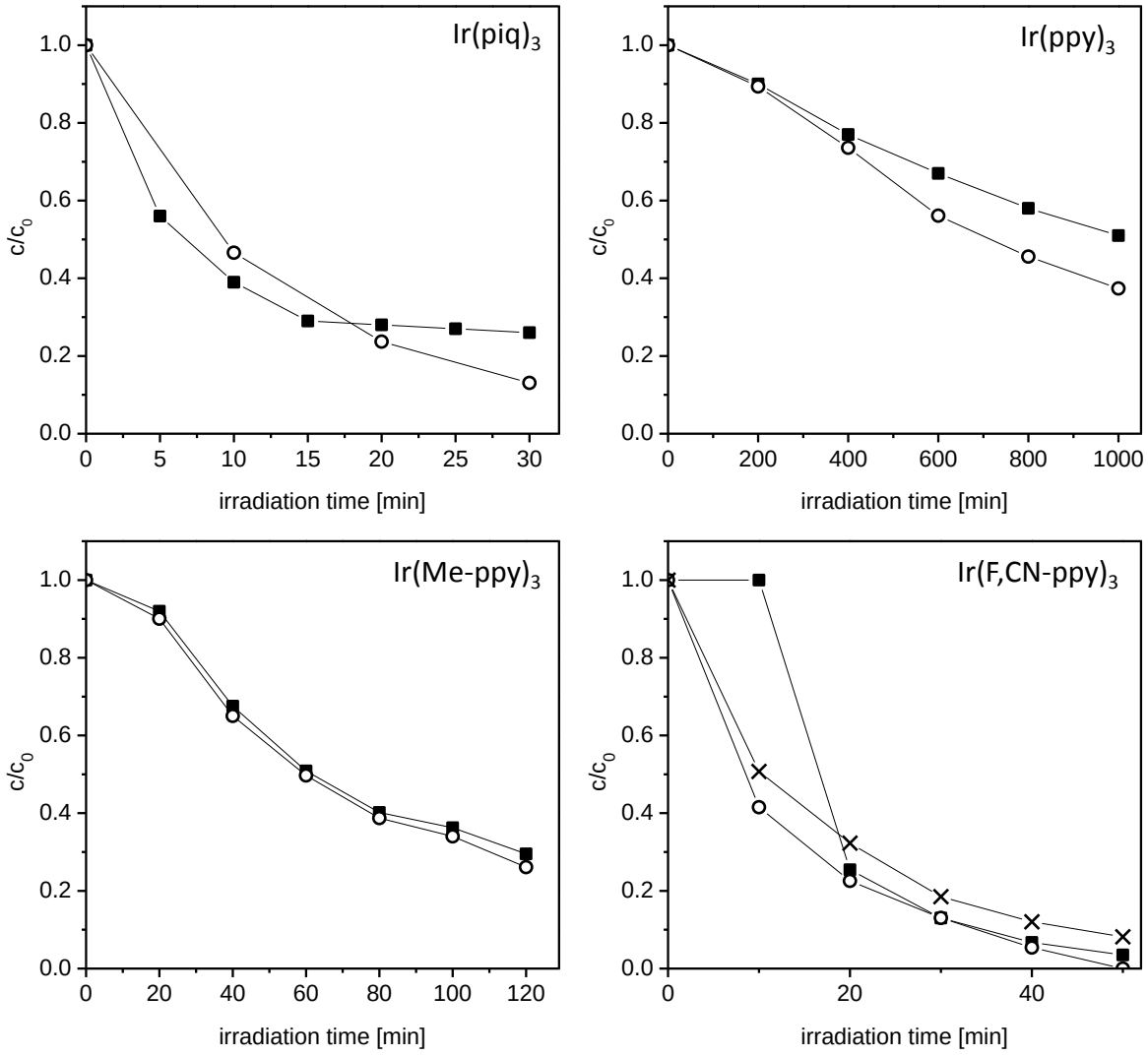

Reproducibility of the degradation studies in a PMMA matrix under ambient conditions:

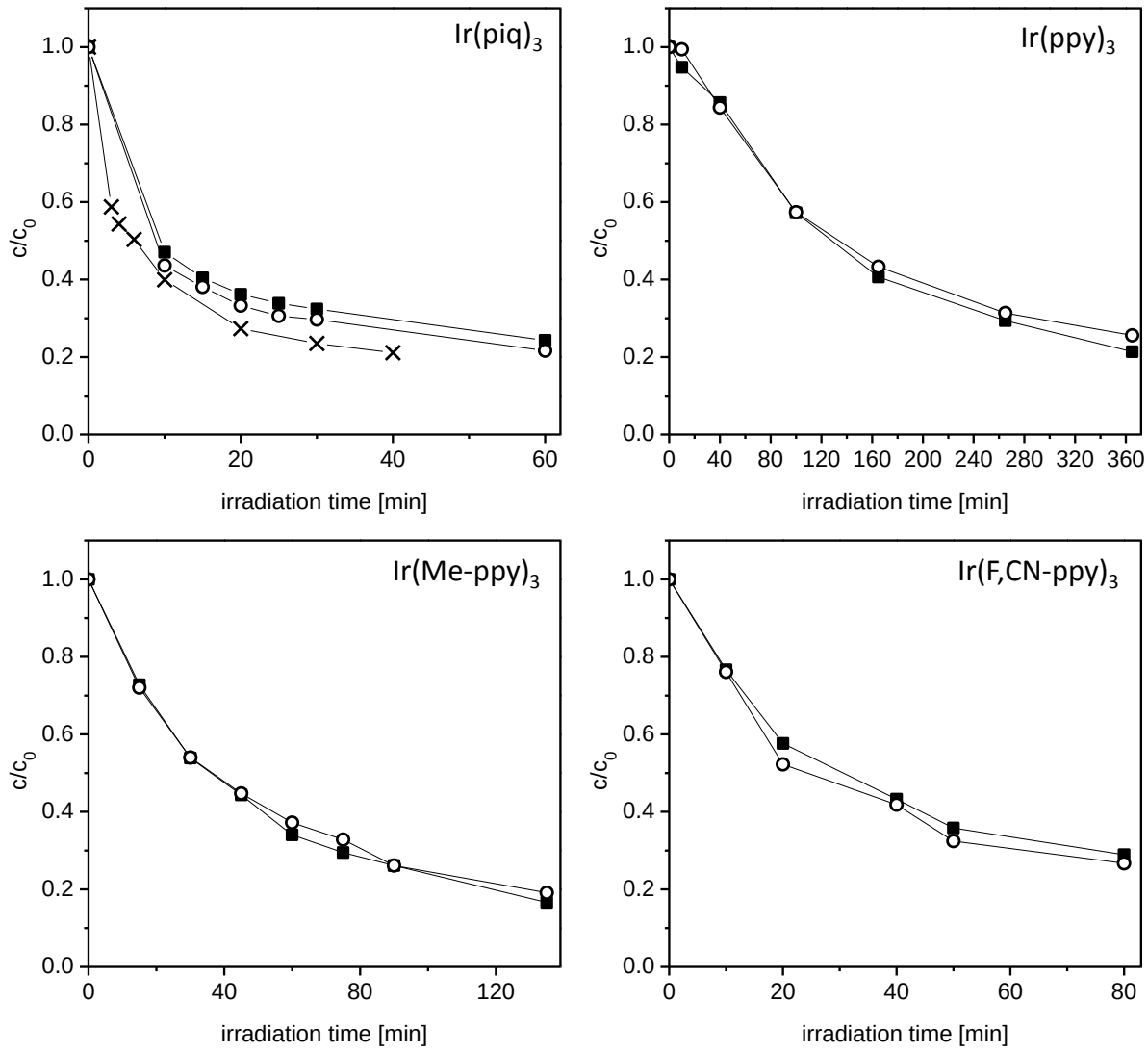

Degradation studies of $Ir(piq)_3$, $Ir(ppy)_3$, $Ir(Me\text{-}ppy)_3$ and $Ir(F,CN\text{-}ppy)_3$ in DCM under ambient and inert conditions:

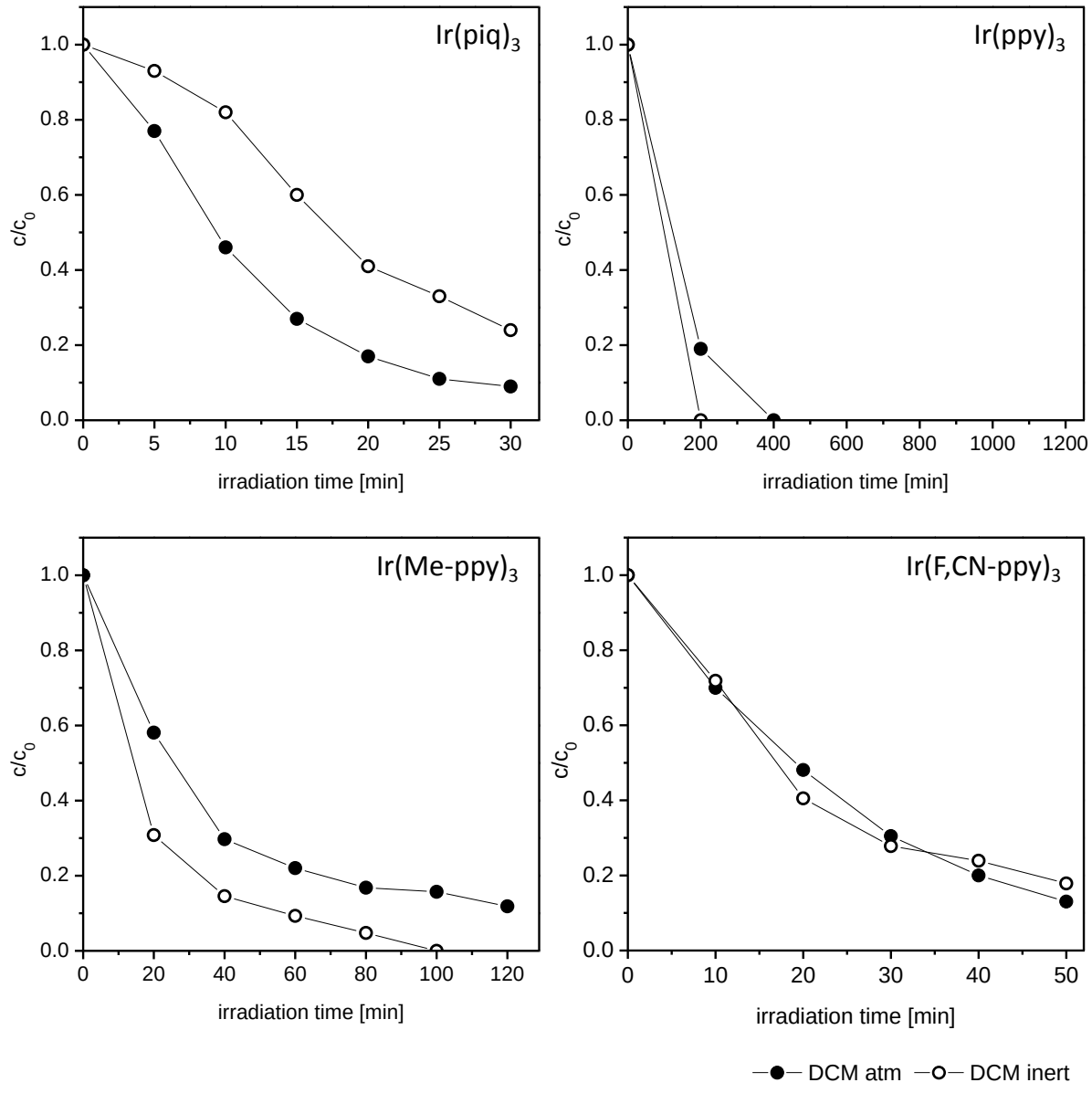

Degradation curves of $Ir(piq)_3$, $Ir(ppy)_3$, $Ir(Me\text{-}ppy)_3$ and $Ir(F,CN\text{-}ppy)_3$ in benzene and toluene under ambient and inert conditions:

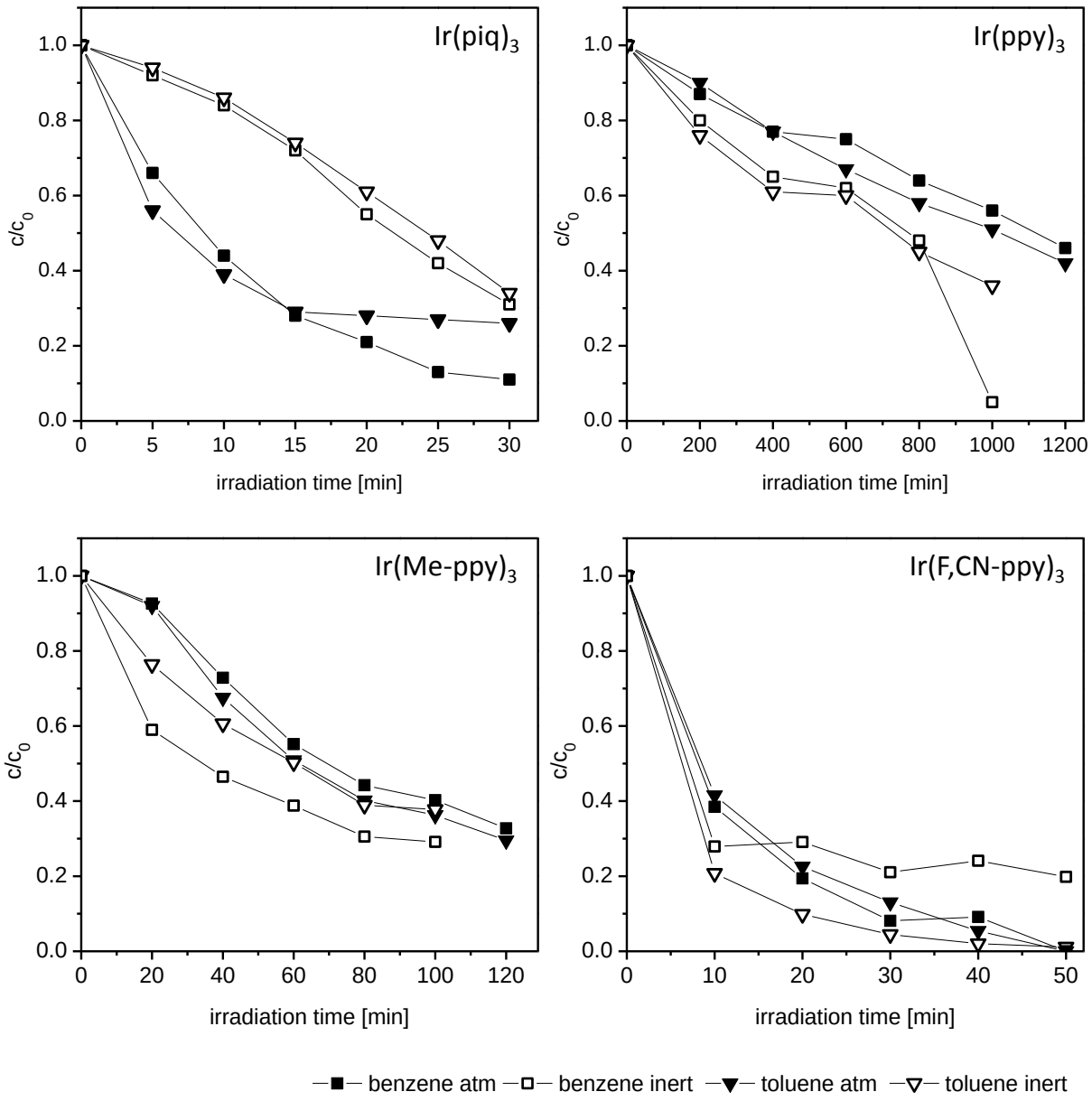

8.3 SUPPORTING INFORMATION FOR CHAPTER 4

8.3.1 PLOTS OF THE STERN-VOLMER QUENCHING EXPERIMENTS

Stern-Volmer plots for $Ir(piq)_3$

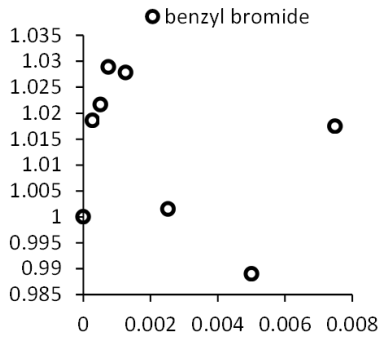

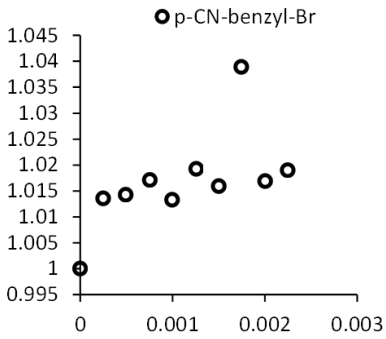

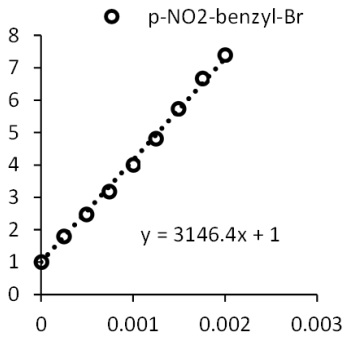

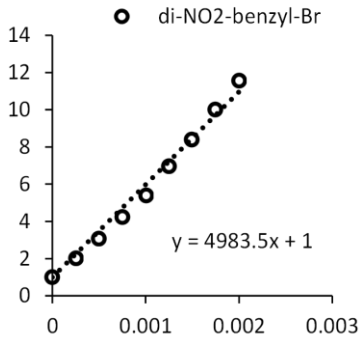

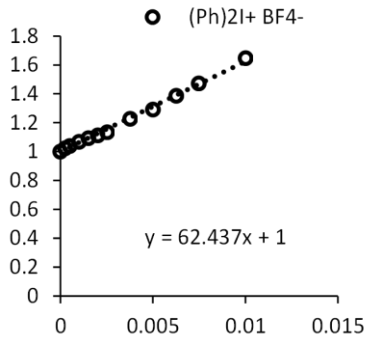

Stern-Volmer plots for $Ir(ppy)_3$

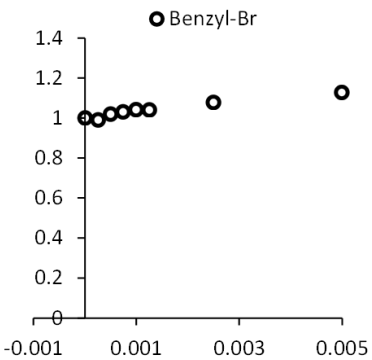

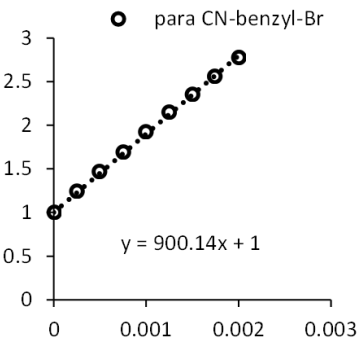

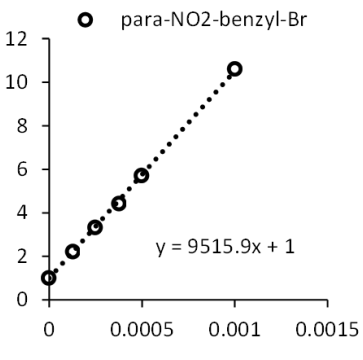

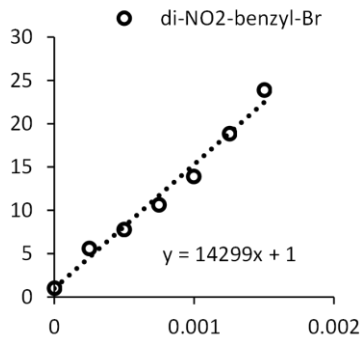

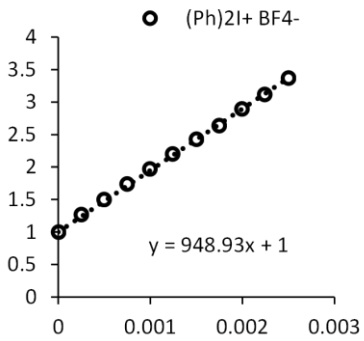

Stern-Volmer plots for **2**

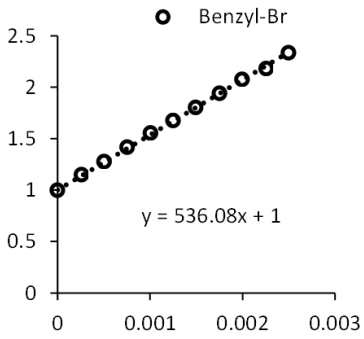

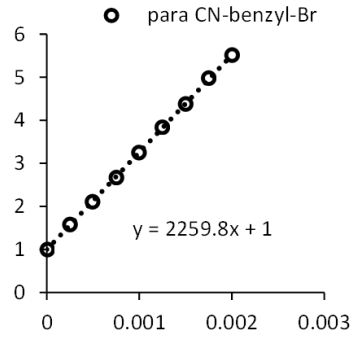

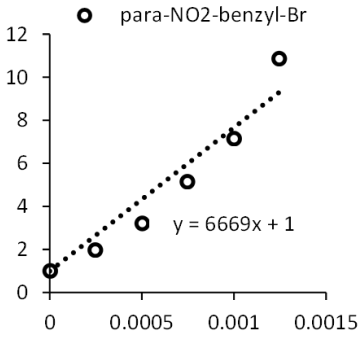

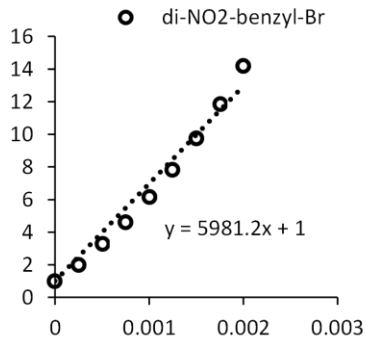

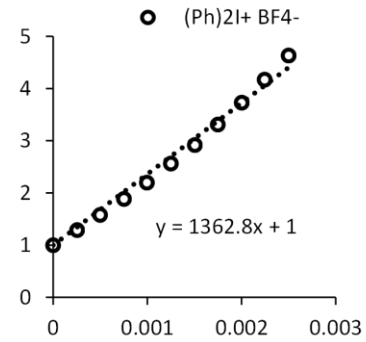

8.4 SUPPORTING INFORMATION FOR CHAPTER 5

^{1}H-NMR of compound **2:**

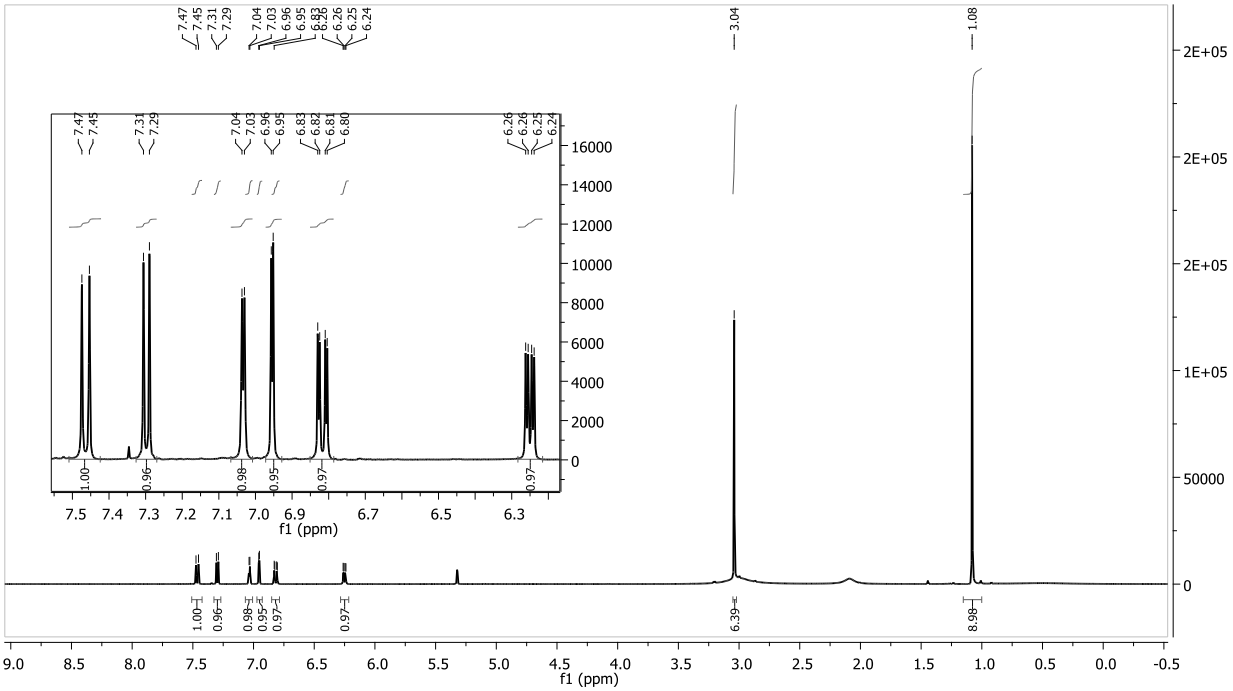

^{13}C-NMR of compound **2:**

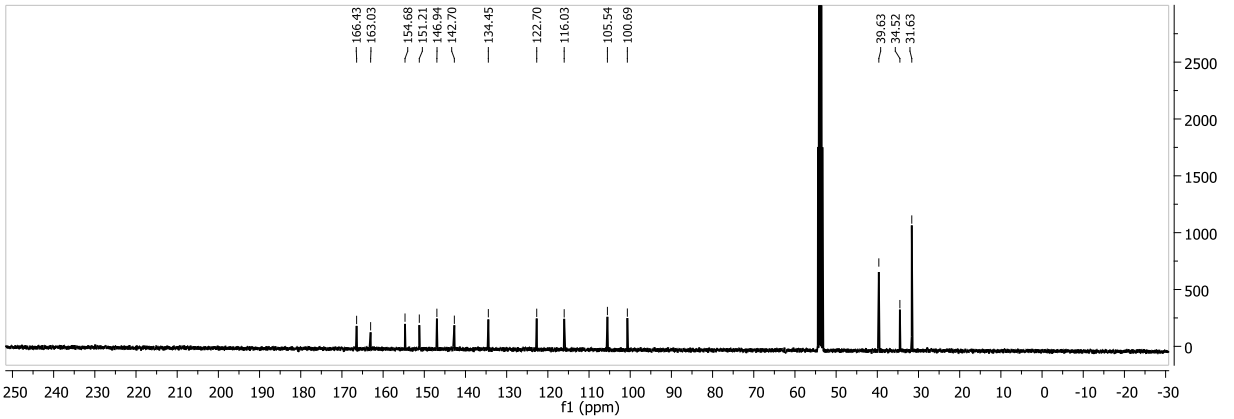

8.5 LIST OF ABBREVIATIONS

3D	three dimensional
^{3}MC	triplet metal centered state
acac	acetylacetonate
AcCN	acetonitrile
ADN	9,10-di(naphth-2-yl)anthracene
AlQ_3	tris(8-hydroxy-quinolinato)aluminium
amu	atomic mass unit
APCI	atmospheric-pressure chemical ionization
BAlQ2	bis(2-methyl-8-quinolinolate)-4-phenylphenolato)aluminium
BCP	2,9-dimethyl-4,7-diphenyl-1,10-phenanthroline
BPC	4-(carbazol-9-yl)biphenyl
BPhen	4,7-diphenyl-1,10-phenanthroline
bzq	7,8-benzoquinoline
CBP	4,4'-bis(carbazol-9-yl)biphenyl
CDBP	4,4′-bis(carbazol-9-yl)-2,2’-dimethyl-biphenyl
CO2	carbon dioxide
d	diameter
d	doublet
DAD	diode array detector

DCM	dichloromethane
dd	doublet of doublets
DFT	density functional theory
DMFL-CBP	2,7-bis(carbazol-9-yl)-9,9-dimethylfluorene
DSSC	dye-sensitized solar cell
DTA	di-p-tolylamine
DTPA	di(p-tolyl)phenylamine
EML	emissive layer
EPR	electron paramagnetic resonance
etc.	et cetera
ETL	electron transport layer
fac	facial
FIrpic	bis(3,5-difluoro-2-(2-pyridyl)phenyl-(2-carboxypyridyl)iridium(III)
FLD	fluorescence detector
FWHM	full width at half maximum
GPC	gel permeation chromatography
h	hour
HBL	hole blocking layer
HOMO	highest occupied molecular orbital
HPLC	high performance liquid chromatography
HR	high resolution
HTL	hole transport material
$Ir(F,CN\text{-}ppy)_3$	*fac*-tris[2-(4-fluoro-3-cyano phenyl)pyridine]iridium (III)

$Ir(piq)_3$	*fac*-tris(phenylisoquinoline)iridium (III)
$Ir(ppy)_3$	*fac*-tris(phenylpyridine)iridium (III)
ISC	inter system crossing
J	coupling constante
K	Kelvin
LC	liquid chromatography
LDE	laser desorption ionization
LED	light emitting diode
LT_{50}	lifetime at half the initial luminance
LUMO	lowest unoccupied molecular orital
m	multiplet
m/z	mass to charge
MALDI	matrix assisted laser desorption ionization
MDQ	2-methyldibenzo-[f,h]quinoxaline
MeOH	methanol
Me-THF	2-methyl tetrahydrofuran
MLCT	metal-to-ligand charge-transfer
mM	millimolar
MS	mass spectrometry
N	normal
nm	nanometer
NMR	nuclear magnetic resonance
NPB	N,N'-bis(naphthalen-1-yl)-N,N'-bis(phenyl)-benzidine

OAc	acetate
OLED	organic light emitting diode
o-tolyl	ortho-tolyl
PC	phenylcarbazole
PEDOT:PSS	poly(3,4-ethylenedioxythiophene) poly(styrenesulfonate)
PhOLED	phosphorescent organic light emitting diode
pim	phenylimidazole
piq	1-phenylisoqchinoline
PL	photoluminescence
pmb	1-phenyl-3-methylbenzimidazolin-2-ylidene- C,C2'
ppm	parts per million
ppy	2-phenylpyridine
PTFE	polytetrafluoroethylene
Q-TOF	quadrupole time-of-flight
QY	quantum yield
s	singlet
TAD	2,2',7,7'-tetrakis(N,N-diphenylamino)-9,9-bifluorene
TAPC	di-[4-(N,N-ditolyl-amino)-phenyl]cyclohexane
TBADN	2-tert-butyl-9,10-di(naphth-2-yl)anthracene
tBu	tert-butyl
TCTA	4,4',4"-tris(carbazol-9-yl)triphenylamine
TDAB	1,3,5-tris(diphenylamino)benzene
Tg	glass transition temperature

THF	tetrahydrofuran
THF	tetrahydrofurane
TPBi	2,2',2"-(1,3,5-benzinetriyl)-tris(1-phenyl-1-Hbenzimidazole)
TPD	N,N'-bis(3-methylphenyl)-N,N'-bis(phenyl)-benzidine
UDC	Universal Display Corporation
UV	ultraviolet
Vis	visible

8.6 CURRICULUM VITAE

Personal data

Date of Birth	18th of January 1985
Nationality	German
Marital status	unmarried
Birthplace	Munich

Education

11/2009 – 02/2013 **PhD studies (organic chemistry),** University of Regensburg Supervisor: Prof. Burkhard König

"New Approaches towards Phosphorescent Iridium Complexes for Applications in Organic Light-Emitting Diodes and Photocatalysis "

- Combinatorial und conventional synthesis of new emitting materials for OLEDs
- Development of a screening for the identification, evaluation and degradation analysis of the emitters via a combination of modern analytic techniques (HPLC-MS/MS, spectroscopy, cyclovoltammetry etc.)

01/2009-10/2009 **Master thesis,** IISC Bangalore and University of Regensburg

"Catalytic Photooxidations in Chiral Bile Acid derived Supramolecular Hydrogels"

10/2007 - 10/2009 **Master of Science (chemistry),** University of Regensburg

Organic Chemistry (mayor), inorganic chemistry and biochemistry, research stays in Bangkok (Thailand) and Bangalore (India)

10/2004 - 10/2007 **Bachelor of Science (chemistry)**, University of Regensburg

General, inorganic, organic, physical and biochemistry

06/2007 **Bachelor Thesis**, University of Regensburg

"Synthesis of Flavin-Guanidino Photocatalysts"

6/2004 **Abitur**, Von Müller Gymnasium Regensburg

International Experience

02/2009 - 07/2009 **Indian Institute of Science (Bangalore, India)**

Research stay with Prof. Uday Maitra for the Master thesis

"Catalytic Photooxidations in Chiral Bile Acid derived Supramolecular Hydrogels"

03/2008 - 04/2008 **Chulalongkorn University (Bangkok, Thailand)**

Research stay with Prof. Tirayut Vilaivan

"Phase-Transfer Catalyzed Addition of Malonates to α-Imidosulphones"

8.8 PUBLICATIONS AND CONFERENCE CONTRIBUTIONS

Publications

J. Bachl, A. Hohenleutner, B. Dhar, C. Cativiela, U. Maitra, B. König, D. Díaz Díaz, Organophotocatalysis in nanostructured softgel materials as tunable reaction vessels: Comparison with homogeneous and micellar solutions. *Submitted.*

S. Schmidbauer, A. Hohenleutner, B. König: Chemical Degradation of Organic Light-Emitting Devices: Mechanisms and Implications for the Synthesis of New Materials. *Accepted*.

A. Hohenleutner, S. Schmidbauer, R. Vasold, D. Joosten, P. Stoessel, H. Buchholz, B. König, Rapid Combinatorial Synthesis and Chromatography Based Screening of Phosphorescent Iridium Complexes for Solution Processing. *Adv. Funct. Mater.* **2012**, *22*, 3406 – 3413.

H. Schmaderer, A. Hohenleutner, B. König, Synthesis of a bicyclic diamine derived from Kemp´s acid. *Syn. Commun.* **2009**, *39*, 2596 – 2604.

Conference Contributions

ORCHEM 2012, 18. Lecture Conference in Weimar, "*Combinatorial Synthesis, Screening and Photodegradation of Phosphorescent Metal Complexes for OLEDs."* (short oral presentation + poster) **09/2012**

4th EuCheMS Chemistry Conference in Prague (Czech Republic), "*Combinatorial Synthesis, Screening and Photodegradation of Phosphorescent Metal Complexes for OLEDs."* (poster) **08/2012**

Gordon Research Conference (GRC) and Seminar (GRS) in Barga (Italy), "*Combinatorial Synthesis, Screening and Photodegradation of Phosphorescent Metal Complexes for OLEDs."* (oral presentation + poster) **06/2012**

3rd EuCheMS Chemistry Conference in Nürnberg, "*Combinatorial Synthesis and High Throughput Screening of new Triplett-emitters for OLED Applications."* (poster) **09/2010**

VIIth International OLED Summer School in Krutyn (Poland), "*Combinatorial Synthesis and High Throughput Screening of new Triplett-emitters for OLED Applications*." (poster) **06/2010**

Workshop OLED in Regensburg, "Schneller zu neuen Emittern: Kombinatorische Synthese und Screening von Triplett Emittern." (oral presentation) **04/2010**

1st INDIGO Research Conference in Hyderabad (India), "Flavin Photocatalysis in Chiral Supramolecular Gels" (oral presentation) **03/2009**